



Desai, Vibhuti H. (2017) *Biotechnological applications of a surfactant protein, ranspumin-2*. PhD thesis.

<https://theses.gla.ac.uk/8609/>

Copyright and moral rights for this work are retained by the author

A copy can be downloaded for personal non-commercial research or study, without prior permission or charge

This work cannot be reproduced or quoted extensively from without first obtaining permission in writing from the author

The content must not be changed in any way or sold commercially in any format or medium without the formal permission of the author

When referring to this work, full bibliographic details including the author, title, awarding institution and date of the thesis must be given

Enlighten: Theses

<https://theses.gla.ac.uk/>
research-enlighten@glasgow.ac.uk



University
of Glasgow

Biotechnological applications of a surfactant
protein, ranaspumin-2

Vibhuti H. Desai

Submitted in fulfilment of the requirements for the Degree of
Doctor of Philosophy

College of Medical, Veterinary and Life Sciences

University of Glasgow

November 2017

Abstract

Surfactant activity is generally associated with small molecules rather than biological macromolecules like proteins. Only a few proteins have good intrinsic surfactant activity, an example being the natural surfactant ranaspumin 2 (Rsn2) from the foam nests of the túngara frog. In solution, Rsn2 has a hydrophobic core and hydrophilic exterior, but when Rsn2 comes in contact with an air-water interface, it changes conformation to expose its hydrophobic core to interact with the air and present a hydrophilic face to the water. The unique combination of biocompatibility along with surface activity offers the possibility of developing biomedical applications based on Rsn2. Some of the possible applications, including cell patterning, functionalising scaffolds and stabilising droplets, have been explored in the work described in this thesis.

The ability of Rsn2 to coat hydrophobic surfaces persistently, rendering them wettable and the nature of coating and interaction with the surfaces were investigated. This formed the basis for the development of a method to coat a range of hydrophobic polymers, which are commonly used for biomedical applications. These Rsn2 coated surfaces were tested for their capability to control cell adhesion on surfaces which usually do not support cell adhesion. Rsn2 coating was demonstrated to promote, and thus allowed the spatial control over, cell adhesion on otherwise non-cell compatible surfaces.

The potential of Rsn2 to be used as a protein fusion partner for the production of further functionalised cell engineering substrates was explored by constructing five different integrin binding sequence (IBS)-Rsn2 conjugates. Specific IBS-Rsn2 proteins proved successful in increasing the adhesion and biomineralising potential of osteoblasts isolated from neonatal rats.

In addition, Rsn2's ability to stabilise microscopic oil droplets, and to solubilise fullerene were investigated. Rsn2 stabilised oil droplets were stable for more than six months.

Thus, the surfactant properties of Rsn2 can be used for many potential biomedical applications.

Table of Contents

List of Tables	5
List of Figures.....	6
Acknowledgements.....	9
Author's declaration.....	10
Definitions/Abbreviations	11
1 Introduction.....	14
1.1 Surfactant.....	15
1.2 Biosurfactants	18
1.3 Pulmonary Surfactant proteins.....	19
1.4 Hydrophobins.....	21
1.5 Biofilm Surface Layer Protein A	23
1.6 Latherin and SPLUNC1	24
1.7 Ranaspumin2	27
1.7.1 Túngara frog	27
1.7.2 Foam nest.....	28
1.7.3 Foam nests components.....	28
1.7.4 Ranaspumin2.....	29
1.8 Comparison of the different surfactant proteins	31
1.9 Aims	34
2 Cell patterning with Rsn2	35
2.1 Introduction	36
2.2 Aim.....	38
2.3 Methods and Materials	39
2.3.1 Rsn2 production	39
2.3.2 Pendant drop tensiometry	41
2.3.3 Wettability.....	42
2.3.4 Contact Angle.....	42

2.3.5	Persistence	43
2.3.6	Routine cell culture	43
2.3.7	Fabrication of PDMS.....	44
2.3.8	Cell Patterning	44
2.3.9	Fluorescence staining	45
2.4	Results	46
2.4.1	Rsn2 and iLOVRsn2 production.....	46
2.4.2	Pendant drop tensiometry	46
2.4.3	Wettability.....	48
2.4.4	Contact angle	49
2.4.5	Persistence	51
2.4.6	Cell patterning.....	53
2.5	Discussion.....	56
3	Functionalisation of PDMS with IBS-Rsn2.....	58
3.1	Introduction	59
3.2	Aim.....	63
3.3	Method and Materials.....	64
3.3.1	IBS-Rsn2 cloning and protein expression	64
3.3.2	Contact Angle.....	65
3.3.3	Silanisation	65
3.3.4	Routine cell culture	65
3.3.5	Isolation and culture of osteoblastic cells.....	65
3.3.6	PDMS fabrication.....	66
3.3.7	Sample preparation.....	67
3.3.8	Differentiation assay.....	67
3.3.9	Immunofluorescence staining	67
3.3.10	Quantification	68
3.4	Results	70

3.4.1	IBS-Rsn2 fusion construct cloning	70
3.4.2	IBS-Rsn2 fusion protein expression.....	73
3.4.3	Contact angle measurements.....	75
3.4.4	Fibroblast cell culture on different IBS-Rsn2 coated PDMS.....	76
3.4.5	Osteoblast cell culture on IBS-Rsn2 coated PDMS	78
3.4.6	Comparison of the cell density of osteoblasts at various time points.....	87
3.4.7	Osteopontin and Osteocalcin expression	89
3.5	Discussion.....	92
4	Stabilisation of micro-emulsions droplets	95
4.1	Introduction	96
4.1.1	Biom mineralisation	96
4.1.2	Molluscan Shell Formation and Extrapallial Fluid.....	97
4.1.2	Rsn2 Protein.....	98
4.2	Aims & Objectives.....	98
4.3	Method and Materials.....	99
4.3.1	Rsn2 stabilised bubbles and droplets.....	99
4.3.2	EP-Rsn2 – cloning and protein production.....	100
4.3.3	Inclusion body preparation	100
4.4	Results	101
4.4.1	EP-Rsn2 cloning	101
4.4.2	Test expression.....	105
4.4.3	EP pET15 protein expression and purification	106
4.4.4	Inclusion body preparation	107
4.4.5	Formation of Rsn2 stabilised bubbles	108
4.4.6	Formation of Rsn2 stabilised droplets.....	109
4.5	Discussion and future work	111
5	General discussion.....	113
6	References.....	116

List of Tables

Table 1-1 Major types of biosurfactants.....	18
Table 1-2 Final reduction in surface tension by the action of surfactant proteins	34
Table 3-1 Integrins and their binding partners.....	61
Table 3-2 Integrin binding sequences (IBS), their molecule(s) of origin, their binding integrins and the citation	62
Table 3-3 Sequences of primers designed to generate IBS-Rsn2.	64
Table 4-1 The EP fusion protein primer sequences.....	102

List of Figures

Figure 1-1 The typical molecular structure of a surfactant	17
Figure 1-2 Diagrammatic representation of water in oil emulsion	17
Figure 1-3 The Schematic structure and relative size of the pulmonary surfactant proteins	20
Figure 1-4 Cartoon representation of the crystal structure of a hydrophobin class II.....	22
Figure 1-5 Cartoon diagram showing structure of BslA1	24
Figure 1-6 Cartoon diagram showing solution structure of latherin.....	25
Figure 1-7 Model showing different stages of Latherin.....	25
Figure 1-8 Foam nest production by mating male and female	27
Figure 1-9 Túngara frog foam nest	28
Figure 1-10 Cartoon representation of the frog foam nest components with their proposed role.	29
Figure 1-11 Cartoon diagram showing solution structure of Rsn2	30
Figure 1-12 Cartoon diagram showing the hypothesised open Rsn2 structure at the air – water interface	30
Figure 1-13 A comparison of the surfactant proteins hydrophobin	32
Figure 1-14 A comparison of the surfactant protein latherin.....	33
Figure 2-1 SDS PAGE of Rsn2 nickel affinity purification	46
Figure 2-2 SDS PAGE of iLOVRsn2 Nickle affinity purification.....	46
Figure 2-3 Rsn2 film relaxation at trioctanoyl glycerol oil/water interface	48
Figure 2-4 Formation of water droplets on a coverslip having coated & non-coated Rsn2 regions.....	49
Figure 2-5 The contact angle of water on Rsn2 coated and non-coated regions	51
Figure 2-6 The persistence of Rsn2 coating on hydrophobic material.....	53
Figure 2-7 Representative light microscopy image taken at the boundary between Rsn2 coated and non-coated regions	54
Figure 2-8 Comparison of coated and non-coted regions of h-Terts cells cultured on Rsn2 coated PS.....	54
Figure 2-9 Scanned image of coomassie blue stained pattern compliant h-Terts cells....	55
Figure 2-10 A montage fluorescence image taken on the edge of the Rsn2 coated and non-coated region	55
Figure 3-1 A representative fluorescent image of the osteoblast cells cultured on IBS-Rsn2 coated PDMS	69

Figure 3-2 A representative fluorescence image of the osteoblast cells cultured on IBS-Rsn2 coated PDMS	69
Figure 3-3 PCR amplification of IBS-Rsn2 product using primers incorporating IBS ...	71
Figure 3-4 Colony PCR.....	71
Figure 3-5 A 1% agarose gel for double digested vector and insert with NdeI and BamHI	72
Figure 3-6 An example of agarose gel electrophoresis of colony	72
Figure 3-7 An example of the sequencing result for IBS-Rsn2 in pET28 vector.....	73
Figure 3-8 SDS-PAGE of PHSRN-Rsn2 affinity purification.....	74
Figure 3-9 SDS-PAGE of the five IBS-Rsn2 samples after Ni ²⁺ -affinity purification	74
Figure 3-10 SDS-PAGE of IKVAV-Rsn2 affinity purification.....	75
Figure 3-11 Graphical representation of the contact angle measurement of the droplet of water on various IBS-Rsn2 coated PDMS surface	76
Figure 3-12 Cell density of fibroblast cells cultured on various IBS-Rsn2	77
Figure 3-13 Immunofluorescence images of osteocytes after 4 hours in culture	79
Figure 3-14 Density of cells on various IBS-Rsn2 coated surface after 4 hours in culture	80
Figure 3-15 Graphical representation of the quantified number of focal adhesion formed per cells on various IBS-Rsn2 coated surfaces after 4 hours in culture	81
Figure 3-16 Immunofluorescence images of osteocytes after 1 day in culture on IBS-Rsn2 coated PDMS	83
Figure 3-17 Density of cells on various IBS-Rsn2 coated surface after 1 day in culture	84
Figure 3-18 Graphical representation of the quantified number of FCA per cells on various IBS-Rsn2 coated surfaces after 1 day in culture	85
Figure 3-19. Immunofluorescence images after 7 days in culture.....	86
Figure 3-20 Density of cells on various IBS-Rsn2 coated surface after 7 days in culture	87
Figure 3-21 Density of cells on day0, day1 and day7.....	88
Figure 3-22. Quantification of the average number of focal cell adhesions per cell on day0 and day1	89
Figure 3-23 Immunofluorescence images for osteopontin after 28 days	90
Figure 3-24 Immunofluorescence images for osteocalcin after 28 days.....	91
Figure 4-1 The common blue mussel.....	97
Figure 4-2 Schematic diagram of the microfluidics chip design used to form bubbles and oil droplets.....	99
Figure 4-3 The binding sites of the three sets of primers design for pET15 EP.....	102

Figure 4-4 PCR amplification from EP pET15.....	103
Figure 4-5 Agarose gel electrophoresis of restriction digests.....	104
Figure 4-6 Agarose gel electrophoresis result	105
Figure 4-7 SDS-PAGE of EP82S-Rsn2 test expressions.....	106
Figure 4-8 SDS-PAGE of large scale expression of EP from pET15	108
Figure 4-9 illustrates the process of Rsn2-stabilized N ₂ bubble formation.....	109
Figure 4-10 Representative image of (A) Rsn2 stabilised oil droplets captured using light microscope and (B) iLOVRsn2 stabilised oil droplets captured using fluorescence microscope	110

Acknowledgements

First of all I would like to thank all my supervisors, Dr. Brian Smith; Dr. Mathis Riehle and Prof Maggie Cusack for providing guidance throughout the course of my PhD. I can't thank Brian enough for his continuous support, wisdom, mentorship, bringing the best out of me and for keep pushing me to "try again" after setbacks, for reading all my draft chapters and giving constructive suggestions, without whom I would not have been able to complete this work. I would like to thank my co-supervisor Mathis for providing his expert insights and for being available when needed, especially for proof reading major chunk of this thesis during Christmas holidays and weekends. I would also like to thank my co-supervisor Maggie for her care, encouragement, directions and detailed inputs throughout PhD, especially during thesis writing. I also like to thank all my supervisors for their incredible support and understanding during my pregnancy and after maternity leave.

Many other people have contributed to the success of my PhD, thank you Dr. Sharon Kelly for your help with SPR. I would also like to thank Prof. Alan Cooper for giving me the opportunity to contribute in C₆₀ solubilisation work. I would like to extend my thanks to Prof Cait MacPhee and Dr. Ryan Morris from the University of Edinburgh for their help in pendent drop method. Thank you Dr. Jonathan McKendry for your help with the microfluidics system and Peter Chung for your help with the ESEM.

Many thanks to all the members of Brian's lab and CCE lab, especially Carrol-Ann, for your co-operation. Thank you Dr. Laphorn, Karen, Andre, Ellen, Ross, Musadiq, Gisela, Donald, Kate and all project students for making the lab lively place. Special thanks to Karen and Ellen for all the laughs, teas/coffees/lunch; it was my pleasure working with you all. Thanks my dear friend Chintan for always being there and lending ears to hear my rants.

I would also like to thank Glasgow University and Kelvin Smith Scholarship programme for giving me an opportunity to pursue this research work.

Finally, I would like to thank Hardik (my husband and my fourth unofficial supervisor), my parents, and my daughter Aarya for their continuous support, motivation, patience and sacrifice. Without you all by my side, I would not have been able to see the other end of this very long tunnel.

Author's declaration

I declare that, except where explicit reference is made to the contribution of others, that this thesis is the result of my own work and has not been submitted for any other degree at the University of Glasgow or any other institution.

Vibhuti Desai

February 2017

Definitions/Abbreviations

°C	Degree centigrade
3D	Three dimensional
Å ²	Angstrom square
ACLAR	A clear, poly-chloro-tri-fluoro-ethylene (PCTFE) film
BPI	Bactericidal permeability increasing protein
BSA	Bovine Serum Albumin
BslA	Biofilm surface layer protein A
CA	Contact angle
Ca ²⁺	Calcium
CCD	Charge-coupled device
CCD camera	Charge-coupled device camera
cDNA	Complementary DNA
DAPI	6-diamidino-2-phenylindole
DGEA	Asp-Gly-Glu-Ala; peptide sequence
DMEM	Dulbecco's Modified Eagle's Medium
DMS	Dimethylsiloxane
DNA	Deoxyribonucleic acid
E.Coli.	Escherichia coli
ECM	Extracellular matrix
EDTA	Ethylenediaminetetraacetic Acid
EP	Extrapallial protein
EP82S-Rsn2/EP76E-Rsn2	First 82/76 amino acid of extrapallial protein – ranaspumin2 fusion protein
EP-Rsn2	Extrapallial protein – ranaspumin2 fusion protein
ESEM	Environmental scanning electron microscope
FA	Focal adhesion
FBS	Foetal bovine serum
FITC	Fluorescein isothiocyanate streptavidin
FL EP	full length extrapallial protein
FMN	Flavin Mononucleotide
g	Gram
g/cm ³	Gram per cubic centimeter
g/L	Gram per litre
GFOGER	Gly-Phe-Hyp-Gly-Glu-Arg; peptide sequence
Glu	Glutamic acid
H ₂ O	Water
H ₂ O ₂	Hydrogen peroxide
HEPES	2-hydroxyethyl-1-piperazine-ethanesulphonic acid
HPA	Hydrophobic Alkane Thiol
h-TERT	Fibroblasts cell line
IBS	Integrin binding sequences
IBS-Rsn2	Integrin binding sequences – ranaspumin-2 fusion protein
Ig	Immunoglobulin G
iLOV	Improved light oxygen voltage
iLOVRsn2	improved light oxygen voltage ranaspumin2 fusion protein

IPTG	Isopropyl β -D-1-Thiogalactopyranoside
IRRAS	Infrared Reflection Absorption Spectroscopy
kDa	Kilo Dalton
L	Litre
LB	Luria-Bertani medium
LPS	Lipopolysaccharide
MEOR	Microbial enhanced oil recovery
mg/ml	Milligram per millilitre
MgCl ₂	Magnesium chloride
mM	Mili molar
mm	Millimetre
mN/m	MiliNewton per metre
NaCl	Sodium chloride
NEB	New England Biolab
Ni ²⁺	Nickel
Ni ²⁺ -NTA	Nickel Nitrilotriacetic acid
nm	Nanometre
NMR	Nuclear Magnetic Resonance
OCN	Osteocalcin
OPN	Osteopontin
PAGE	Polyacrylamide Gel Electrophoresis
PBS	Phosphate buffered saline
PC	Polycarbonate
PCR	Polymerase Chain Reaction
PDA	Polydopamine
PDB	Protein data bank
PDMS	Polydimethylsiloxane
PEG	Polyethylene glycol
pg/mm ²	Picogram per millimetre square
pI	Isoelectric point
PLUNC	Palate, Lung and Nasal Epithelium Clone
PMMA	Para-methoxymethamphetamine
PP	Polypropylene
PS	Polystyrene
PTFE	Polytetrafluoroethylene
RGD	Arg-Gly-Asp; peptide sequence
RH	Relative humidity
RNA	Ribonucleic Acid
RP-HPLC	Reversed-Phase High-Performance Liquid Chromatography
Rpm	Rounds per minute
Rsn2	Ranaspumin-2
RU	Response unit
SDS	Sodium Dodecyl Sulphate
SDS-PAGE	Sodium dodecyl sulphate polyacrylamide gel electrophoresis
SiO ₂	Sillicon dioxide
SP	Pulmonary surfactant protein
SPLUNC	Small Palate, Lung and Nasal Epithelium Clone
SWNT	Single-wall nanotubes

Taq	Thermus aquaticus polymerase
TFA	Trifluoroacetic acid
UV	Ultraviolet
μL	Microliter

1 Introduction

Introduction

Almost all proteins display some surface activity when agitated sufficiently vigorously, but this property is certainly not one that they have evolved to possess. However, there are a small number of proteins whose intrinsic surface activity appears to fulfil one of their primary functions. One such protein is ranaspumin-2 (Rsn2) found in foam nest of túngara frog. The physical properties of Rsn2 offer an attractive opportunity for many biotechnological applications, including, coatings for nano-devices or medical implants and as an emulsifier in food and personal-care products. Work described in this thesis is mainly focused on using Rsn2's ability to coat surfaces for developing a variety of biotechnological applications.

1.1 Surfactant

Surface tension is one of the important properties of a liquid and it arises from the interactions between the molecules that constitute a liquid. These molecules have cohesive forces between them, which attract them to each other and allow the surface of a liquid to resist an external force.

Surface tension is the measure of the free energy of the surface per unit area (Myers, 2005b). Surface tension is one of the important properties of liquids and it arises from the interactions between the molecules that constitute them. These molecules have cohesive forces between them, which attract them to one another and allow the surface of a liquid to resist an external force. Surface tension of a pure liquid, which is a constant value, can be measured by static surface measurements. For example water, which forms relatively strong intermolecular hydrogen bonds, generates a high surface tension (74.2 mN m^{-1}) compared to other liquids, for example ethanol (22.3 mN m^{-1}) and acetone (23.7 mN m^{-1}) where dipole-dipole interactions and van der Waal forces also exists (Myers, 2005b).

Surface tension measurements are commonly made by the capillary rise method, Du Noüy ring tensiometer, pendant drop or sessile drop method, and micro trough tensiometry method.

In the capillary rise method, a thin circular glass capillary is dipped into the liquid to be tested. If the liquid interaction with the capillary wall is favoured, then the liquid level will rise in the capillary and will generate a concave meniscus. In the opposite situation, a decrease in the liquid level will be observed in the capillary along with a

semispherically convex meniscus (Liu et al., 2016, Zhmud et al., 2000). The below formula is used for measuring surface tension in capillary rise method

$$\gamma = rh dg/2$$

Where γ is the liquid surface tension, r is the capillary radius, h is the height, d is the liquid density and g is the acceleration of gravity.

The Du Noüy ring tensiometer uses a platinum ring, which is generally lowered into the liquid to be tested and lifted upwards, raising a meniscus of liquid along with it. The force required to raise the ring increases until the meniscus breaks, releasing the ring. The maximum force encountered by the ring is measured by a balance and used to calculate surface tension (Fox and Chrisman, 1952). The below formula is used for measuring surface tension in method the Du Noüy ring tensiometer

$$W_{tot} = W_r + 4\pi R \gamma = W_r + 2l\gamma$$

Where W_{tot} is the total force needed to detach the ring, W_r is the ring weight, R is the ring radius, γ is the liquid surface tension, and l is the width.

The micro trough tensiometry method, also known as the Wilhelmy plate method, measures the surface tension of a test solution. For this a platinum rod attached to a computer-monitored microbalance is submerged into the test solution. The downward force exerted upon the rod by the surface is then calculated. The principle of the technique is similar to that of the du Noüy ring, however this gives the advantage of being able to measure surface tension in time-dependant manner (Vance, 2012, Wu et al., 1999). The below formula is used for measuring surface tension in method the micro trough tensiometry

$$W_{tot} = W_{plate} + 2 l \gamma \cos\theta$$

Where W_{tot} is the total force needed to detach the ring, W_r is the ring weight, R is the ring radius, γ is the liquid surface tension, and l is the width of the plate.

The pendant drop or sessile drop method involves taking measurements of an axisymmetric fluid droplet, and using the Young–Laplace equation to calculate interfacial tension (Berry et al., 2015) The method is described in detail in section 2.3.2 and 2.3.4 of the thesis.

Surfactants are surface active molecules which modify the surface tension of the liquid by modifying the inter-molecular forces between molecules at the surface. Surfactants have the ability to reduce the surface tension at an interface, even though present in small concentrations as measured in the bulk solution. Synthetic surfactants are usually organic molecules with amphiphilic properties, and they are made up of hydrophilic (polar head) and hydrophobic (non-polar tail) groups. Consequently, they are soluble in both aqueous and non-aqueous solutions. The conventional surfactants are grouped as non-ionic, cationic, anionic or zwitterionic, depending upon the nature of their head group (Myers, 2005a).

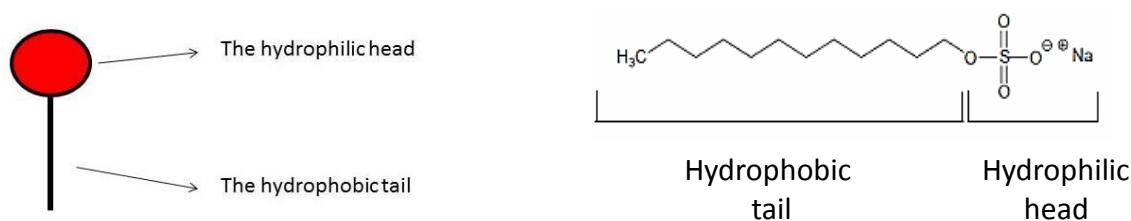


Figure 1-1 The typical molecular structure of a surfactant (A) and an example of a synthetic surfactant Na-dodecyl sulphate (B).

Upon mixing water and an immiscible hydrophobic liquid such as oil with surfactant, the surfactant occupies the water-oil interface and forms emulsions or micro-emulsions to avoid the direct oil/water contact. The surfactant molecules act cooperatively at an interface, and change the interfacial energy to function as wetting; emulsifying; foaming or suspending agents.

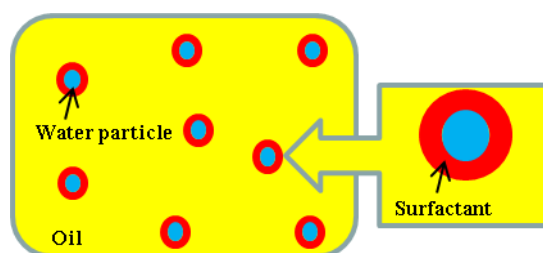


Figure 1-2 Diagrammatic representation of water in oil emulsion stabilised by surfactant

A wide variety of applications have increased the demand and production of surfactant molecules at global level. The global surfactant market was of US \$30.65 billion in 2015 and their demand is expected to increase by 4.4% in coming years (Market, 2016). Most of the synthetic surfactants are chemically derived from petroleum; nevertheless the interest in biological surfactants has been increasing steadily for environmental and industrial applications (Joshi et al., 2015).

1.2 Biosurfactants

Biosurfactants, a type of surfactant, are amphiphilic molecules secreted extracellularly by cells to facilitate many physiological functions including antimicrobial activity, protecting them against wetting and allowing them to grow on water-immiscible substrates (Desai and Banat, 1997). Like surfactants, biosurfactants also contain hydrophobic and hydrophilic groups, and have the ability to reduce surface tension at the interface. They have generally been found to be low molecular weight molecules. According to their chemical composition, biosurfactants are classified as glycolipids, lipopeptides and fatty acids (Reis et al., 2013). The current mass produced sources and possible applications of a range of biosurfactants are shown in below (Table 1-1).

Biosurfactants potentially offer notable advantages of reduced toxicity, biodegradability, eco-friendliness, bioremediation and digestibility (Banat et al., 2010) over the traditional chemical surfactants, and have found their applications in coatings and lubricants, pharma, crude oil recovery, health care, cosmetics and food processing industries (Desai and Banat, 1997).

Biosurfactant	Class	Micro organism	Application
<i>Glycolipids</i>	<i>Rhamnolipids</i> (Edwards and Hayashi, 1965)	<i>P. aeruginosa</i> and <i>P. putida</i>	<i>Bioremediation, Biocontrol agent, Antifungal agent, Bioremediation</i>
	<i>Sphorolipids</i> (Gautam and Tyagi, 2006)	<i>Candida bombicola</i> and <i>C. apicola</i>	<i>Emulsifier, MEOR, alkane dissimilation</i>
	<i>Trehalose lipids</i> (Asselineau and Asselineau, 1978)	<i>Rhodococcus spp.</i> and <i>Arthrobacter sp.</i>	<i>Bioremediation, Antimicrobial agent</i>
	<i>Mannosylerythritol lipids</i> (Reis et al., 2013)	<i>Candida antartica</i> <i>Neuroreceptor antagonist</i> and <i>Kurtzmanomyces sp</i>	<i>Antimicrobial agent, Biomedical application</i>
<i>Fatty acids</i>	<i>Fatty acids, phospholipids and neutral lipids</i> (Gautam and Tyagi, 2006)	<i>Acinetobacter spp</i>	<i>Biomedical applications</i>
<i>Lipo Peptides</i>	<i>Surfactin</i> (Arima et al., 1968)	<i>Bacillus subtilis</i>	<i>Antimicrobial agent, biomedical application</i>
	<i>Lichenysin</i> (McInerney et al., 1990)	<i>B. licheniformis</i>	<i>Hemolytic and chelating agent</i>

Table 1-1 Major types of biosurfactants

The surfactant property is generally associated with the low molecular weight molecules, but some macromolecules, like proteins, are also surface active. Nearly all proteins are composed of amphiphilic polypeptides, but generally have the hydrophilic parts exposed on their surface and the hydrophobic parts buried. Most proteins are sensitive to surface effects and foaming will result in denaturation. This denatured proteins exhibits surfactant properties attributed to the exposure of hydrophobic groups, which were buried in their native structure (Cooper and Kennedy, 2010). Thus while most proteins are surfactant to a certain extent, they are not usually surface active in their native state. However, proteins that have intrinsic surfactant activity are termed as surfactant proteins. The surfactant proteins generally adsorb at air water interfaces. The process of adsorption at an air water interface gives rise to an emulsion.

The surfactant proteins can be grouped into two classes: those that are active in presence of associated lipids (e.g., the pulmonary surfactants), and non-lipid-associated globular proteins. Both types of proteins and their mechanism of action are further discussed in the next sections, with the focus on the non-lipid associated surfactant proteins.

1.3 Pulmonary Surfactant proteins

The pulmonary surfactant proteins (SP) are the most well studied group of proteins linked with surfactant activity. Pulmonary surfactants are produced by the alveolar epithelial cell lining of the lungs to prevent alveolar collapse upon exhalation. Pulmonary surfactant is heterogeneous being composed of 90% lipids and 10% proteins by weight, the latter representing four surfactant associated proteins, designated as surfactant protein (SP)-A, SP-B, SP-C and SP-D. These proteins can be divided into two types, SP-B and SP-C are small hydrophobic proteins, while SP-A and SP-D are large hydrophilic proteins (Goerke, 1998).

SP-A and SP-D have collagen-containing calcium-dependent lectins, and are therefore referred to as “collectins”. Both proteins are hydrophilic and have calcium dependent carbohydrate binding domains involved in innate host-defence functions (Kishore et al., 2006, Sano and Kuroki, 2005).

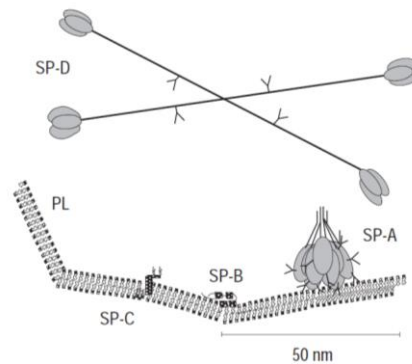


Figure 1-3 The Schematic structure and relative size of the pulmonary surfactant proteins. SP-A, SP-B, SP-C, and SP-D stands for the four different types of surfactant proteins acting near a phospholipid bilayer (PL). Image taken from (Griese, 1999)

The most abundant SP by weight is SP-A. SP-A is an octadecamer made up of ~ 32 kDa monomers, interacting with each other via disulphide linkages and noncovalent interactions (Griese, 1999). Each SP-A monomer has three structural motifs, a linking region that connects a long collagenous region to a globular region (Kishore et al., 2006). SP-A and SP-B along with endogenous surfactant are involved in the formation of tubular myelin (Goerke, 1998).

The membrane associated SP-B is a 79 amino acid peptide weighing almost a 17.4- kDa (Zaltash et al., 2000, Johansson and Curstedt, 1997). Sp-B has a direct impact on the respiratory physiology and absence of it can result in lethal respiratory failure in deficient individuals (Melton et al., 2003). SP-B is mainly found in a dimeric state, where monomers are linked through three intrachain and one interchain disulphide linkages (Zaltash et al., 2000).

The highly hydrophobic SP-C is expressed by alveolar type II cells (Griese, 1999). SP-C is a 35 amino acid, valine rich lipopeptide (Gustafsson et al., 1997). The structure of SP-C mainly consists of a rigid 3.7 nm long alpha helix and a 2.3 nm central aliphatic domain, which is attached to the alpha helix (Johansson and Curstedt, 1997). Two palmitoyl chains are also linked to the N-terminus of SP-C via thio-ester bonds, allowing it to incorporate into the phospholipid monolayer (Gustafsson et al., 1997). The main function of SP-C is to facilitate the spreading of surfactant at the air/water interface (Pinto et al., 1995). SP-B is required for the full processing of SP-C and absence of SP-C is associated with severe respiratory diseases (Glasser et al., 2003).

Hydrophilic SP-D surfactant protein weighs almost 43 kDa as a monomer (Zhang et al., 2001). Electron microscopy shows that the native SP-D consists of 12 monomers forming four homologous trimers stabilised by interchain disulfide bonds (Zhang et al.,

2001). The four trimers are directly linked to the long collagen-like regions forming a cross shaped molecule with a width of approximately 92 nm (Griese, 1999). SP-D has an immunological role, but has no surfactant function. It has specific binding sites for macrophages and bacterial lipopolysaccharide and modulates the chemotaxis and oxidative bursts of macrophages and opsonizes various micro-organisms for easier phagocytosis (Griese, 1999).

To summarise, pulmonary surfactant proteins play an important role in vital respiratory process in humans. However, these proteins rely mostly on their exposed amphiphilicity for their function and play a crucial role in organising lipids at the interface. It is the lipid rich surfactant mixture, which goes on to decrease the surface tension at the interface rather than the proteins themselves. Thus these proteins can be considered as mediators rather than the principal surfactants.

1.4 Hydrophobins

Another type of amphiphilic surfactant protein that has been studied in detail is the hydrophobin family. Hydrophobins are a group of surface active proteins that are secreted by filamentous fungi. Hydrophobins are known to fulfil many important functions in fungal physiology, forming surface coatings for protection against desiccation and wetting, and reducing the surface tension of water to allow growth of aerial structures including hyphae and spores (Linder et al., 2005).

Hydrophobins are small proteins of about 100 amino acids and 10 kDa in size. They have four disulphide bridges formed by eight conserved cysteine residues (Hou et al., 2009). Hydrophobins are divided into two classes (class I and II) based on differences in hydrophathy pattern and biophysical properties. Both types self-assemble into an amphipathic film at a hydrophilic–hydrophobic interface. The protein aggregates of class I hydrophobins are more stable. They resist boiling in detergent and can only be dissolved in strong acids such as trifluoroacetic acid (TFA) and formic acid. In contrast, class II aggregates are less stable and can be dissolved using aqueous dilutions of organic solvents (Bonazza et al., 2015, Hou et al., 2009).

Upon self-assembling at an interface, hydrophobins can very effectively invert the polarity of the surface. The N-terminal part determines wettability of the hydrophilic side of the assemblage (Hou et al., 2009). Class I hydrophobins self-assemble at interfaces into a monolayer of highly ordered mosaic ultrastructure of 10 nm wide rodlets (Wosten and de Vocht, 2000), which share some structural similarity to amyloid-like fibrils. By

contrast, class II hydrophobins lack fibrillar structure, but form films with a hexagonal structure and distinct repeating units (Paananen et al., 2003). Both the class of hydrophobins exist in an initial soluble state (monomeric for class I, and dimeric or tetrameric for class II) and transform to the final beta-sheet state, in which they are insoluble in water (Wosten and de Vocht, 2000, Meister et al., 2016). Their actions result in the formation of different types of highly ordered coatings, as mentioned earlier.

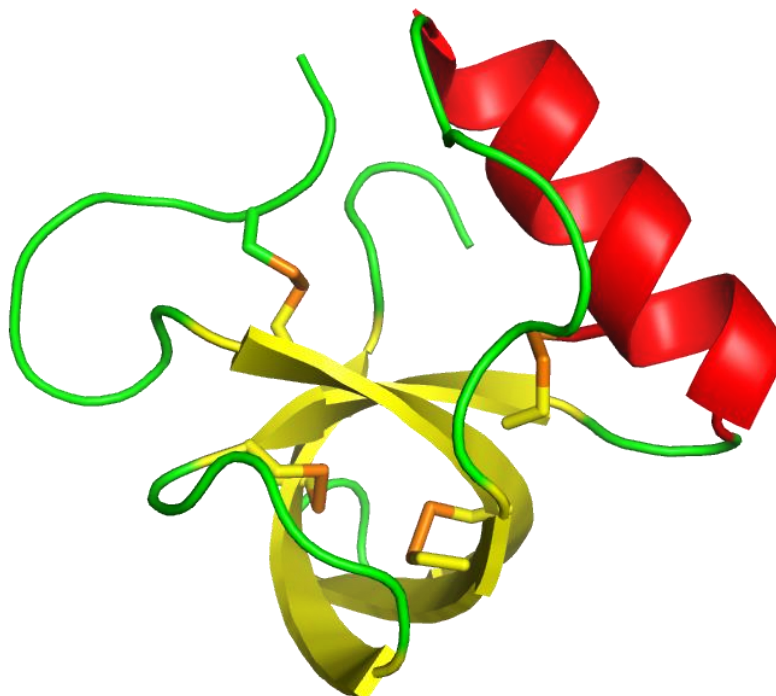


Figure 1-4 Cartoon representation of the crystal structure of a hydrophobin class II monomer showing four symmetrically arranged disulphide bridges in yellow and orange, with the α -helix shown in red and the strands of the β -barrel in yellow. Diagram was created from PDB file 2b97 using PyMOL software (Hakanpää et al., 2006).

The first crystal structure of a class II hydrophobin from *Trichoderma reesei* was solved at 1.0 Å resolution revealing that this globular protein is made up of a central β -barrel structure, consisting of two β -hairpins, and one short α -helix (Hakanpää et al., 2004). Hydrophobin exhibits a novel fold, which is as shown in Figure 1-4.

Hydrophobin exposes about half of its hydrophobic aliphatic residues to the surface, unlike most soluble proteins, and has a hydrophobic residues in the core that stabilises the structure (Linder et al., 2005). The disulphide bridges formed by cysteine residues provide further stabilization, and ensure that the protein will remain globular. To contrast,

other protein surfactant like Rsn2, Latherin/SPLUNC1 (discussed later in detail) also contain a disulphide each, but are not as topologically constrained by them.

The unique properties of the hydrophobins have been appreciated and applied in numerous roles including: biomedical applications, fusion partners for protein purification and anti-fouling agents (Wösten and Scholtmeijer, 2015).

1.5 Biofilm Surface Layer Protein A

Bacillus subtilis is a gram-positive bacterium dwelling in soil. The bacteria often aggregate to form a community of individuals referred to as a biofilm (Ostrowski et al., 2011). This biofilm provides resistance to liquid wetting. Studies have shown that the surface topology of biofilms plays a vital role in water repellence (Epstein et al., 2011, Ostrowski et al., 2011). Further investigation has shown that in *B. subtilis*, a biofilm surface layer protein A (BslA1) is the main contributor for repellence to surface wetting (Kobayashi and Iwano, 2012). BslA1 is a surfactant protein that forms a hydrophobic coating outside of the biofilm matrix, and is therefore referred to as bacterial raincoat (Hofer, 2013).

Structure of BslA1 was recently solved using X-ray crystallography and its fold revealed that BslA1 belongs to a member of the immunoglobulin superfamily. The structure of BslA1 consists of one 3_{10} -helix and two β -sheets, one four stranded and one three stranded, stacked together. Linked to this main scaffold is a highly hydrophobic “cap” β -sheet region, comprising three short β -strands (Hofer, 2013). The crystal structure revealed two forms of the protein, one in which hydrophobic amino acids of the cap region are buried within the structure, which allows the protein to be monomeric in aqueous solution. The alternative conformation is believed to reveal what happens when BslA1 is at an air-water interface. The protein undergoes a limited conformational change, exposing the hydrophobic amino acids of the cap region to the hydrophobic surface and can then self-assemble into an ordered 2D rectangular lattice that stabilizes the interface (Bromley et al., 2015, Brandani et al., 2015).

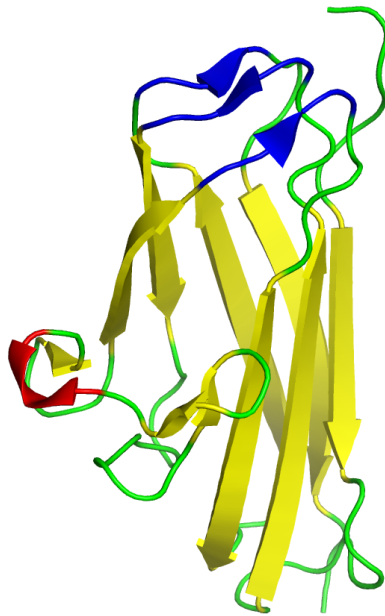


Figure 1-5 Cartoon diagram showing structure of BslA1 determined by X-ray crystallography coloured red for α -helix and yellow for β -strand. The cap region, made up of three β -strands, is highlighted using blue colour. Image created from PDB file 4bhu using PyMOL software (Hobley et al., 2013b)

The importance of the “cap” region residues was confirmed by replacing individual leucines with lysine residues in the centre of the cap. The resulting disruption in the formation of the 2D lattice suggests that leucine residues are involved in inter-monomer interactions. Thus proving the importance of the hydrophobic residues in cap region needed for interfacial stabilization of biofilms (Hobley, 2013).

1.6 Latherin and SPLUNC1

Latherin is a surfactant protein, identified from the sweat and saliva of horses and other equine species. It is believed to play a vital role in the process of evaporative cooling by wetting the waterproofed pelt (McDonald et al., 2009). Like humans, horses regulate their body temperature by sweating, but equine sweat has low salt and high protein (5-10 g/L) content compared with that of humans. The horse sweat gets readily converted into foam and this foaming property is attributed to latherin, a surfactant protein. Even at low concentrations, latherin has the ability to reduce water surface tension. (Eckersall et al., 1982, McDonald et al., 2009).

Latherin, a 22.6kDa protein, is acidic and has a pI of 4.11 (McDonald et al., 2009). Latherin is composed of 228 amino acids and is exceptionally rich in leucine residues (Vance et al., 2014).

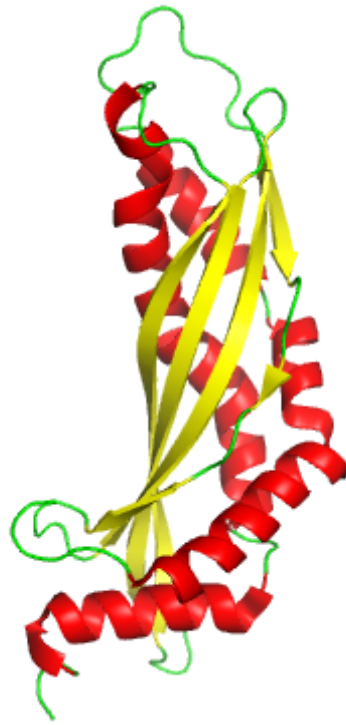


Figure 1-6 Cartoon diagram showing solution structure of latherin coloured red for α -helix and yellow for β -sheet. Image created from PDB file 3ZPM using PyMOL software (Vance et al., 2013a)

Latherin is monomeric in solution and displays an approximately cylindrical-shaped structure, as determined by NMR spectroscopy (Figure 1-6). Latherin's structure consists of a four stranded β -sheet, two antiparallel α -helices, and two flexible, leucine-rich loops at one end. Like most globular proteins, latherin has a hydrophobic core and displays no obvious signs of being particularly amphiphilic (Vance et al., 2013a).

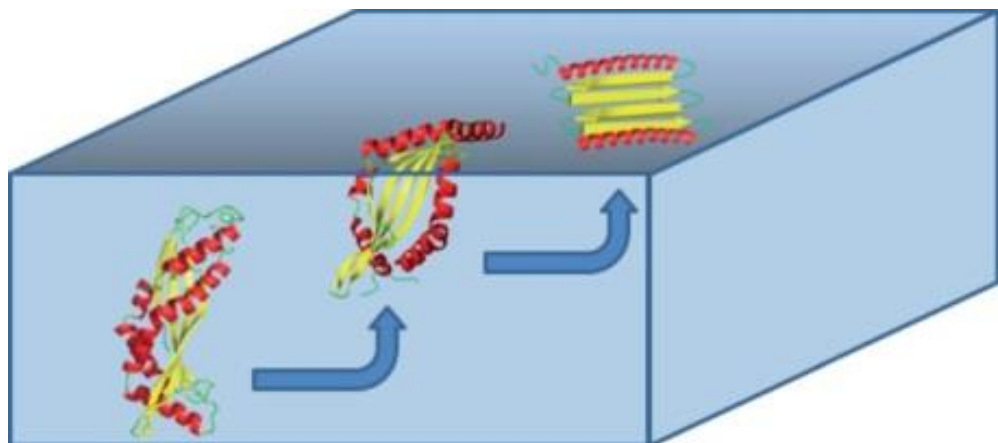


Figure 1-7 Model showing different stages of Latherin unfolding from globular solution state to planar conformation state at an air : water interface. Taken from (Vance et al., 2013a).

During interfacial association, latherin is proposed to undergo major conformational changes as shown in Figure 1-7. This is backed by the neutron-reflection measurements data, which show that latherin adsorbs at the interface forming a 1 nm thick monolayer

(Kennedy, 2011). Initial interfacial recognition is thought to be driven by the leucine rich flexible loops followed by opening of the two helices into a planar conformation, in which its hydrophobic core is exposed to the interface, retaining its secondary structure (Vance et al., 2013a).

The conserved amino acid sequence of latherin belongs to a family of the palate, lung, and nasal epithelium clone (PLUNC) proteins (Kennedy, 2011). PLUNCs are the group of hydrophobic proteins with a pair of highly conserved cysteines and are encoded by sequential genes present on chromosome 20 (Gakhar et al., 2010, Bingle et al., 2004). PLUNCs have a role in host defence system and have been shown to be bactericidal to a number of bacteria including *Pseudomonas aeruginosa* and *Mycoplasma pneumoniae* (Di, 2011, Britto and Cohn, 2015).

SPLUNC1, also known as Human short PLUNC, is a member of the PLUNC family (Garcia-Caballero et al., 2009). SPLUNC1 has been found to be present in human respiratory system, mammalian salivary glands and oral cavities (Tarran and Redinbo, 2014). SPLUNC1, a 237 amino acids protein, share high leucine composition and 28% sequence similarity with latherin (Kennedy, 2011).

SP-B and SP-C are the surface active proteins found in lungs but not in the upper respiratory tract, suggesting that a different surfactant molecule might be present. SPLUNC1, the most abundant secreted protein in the airways, is surface active at below physiological concentration in many assays (Gakhar et al., 2010).

The recently solved X-ray crystal structure of SPLUNC 1 shows that, a SPLUNC1 monomer consists of a central six-stranded antiparallel β -sheet, flanked by six α -helices. SPLUNC1 exhibits structural similarity to the Latherin and N-terminal half of BPI (bactericidal permeability increasing protein). Like latherin, SPLUNC1 is suggested to undergo a conformational change at an interface. (Garland et al., 2013).

Mutation of four leucine residues to alanine in α -helix (α 4) and/or addition of a disulphide mutation have inhibited bacteriostatic, surfactant, and LPS binding ability of the SPLUNC1 protein. Introduction of the disulphide bond is expected to restrict the conformational freedom of the protein and inhibited the SPLUNC1's ability to function. (Walton et al., 2016).

1.7 Ranaspumin2

The surface tension at an air–water interface is reduced by one of the component of Túngara frog foam nest, named Ranaspumin 2 (Rsn2). The remarkable features of this protein of being both surface active and biocompatible have formed the basis of this investigation.

1.7.1 Túngara frog

Túngara frog (*Engystomops pustulosus*; formerly known as *Physalaemus pustulosus*) (Figure 1-8) is one 650 of species belonging to the Leptodactylidae family (Ron et al., 2006). This frog is very commonly found in moist, lowland sites from South and Central America and the Caribbean (Weigt et al., 2005). The frog's skin has many small lesions (pustular), hence known as *pustulosus* (Ryan, 1985).



Figure 1-8 Foam nest production by mating male and female Engystomops pustulosus Image courtesy of Alan Cooper and Malcolm Kennedy.

Once a female has selected to mate with one of the calling males, the female frog carries the male in amplexus to a nesting spot, different from the calling site. There she lays a combination of eggs and foam precursor fluid. The male fertilises the eggs and whip up the fluid with their feet to make a foam nest for the eggs at the side of the pond (Ryan, 1980). The well-studied nesting process usually takes about an hour and results in formation of surface floating foam nest containing 100–200 eggs (Dalgetty and Kennedy, 2010). The foam nests are then left unattended for the remaining development from eggs to tadpoles. The eggs in the foam will hatch in two days giving rise to tadpoles. The tadpoles will survive by eating detritus in the water and will metamorphose in about 4 weeks. If the pool dries out, the tadpoles will congregate beneath the foam, where they

can survive for up to five days. Tadpoles are sexually mature after a few months (Ryan, 1985). At the point when tadpoles are ready to hatch, the foam dissolves allowing the tadpoles to escape into surrounding water.

1.7.2 Foam nest

The frog foam nest displays interesting biochemical and biophysical properties. They are also stable for up to 10 days (without eggs), although made up of foam is remarkable in itself. It can also maintain a stable environmental temperature and act as a mini-incubator for developing eggs and tadpoles. Being rich in carbohydrate, which naturally holds water, the nest resists evaporation in the tropical heat.

These foam nests are not only mechanically stable to physical handling, but are also flexible enough to adapt to various conformations. They are rich in carbohydrates and proteins, but are not vulnerable to predation. They have also developed a mechanism for resistance to microbial attack, but this is not due to the foaming surfactant causing cell membrane disruption, as the foams are compatible with the eggs and young embryos. This striking feature of biocompatibility along with surface activity has suggested many potential biomedical applications and further research.



Figure 1-9 Túngara frog foam nest with eggs seen as dots. Image courtesy of Prof Malcolm Kennedy.

1.7.3 Foam nests components

The túngara foam nests have a density of approximately 0.1 g/cm^3 . Analysis of the foam fluid components revealed that it is made up of 1–2 mg/ml of total protein and similar quantities of carbohydrate. There was an absence of fat and lipid, signifying a lack of any conventional small molecule surfactants. (Cooper and Kennedy, 2010). Further investigations resulted in discovery of six proteins, consequently named as “ranaspumins” (Latin: rana = frog; spuma = froth, foam).

Rsn1, an 11.4 kDa protein, belongs to the cystatin super family. It shows sequence similarity and fold similarity with the cystatins. Its exact function is unknown, but it is believed to function alongside Rsn2 to maintain surface activity of the bulk foam (Fleming et al., 2009).

Rsn2, an 11 kDa protein, is the main surfactant protein in the foam nest (Cooper et al., 2005). Rsn2 is discussed in detail in the next section 1.7.4.

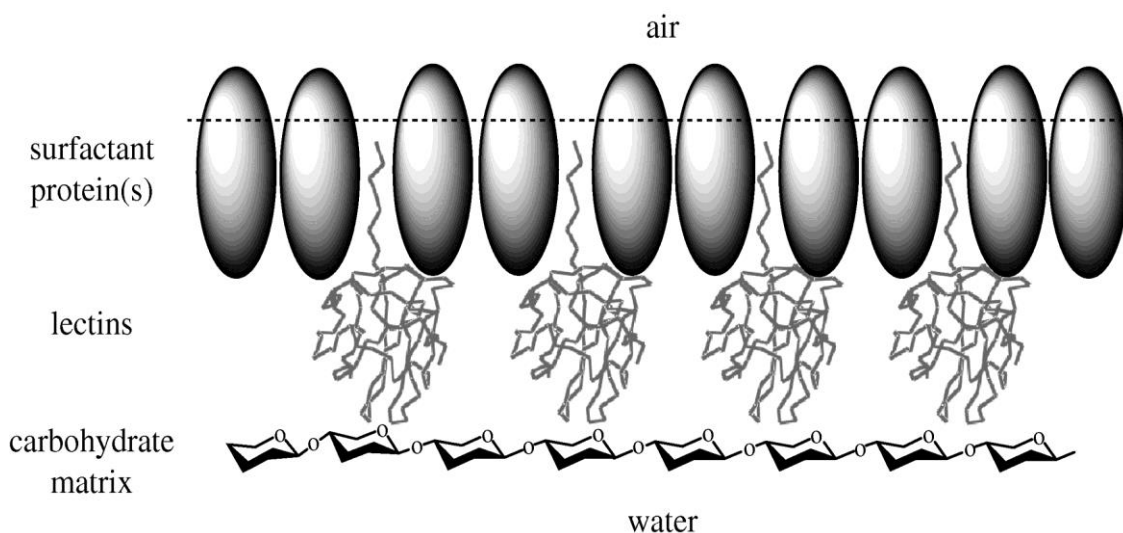


Figure 1-10 Cartoon representation of the frog foam nest components with their proposed role. (Fleming et al., 2009)

Rsn 3, 4, 5 & 6 fall in the range of 18-26 kDa in weight and have sequence similarities to the sugar binding, lectin family of proteins. Rsn6 is a galactose binding C-type lectin; whereas Rsn3, 4 & 5 are fucose binding F-type “fuclectins”. They may play a defensive role in protection of foam nest against microorganisms and insects like predators. Some of the lectins bind to target sugars on the surface of bacteria and decreases their ability to form aggregates. The agglutination activity of lectins has been shown to upset the gut of insects, perhaps discouraging them from using foam as a food (Cooper and Kennedy, 2010, Fleming et al., 2009). The lectin's sugar binding site is hypothesized to interact with the carbohydrates and provide mechanical resilience to the foam.

1.7.4 Ranaspumin2

Ranaspumin 2 (Rsn2) is a small, moderately surfactant protein secreted by female túngara frog (Kennedy, 2011). Rsn2 is rich in polar amino acids like lysine and aspartic acid, and has acidic pI of 5.16 (Fleming et al., 2009). At the C-terminus, Rsn2 displays unusual amino acid sequence where 6 out of its 21 aspartic acid residues are found consecutively, making the C-terminal region highly negatively charged.

Rsn2's monomeric solution structure was solved using NMR spectroscopy (Mackenzie et al., 2009). The structure of Rsn2 consists of a four stranded antiparallel β -sheet and a kinked α -helix lying perpendicular to the β -sheet. A disulphide bond links the third and fourth strands of the β -sheet, while the hydrophobic N-terminus and hydrophilic C-terminus remain mostly disordered. Rsn2 exhibits a cystatin-like fold but cystatin protease inhibitor activity has not been detected (Mackenzie et al., 2009).

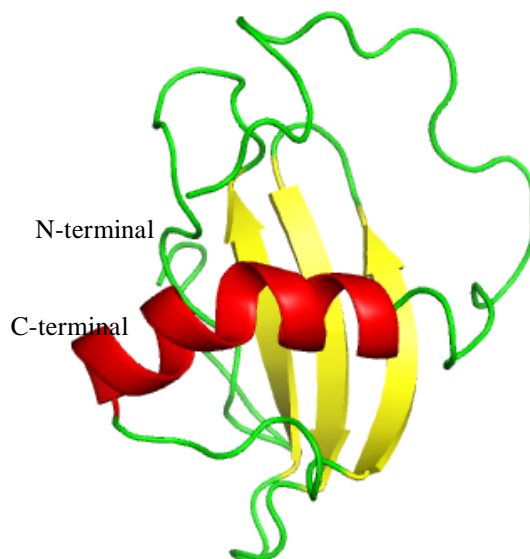


Figure 1-11 Cartoon diagram showing solution structure of Rsn2 coloured red for α -helix and yellow for β -sheet. Image created from PDB file 2WGO using PyMOL software (Mackenzie et al., 2009).

Rsn2 is monomeric in solution and its structure does not obviously establish it as an amphipathic protein. It has been hypothesised, based on the neutron reflectivity data, that Rsn2 needs to undergo a conformational change to enable its interfacially active. It has been proposed that Rsn2 might undergo a clamshell-like opening when it approaches the interface (Mackenzie et al., 2009).

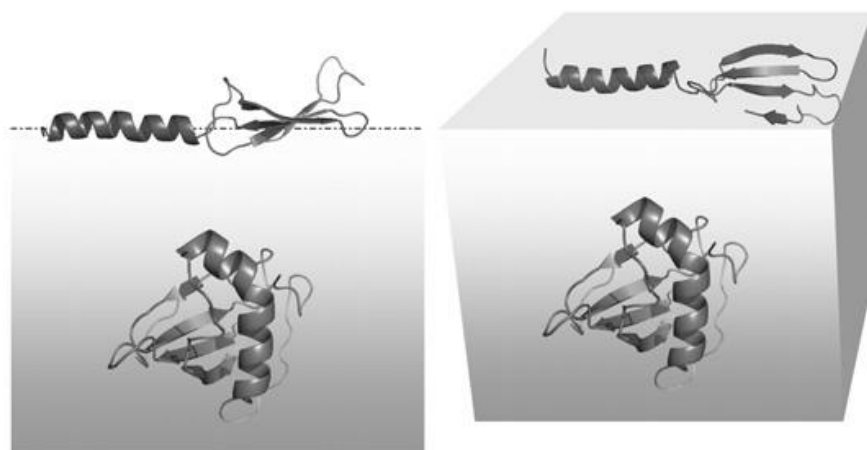


Figure 1-12 Cartoon diagram showing the hypothesised open Rsn2 structure at the air –water interface and the closed globular form in solution (Mackenzie et al., 2009).

Further investigation using coarse-grained molecular dynamics simulations showed that interfacial adsorption of Rsn2 is a two-step process. The initial interaction with an interface is made by the flexible N-terminal tail, which is followed by a conformational change in which the helix ‘unhinges’ from the β -sheet exposing its hydrophobic core. Thus aligning the hydrophilic exterior in one plane, directed into the water, and retaining its secondary structure (Morris et al., 2016). The infrared reflection absorption spectroscopy (IRRAS) data and the Neutron-scattering data confirm that this is the case (Mackenzie et al., 2009).

1.8 Comparison of the different surfactant proteins

The foremost difference between the non-lipid-associated globular surfactant proteins, described earlier in this chapter is the diversity in their origin. Proteins with intrinsic surfactant activity are produced by organisms ranging from single-cell prokaryotes to mammals, in each case supporting a different biological function.

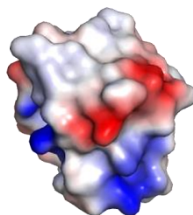
Even though they have similar surfactant properties, none of the proteins show a similarity in their structure, nor do they have any obviously conserved amino acid sequence. Even the mechanism of action by which they interact at the interface is different, as mentioned earlier in each respective protein section.

Although all surfactant proteins are ultimately amphipathic in nature, not all proteins have amphiphilic surface charge in their “native” conformation (Figure 1-13). Proteins like hydrophobin and BslA1 have patches of polar and non-polar regions, while Rsn2 and latherin have predominantly polar surfaces similar to the majority of globular proteins (Hakanpää et al., 2004, Mackenzie et al., 2009, Vance et al., 2013a). The later rely on their ability to undergo conformational change to expose the core hydrophobic residues to interact at the interface (Mackenzie et al., 2009, Vance et al., 2013a). In contrast hydrophobin and BslA1 rely on their ability to generate a surface active film via intermolecular association (Meister et al., 2016, Hogley et al., 2013b). Unlike hydrophobin, BslA1 also undergoes a small conformational change in the cap region to make hydrophobic interactions (Hogley et al., 2015).

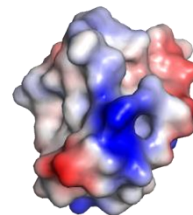
A1



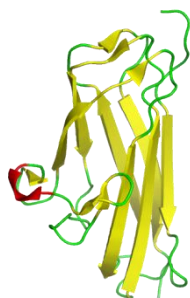
A2



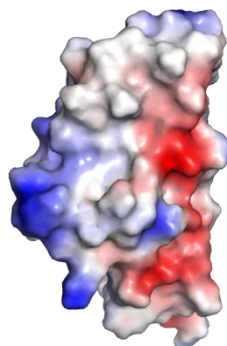
A3



B1



B2



B3

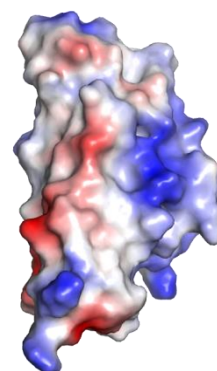


Figure 1-13 A comparison of the surfactant proteins hydrophobin II (A) and BslA1 (B) is shown. The cartoon figures (A1 and B1) represent the structure of each protein with α -helices shown in red, β -strands in yellow and loops in green. The surface charge of the proteins are represented in figures (A2, A3, B2, B3) by red for negative electrostatic potential, blue for positive and grey for neutral, where the panels 2 and 3 show opposite faces of proteins. All the surface charge figures are contoured to same range of potentials (-80 to +80) and the proteins are shown at the same scale.

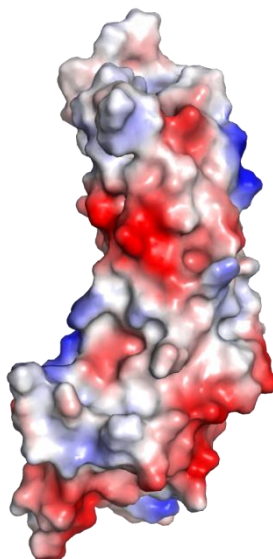
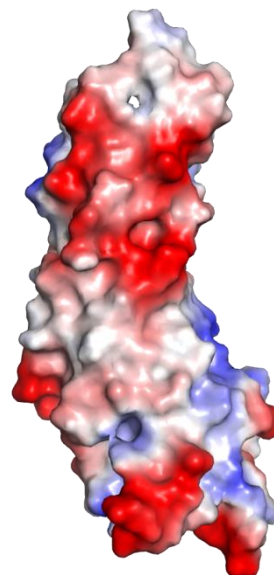
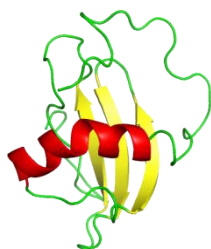
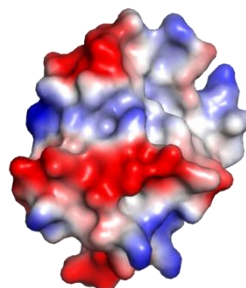
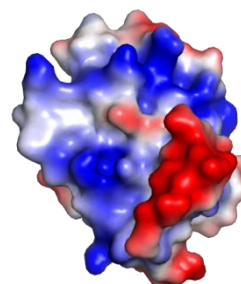
C1***C2******C3******D1******D2******D3***

Figure 1-14 A comparison of the surfactant protein latherin (C) and Rsn2 (D) is shown. The cartoon figures (C1 and D1) represent the structure of each protein with α -helices shown in red, β -strands in yellow and loops in green. The surface charge of the proteins are represented in figures (C2, C3, D2, D3) by red for negative electrostatic potential, blue for positive and grey for neutral, where the panels 2 and 3 show opposite faces of proteins. All the surface charge figures are contoured to same range of potentials (-80 to + 80) and the proteins are shown at the same scale.

Among the globular surfactants, hydrophobins are the strongest surfactant followed by BslA1, and then by latherin and Rsn2. Rsn2 and latherin are considered moderate surfactant proteins. This comparison is made on the basis of the final interfacial surface tension obtained after the action of the surfactant proteins, which for hydrophobin is $20 \text{ mN}\cdot\text{m}^{-1}$, compared to $50 \text{ mN}\cdot\text{m}^{-1}$ for Rsn2 (table1-2). The aim of this work is to apply the surfactant and biocompatible property of Rsn2, for various cell based biological applications.

<i>Surfactant protein</i>	<i>Final Interfacial surface tension</i>	<i>Reference</i>
<i>Hydrophobin (class II)</i>	$20 \text{ mN}\cdot\text{m}^{-1}$	<i>(Alexandrov et al., 2012)</i>
<i>BslA1</i>	$27 \text{ mN}\cdot\text{m}^{-1}$	<i>(Bonmatin et al., 1994)</i>
<i>Latherin</i>	$43 \text{ mN}\cdot\text{m}^{-1}$	<i>(Vance, 2012)</i>
<i>Rsn2</i>	$50 \text{ mN}\cdot\text{m}^{-1}$	<i>(Morris et al., 2016)</i>

Table 1-2 Final reduction in surface tension by the action of surfactant proteins. Final interfacial surface tension measurements for Hydrophobins, BslA1 and Rsn2 were made using pendant drop method; while microtrough tensiometer was used for Latherin. Note – The final interfacial surface tension value gives an estimate for comparison among the surfactant proteins. The method used, along with time and protein concentration required to reduce the interfacial surface tension are not the same in every instance, so some minor difference is expected in the values .

1.9 Aims

The aim of this project was to use the unique features of Rsn2 protein to develop various biotechnological applications with a particular focus on cell engineering.

The project developed along four main themes: approaches for cell patterning by controlling cell adhesion on surfaces that do not otherwise support cell adhesion; analysis of bone cell growth on surfaces coated with integrin binding sequence-Rsn2 fusion proteins; production of Rsn2 stabilised droplet emulsions; and, a method to solubilise C60 (Fullerene). These will each be described in the subsequent chapters.

2 Cell patterning with Rsn2

2.1 Introduction

For many tissue engineering approaches, cells are seeded into scaffolds that support subsequent tissue formation. A range of scaffolds that have desirable mechanical properties are available, but most of them are hydrophobic (non-wettable) polymer to which cells have difficulty attaching (Chan and Leong, 2008a). Thus there is a need to engineer a material surface to promote cell adhesion and enhance tissue function.

The factors that influence cell-adhesiveness to the surface materials are of significant interest in the bioengineering of complex tissues. Many approaches have been tested, including modifying the chemical and topographical properties of the surfaces to enhance cell adhesion. These alterations in the physicochemical properties of the material surface will influence protein adsorption and thereby cell adhesion (Welle et al., 2014). Cell adhesion is mediated by cell adhesion molecules like cadherins and integrins. Modification of the material surface to enhance cell adhesion is described in detail in section 3.1 of this thesis.

The interaction of living cells with a scaffold material is mediated through the integrin receptors, which will interact with the protein film deposited on the material surface. This provides an opportunity to guide cell attachment and development by controlling the pattern of protein deposition. Cell patterning provides a useful tool for research in overcoming the limitation of conventional cell culture techniques. Even cell patterning has some limitations, such as having only two dimensions, though research is underway to develop 3D scaffolds, but it brings us a step closer to tissue engineering.

Patterns of proteins and cells have been generated using photolithographic, soft lithographic, micro-contact printing, Inkjet printing and dip coating techniques. A brief overview of these widely used patterning techniques is follows.

Kleinfeld and colleagues used the photolithography process from electronics and created new methods for cell patterning (Kam et al., 2013). Photolithography works on the principle that when radiation is applied to the photoresist material layered on a master, only the photoresist to which radiation is applied becomes soluble in particular solvents, which depends on the type of the photoresist used. Thus a pattern is developed by washing the soluble photoresist with a solvent and leaving the insoluble photoresist intact. This method can be used to create patterns on substrate with features at the precision of submicron level (less than 100 nm) (Nie and Kumacheva, 2008). This

method is one of the most popular methods for patterning cells and proteins. Although this method is highly reproducible, it requires specialised equipment and clean room facilities for producing the substrate along with being laborious and expensive. Soft lithography, a modified version of lithography, is a versatile technique for generating patterns of proteins and cells.

Soft lithography, initially developed by Whitesides and colleagues, are so called because they involve production of a stamp, mould or mask made from a soft elastomeric material by means of lithography. (Qin et al., 2010a). This elastomeric stamp can be used to copy patterns on to another material through surface direct printing, position limited adsorption, or masking. Typically poly(dimethylsiloxane) (PDMS) is used as a soft elastomeric material of choice. This technique overcomes many limitations of photolithography and offer some advantages such as being inexpensive, being easy to develop, having the ability to pattern a variety of substrates, and not requiring specialized equipment or chemicals (Ratner and Bryant, 2004). However, most of the soft lithography techniques are restricted to substrates such as gold, silver, or silicon, whereas for many applications, other substrates such as polymers are more desirable. To overcome this, micro-contact printing (μ CP) techniques have been developed.

In the μ CP approach, different patterns can be generated on a variety of substrate surfaces (James et al., 1996), including patterned self assembled monolayers (SAMs) (Kumar and Whitesides, 1993). μ CP has been used to generate patterns on different substrates and functionalised them using proteins, DNA as well as the organic thiol solutions used for gold functionalisation (Bernard et al., 2000, Hui et al., 2002)

Another method for delivering fine patterns using liquid "inks" is inkjet printing. In this method, cell-adhesive materials are used instead of ink to produce a patterned substrate. Inkjet printers are an alternative patterning technology that produces droplets of tens of microns in diameter, which are deposited onto a material surface, and develop into a pattern when the solvent evaporates (Cui et al., 2014, Cui et al., 2012) (Nie and Kumacheva, 2008). The inkjet printing technique offers advantages of being cost effective and, unlike for soft lithography, it is easy to change the pattern from one printed item to another at a resolution of 1,400 dpi in 3D (Cui et al., 2014)

Some other proteins and peptides, like hydrophobins and polydopamine (PDA), have been used for cell patterning. Like Rsn2, hydrophobins and PDA can be used to make proteinaceous coatings on the polymer surface and render them biocompatible (Janssen

et al., 2002a, Huang et al., 2016). Thus different proteins have been tested in the past to promote cell adhesion. This chapter will focus on the development of patterned scaffolds using a naturally surfactant protein, Rsn2.

As described earlier in section 1.7.4, Rsn2 was identified as one of the foam nest components of the *Túngara* frog (Fleming et al., 2009). The foam protein from these nests showed significant surfactant properties while retaining biocompatibility with fertilized eggs, sperms and young embryos (Cooper and Kennedy, 2010). It is unusual for a protein to be highly surfactant and this feature of the Rsn2 protein was used to develop approaches to pattern hydrophobic surfaces thereby directing cell adhesion.

It was hypothesized that the use of Rsn2 was expected to be beneficial compared to other patterning techniques because of the removal of any need for chemical treatment.

Cell patterning is a process to control the spatial position of the cells onto a substrate. In this chapter, the cell patterning is obtained by dip coating Rsn2 protein onto the surface and seeding it with cells. Strictly speaking, this is more of controlling cell adhesion onto a large surface area and not forming fine cell patterning in microns.

2.2 Aim

The aim of the project was to develop a set of tools that allow cell patterning on a range of hydrophobic scaffolds.

2.3 Methods and Materials

2.3.1 Rsn2 production

Recombinant Rsn2 and iLOVRsn2 expression constructs (generated by Dr S.J. Vance) were utilised for Rsn2 and iLOVRsn2 expression and purification.

2.3.1.1 Protein Expression

Rsn2 and iLOVRsn2 were expressed using Novagen's pET28 expression system. The strong bacteriophage T7 promoter has the control of the gene cloned into a pET plasmid. This has an advantage over host transcription as T7 RNA polymerase is selective and much more active as compared to its host counterpart. Basal expression is inhibited by a Lac repressor binding sequence incorporated in the promoter assisted by expression of lac repressor protein. This control element regulates expression of both the target gene and the T7 polymerase gene integrated into the host genome. Once induced using the lactose analog, isopropyl β -D-1-thiogalactopyranoside (IPTG), almost all of the host cell's resources are transferred towards the target gene expression. As a result, high levels of expression of the desired protein can be achieved in just a few hours after induction. Also, it is possible to modulate the expression level by varying the concentration of IPTG, which can help to optimise the soluble yield of target protein (Rosano and Ceccarelli, 2014).

2.3.1.1.1 Transformation

Competent *E.Coli.* were transformed with a pET28(b) based, kanamycin resistant expression vector carrying the coding sequence for Rsn2 expressed as a fusion protein with a thrombin cleavable N-terminal 6-His tag. Plasmid was incubated with chemically competent BL21 (DE3) cells (Novagen) for 30 minutes on ice. The mixture was then heat-shocked at 42°C for 30 seconds and immediately returned to ice. Transformed cells were grown in SOC media for 1 hour and were spread on LB plates containing kanamycin. Plates were then incubated overnight at 37°C.

2.3.1.1.2 Protein Production

Overnight cultures were set up and used at 1:100 dilutions to seed 8 × 500 mL LB broth in 2 L conical flasks. The 500 mL cultures were incubated with shaking (200 rpm) at 37°C until the OD₆₀₀ reached 0.6-0.8. The cells were then induced using IPTG at a final concentration of 1 mM and were incubated for a further 3 hrs. Cells were harvested by centrifugation at 4°C for 25 minutes. The supernatant was discarded and the cells were

re-suspended in 20 mL of binding buffer (20 mM Tris, 500 mM NaCl, 5 mM Imidazole, pH 8) for 4 L of culture.

2.3.1.2 Protein Purification

The process of Rsn2 and iLOVRsn2 purification can be divided into three key steps: cell lysis and insoluble cell debris removal; Ni²⁺-affinity chromatography; and analysis using SDS-PAGE.

2.3.1.2.1 Cell Lysis and Insoluble Cell Debris Removal

Two methods were assessed for cell lysis, namely detergent lysis and sonication. The test expression using detergent solution (Bugbuster, Novagen) for cell lysis resulted in a greater proportion of target protein being seen in the insoluble fraction. Thus sonication was used for cell lysis in large scale expressions, which gave less insoluble target protein. A plausible explanation for the difference between the lysis methods is that the amphiphilic nature of the detergent causes denaturation of protein resulting in aggregation. Thus sonication was deemed acceptable for cell lysis.

For sonication, 500 U Benzonase (Novagen) and an EDTA free protease inhibitor tablet (Roche) were added to the re-suspended bacterial pellets and sonicated on ice at 10 microns amplitude for 15 cycles of 30 seconds on and 30 seconds off.

Following sonication, insoluble cell debris was removed by high speed centrifugation at 40,000 g for 25 minutes and careful decanting of the supernatant. The supernatant was filtered using 0.2 µm filter leaving a solution containing the protein of interest along with the remaining soluble cell components.

2.3.1.2.2 Ni²⁺-Affinity Chromatography

Rsn2 and iLOVRsn2 fusion proteins were expressed with six consecutive histidine residues at the N-terminus and purified using metal chelation chromatography (Ni²⁺ bound within a nitrilotriacetic acid (Ni²⁺-NTA) column). Ni²⁺-affinity chromatography was chosen for protein purification because of its simplicity and reliability (Bornhorst and Falke, 2000).

The cleared lysate was passed through an Econo pack (BioRad) column loaded with 5 x ml bed of Ni-NTA His-bind Super flow (Novagen), previously equilibrated with binding buffer. The flow through was collected and the column washed with binding buffer containing 5 mM imidazole. The poly-histidine fusion tag (His-tag) protein sequence binds to Ni²⁺ ions, which are immobilized on the Ni-NTA Resin (Bornhorst and Falke,

2000, Khan et al., 2006). Non-specific binding via electrostatic interactions was inhibited by the presence of NaCl in the buffer. The column was then washed with wash buffer (20 mM Tris, 500 mM NaCl, 25 mM Imidazole, pH 8) containing 25 mM imidazole to remove weakly bound proteins. This was followed by elution in buffer containing a high concentration of imidazole (300 mM), which displaces the bound histidines. Finally a 1 M imidazole wash was applied to ensure that the column was clean before re-equilibration in binding buffer.

2.3.1.2.3 SDS-PAGE

The success of the protein purification was determined by SDS-PAGE (sodium dodecyl sulphate polyacrylamide gel electrophoresis). The underlying principle is to use an electric field to displace charged protein-SDS complexes through a porous matrix and separating them on the basis of their molecular weight.

The lysate and flow through samples were diluted to a final volume (in μl) which was 150 times the OD_{600} at harvest to ensure even loading of the gel. The samples were mixed with SDS-PAGE loading buffer and then heated at 85°C for ten minutes before loading on the gel. SDS was added to mask protein intrinsic charge and to impart negative charge to the protein, generating unfolded proteins into linear chain depending on its size. Glycerol was added to render density to the loading sample and the bromophenol blue to track the electrophoresis progress of the gel. Upon application of electric voltage, the proteins will get separated based on their size by a sieving mechanism. Gels were then stained with Coomassie Brilliant Blue Stain and destained in 'Coomassie Destain Solution' (70% distilled H_2O , 15% CH_3OH and 15% CH_3COOH) to visualise the protein bands.

2.3.2 Pendant drop tensiometry

The purified Rsn2 proteins were assessed for functionality by evaluating their surface activity by pendant drop measurement. Rsn2, being a surfactant protein, should act on the air-water/air-oil interface and reduce the surface tension and so affect the shape of the pendant shaped droplet formed during the experiment.

Pendant drop experiments were performed on a Krüss EasyDrop tensiometer. Rsn2 was diluted in MilliQ water and immediately placed in a syringe with a needle diameter of 1.83 mm. Images of the pendant drop were captured by a CCD camera and their shapes fitted to the Young-Laplace equation using Krüss software to determine the interfacial tension.

2.3.3 Wettability

The effect on the wettability of surfaces coated with Rsn2 was assessed using an environmental scanning electron microscope (ESEM) by observing the formation of microscopic water droplets on samples in an environment held at 100% relative humidity (RH).

Glass coverslips to be used were thoroughly cleaned with concentrated nitric acid, rinsed twice with distilled water and dried overnight. Hydrophobic surfaces were prepared by dipping only half of the coverslip in silanizing reagent (dimethyldichlorosilane) for 5 minutes and again drying overnight. Only the silanized half of the coverslip was dipped in 1 mg/ml of Rsn2. Any excess Rsn2 was removed by dipping in distilled water twice before subjecting to ESEM.

Then the images of Rsn2 coated and non-coated surface were taken after 30, 70 & 120 minutes. The obtained ESEM images were subjected to ImageJ analysis to calculate the percentage of the area covered by water droplets on coated and non-coated surfaces.

2.3.4 Contact Angle

Contact angle measurements were performed by dip coating half of a clean glass slide with protein sample (1 mg/ml). Any excess Rsn2 was removed by dipping in distilled water twice and air drying before subjecting to water contact angle measurements. Then water drops of uniform volumes of 20 μ L were transferred onto a half coated glass slide and the contact angle of each droplet measured at room temperature. Contact angle measurements were carried out using the sessile drop technique with a KSV CAM 100 contact angle goniometer (KSV Instruments, USA) on Rsn2 coated and non-coated surfaces. High contrast images of static water droplets were recorded and CAM 100 software was used to determine the water contact angle.

Similarly to assess relative hydrophobicity, water contact angle was measured on a range of materials including silanized glass, polycarbonate (PC), polytetrafluoroethylene (PTFE), poly(methyl methacrylate) (PMMA), Nylon, polystyrene (PS), polypropylene (PP), ACLAR and polydimethylsiloxane (PDMS). Contact angle measurements were made on the Rsn2 coated and non-coated surfaces for each material. Mean and standard deviation were calculated using data from three set of experiments.

2.3.5 Persistence

Fluorescence from the FMN of the iLOV fusion protein in iLOVRsn2 was used to check the longevity of Rsn2 coating on a range of hydrophobic surfaces. All the surfaces used were cleaned with 70% ethanol and then rinsed twice with water. Thereafter fluorescent iLOV-Rsn2 protein (1 mg/ml) was applied onto each material surface and incubated for one minute. Excess protein was removed by extensive, rapid rinsing with water. The protein-coated material was incubated in PBS at 37°C and fluorescence microscopy was carried out every day for 10 days. The range of materials tested in this experiment were – ACLAR (Agar scientific Ltd.), silanized glass, Nescofilm™, nylon (Good Fellow, Ltd.), polycarbonate (PC) (Good Fellow, Ltd.), polydimethylsiloxane (PDMS), Polymethyl methacrylate (PMMA) (Good Fellow, Ltd.), polypropylene (PP) (Good Fellow, Ltd.) and polystyrene (PS) (Good Fellow, Ltd.).

To avoid the loss of fluorescence signal due to photobleaching, optimisation was done in order to find out the duration of exposure after which bleaching effects may occur. Once determined, all the samples were exposed under blue light for the same duration (400 nm, which is less than the time required for photobleaching), while keeping numerical aperture constant.

To calculate and eliminate the effects of fluctuations in the intensity of the light source, autofluorescence from the white filter paper (whatman lens cleaning tissue, GE healthcare) was used as a control along with neutral density filters (Zeiss). Fluorescence images of iLOVRsn2 coated and non-coated regions were exported to ImageJ to quantify the intensity of fluorescence. Obtained intensity of fluorescence were then normalised by dividing with the value of intensity obtained using filter-2 (% transmission = 53.6%).

While conducting fluorescence microscopy, background signals can affect the reliability and quality of the results, hence background signals were subtracted before making any quantifications using the formula, T (total signal) = Signal + Background.

2.3.6 Routine cell culture

Cell culture work was performed aseptically at room temperature using laminar flow cell culture hoods and cells were cultured in an incubator at 37°C under humidified conditions with ventilation of 5% CO₂. Cells were maintained in Dulbecco's Modified Eagle's Medium (DMEM) (PAA Laboratories) supplemented with 10% Foetal bovine serum (FBS, Invitrogen) and 1% penicillin and streptomycin (Sigma) unless otherwise stated

Fibroblast cell lines (h-TERT, Lonza, USA) were seeded into a 75 cm² (T-75) culture flask (BD Biosciences, San Jose, CA, USA) containing medium and incubated. After 48 hrs in culture, the non-adherent cells were discarded and cells were fed with fresh medium. Medium was replaced once a week. Cells were allowed to reach 70-80% confluence and then the cells were passaged. Briefly, the culture medium was aspirated and the cells washed in HEPES saline following which 5 ml trypsin was added (PAA Laboratories) and incubated at 37°C for 5 minutes. The action of trypsination was neutralised by adding 5 ml medium and a cell count was performed using a Neuber chamber. The cells were then seeded in a 150 cm² culture flask (BD Biosciences, San Jose, CA, USA) for sub culture.

2.3.7 Fabrication of PDMS

Polydimethylsiloxane (PDMS) was made by properly mixing PDMS 184 polymer solution 90% (Wt/Wt) (Sylgard® 184 Silicone Elastomer, Dow Corning, UK) with 10% (Wt/Wt) curing agent. The mixture was kept under vacuum for 30 minutes to de-gas it and remove any bubbles. The mixture was then transferred to a sterile petri dish and left to set overnight at 180°C. Solidified PDMS was treated with n-pentane to remove unbound DMS in order to remove the capacity for self-healing of the PDMS surface thus avoiding peeling off of the protein coat (Lee et al., 2003). PDMS casts were sterilised by washing in 70% alcohol followed by rinsing in sterile water twice. PDMS casts were then dried using sterile-filtered nitrogen gas in preparation for cell patterning experiments.

2.3.8 Cell Patterning

Cell culture substrates made of PDMS, PS and glass were rinsed with 70% alcohol to sterilise them and dried. Glass was further subjected to salinization, by adding a organofunctional alkoxy silane molecules to the surface of the glass, which will increase its hydrophobicity and cell selectivity. A pattern was developed on each substrate by dip coating half of each substrate with Rsn2 at a concentration of 1 mg/ml for 1 minute before rinsing with sterile PBS. A confluent flask of h-TERT cells was trypsinised and used to seed the substrates homogenously. Cells were incubated at 37°C for up to 72 hrs before fixing them with 4% formaldehyde and stained with coomassie blue. Cell density and cell surface area measurements were performed using ImageJ software. Paired T-test was used for significance analysis.

2.3.9 Fluorescence staining

Samples were washed with PBS and fixed with 10% v/v formaldehyde/PBS for 15 minutes at 37°C. Cells patterned were stained with 4', 6-diamidino-2-phenylindole (DAPI) mountant and visualised using Olympus fluorescence microscope at 10X magnification.

2.4 Results

2.4.1 Rsn2 and iLOVRsn2 production

Recombinant His-tagged Rsn2 proteins were produced in *E. coli* and purified to a high degree by Ni²⁺-affinity chromatography as seen in Figure 2-1. A good yield for Rsn2 (19.23 mg/L) and for iLOVRsn2 (7.5 mg/L) were obtained. A right size band appeared for both the protein as observed by SDS-PAGE.

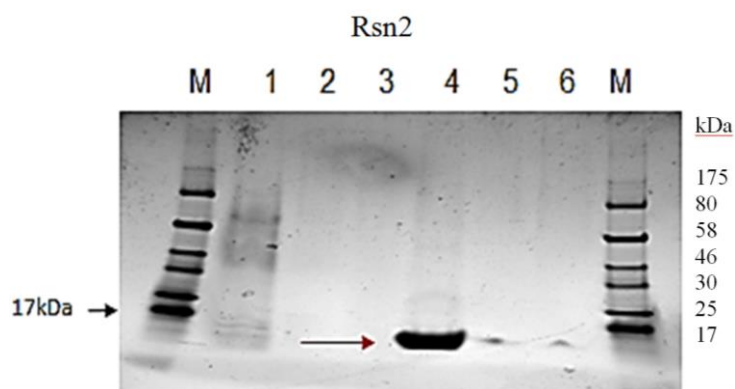


Figure 2-1 SDS PAGE of Rsn2 nickel affinity purification, (1) Cell lysate flow through; washes with (2)binding buffer and (3) wash buffer; (4 & 5) Elutions; (6) 1M imidazole and (M) Marker (NEB pre stained protein ladder). Mw of iLOVRsn2 is ~ 14 KDa, which is where the band is obtained in elution fraction.

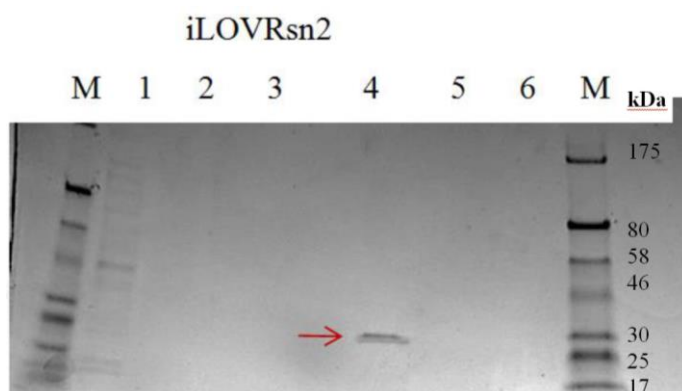


Figure 2-2 SDS PAGE of iLOVRsn2 Nickel affinity purification (1) Cell lysate flow through; washes with (2)binding buffer and (3) wash buffer; (4 & 5) Elutions; (6) 1M imidazole and (M) Marker (NEB pre stained protein ladder). Mw of iLOVRsn2 is ~ 27 KDa, which is where the band is obtained in elution fraction.

2.4.2 Pendant drop tensiometry

Pendant drop experiments were performed to explore the behaviour of Rsn2 at an air/water and oil/water interface. A droplet of Rsn2 (1.3 mg/ml) in low salt buffer was

formed in trioctanoyl glycerol to produce an oil-water interface. The obtained droplet was fitted using the Young-Laplace equation to estimate the surface tension,

$$\Delta p = \sigma \cdot \left(\frac{1}{r_1} + \frac{1}{r_2} \right)$$

where Δp stands for the pressure difference, r_1 and r_2 for the radii of curvature of the surface and the interfacial tension is calculated (KRUSS).

Rsn2 reduced the interfacial surface tension from the initial interfacial surface tension of 72 mN/m to 50 mN/m (Figure 2-4 A). The control, the interfacial surface tension of a droplet of buffer alone formed in trioctanoyl glycerol, also was 72 mN/m. This result of final interfacial surface tension is in close agreement with measurements of surface tension depression by Rsn2 measured by micro trough tensiometry (Vance, 2012).

To gain further insight into Rsn2's behaviour at the interface, the droplet was compressed after a curing time of 10 minutes. It was observed that upon compression of the droplet, transient wrinkles were formed (Figure 2-3), indicating that Rsn2 forms a film at the interface. The wrinkles in the film completely relaxed after 5 seconds indicating that this process of film formation is fully reversible. The observations of depression of the surface tension is similar to other surfactant protein such as hydrophobin (Szilvay et al., 2007) and BslA (Hobley et al., 2013a), confirming recombinant Rsn2 is a functional surfactant protein. Interestingly, the rapid resolution of the wrinkles for Rsn2 is in contrast to hydrophobins and BslA, whose wrinkles did not relax after 10 minutes (Bromley et al., 2015).

Wrinkles are a sign of hysteresis that is due to the interfacial structures being thermodynamically stable and therefore long-lived. This is because of the interactions between the surfactant molecules at the surface and the energy barrier that must be overcome to drive them back into bulk solution. The difference in wrinkle characteristics between Rsn2 and hydrophobins can be attributed to the way the individual protein interacts at the interface. Rsn2, a monomer in solution, undergoes a conformational change upon interaction with the interface where it does not appear to act cooperatively with its neighbouring Rsn2 monomers. The hydrophobins, dimers or tetramers in solution, form a homogeneous film at the interface by interacting with neighbouring molecules using H-bond together making continuous β -sheets. Thus upon retraction of the droplet in pendant drop method, individual Rsn2 molecules can undergo

conformational change in to a globular shape monomer that can re-dissolve into the bulk solution and thus the interfacial surface area can decrease rapidly allowing the wrinkles to relax. In contrast, the hydrophobins are arranged in a relatively rigid, cooperative conformation such that they do not go back into the solution rapidly upon retraction and the wrinkles remain stable.

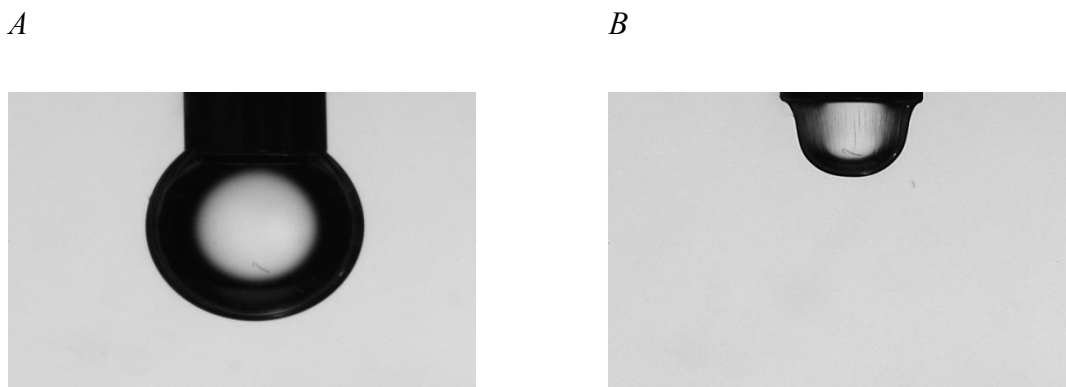
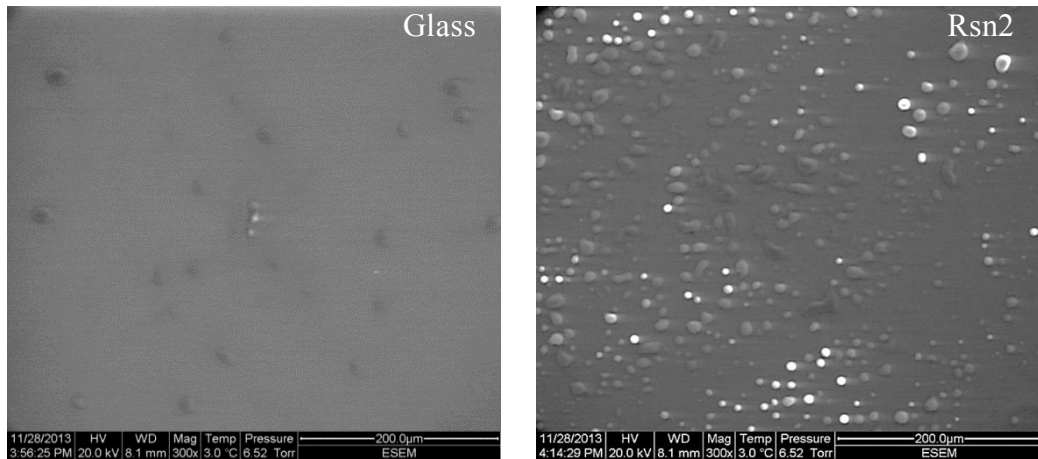


Figure 2-3 Rsn2 film relaxation at trioctanoyl glycerol oil/water interface. (A) Droplet of 1.3 mg/ml Rsn2 before compression. (B) After surface compression induced by reducing the drop's volume. Large wrinkles or folds appear in the surface layer which rapidly relax.

2.4.3 Wettability

Wettability experiments were performed to investigate Rsn2 ability to coat surfaces and make them hydrophilic or wettable. In each ESEM experiment, half of a coverslip was coated with Rsn2 and subjected to ESEM. At 100% RH, water droplets started to form on both the parts of the coverslip. The percentage area covered by condensation was calculated for Rsn2 coated and uncoated regions and compared. After 30 minutes incubation, droplets started to develop on protein coated regions only and the number and size of the droplets had increased by 70 minutes. Only after 120 minutes incubation, were droplets formed on non-coated regions. At the 120 minute time point, Rsn2 coated regions showed significantly higher area of condensation compared with non-coated regions.

A



B

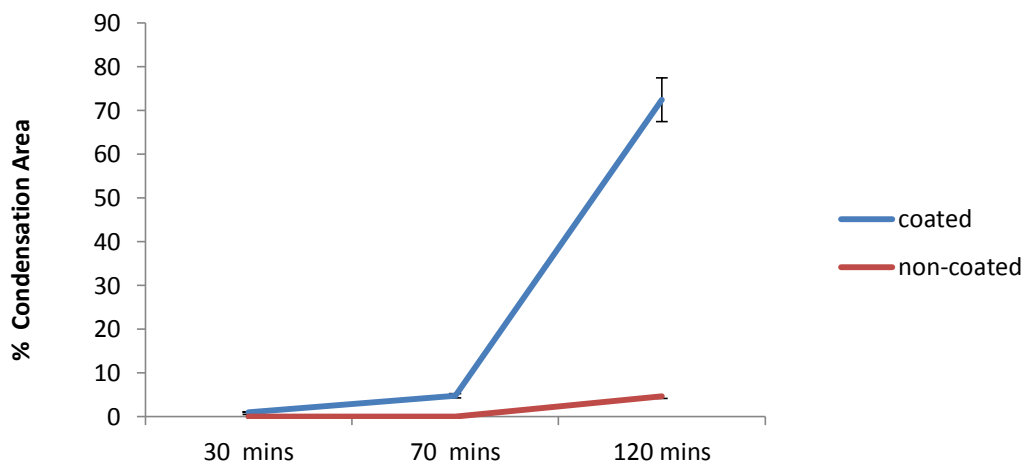


Figure 2-4 Formation of water droplets on a coverslip having coated & non-coated Rsn2 regions subjected to ESEM at 100% RH, where (A) is a representative ESEM images of water droplet formation on Rsn2 coated & non-coated region after 120 minutes and (B) is a graphical representation of condensation area of Rsn2 coated vs. non-coated surface.

2.4.4 Contact angle

Investigations were made to assess the range of surfaces that Rsn2 can coat, using contact angle measurements. Rsn2, being a surfactant protein, should reduce the surface tension of the droplet, thereby reducing the contact angle of the droplet.

Except glass, all the materials chosen are hydrophobic, as shown by angle of contact of a pure water droplet on their uncoated surface, and display a range of hydrophobicities. When an Rsn2 coat was applied, water droplets spread out, decreasing the angle of contact indicating decreased hydrophobicity.

Upon coating with Rsn2, the wettability of all the material surfaces improves noticeably, except for the PTFE in which nearly no change in the contact angle was observed between coated and non-coated surface. The difference in the change of contact angle

among different surfaces could be attributed to the initial loading of Rsn2, which is dependent on the nature of the surfaces and could be different for different substrates.

The contact angle result shows that the initial loading of Rsn2 was higher on to PC, Glass, PP, ACLAR, PS, PMMA and Nylon. Consequently, an increase in wettability is observed the most in case of PC, followed by Glass and PP, while the least change in wettability was observed in PTFE and PDMS.

In case of PDMS, the difference in contact angle is not much, suggesting low initial loading of Rsn2 on PDMS surface. But the result of persistence experiment suggests that the initial loading of Rsn2 is very decent in case of PDMS. This difference in initial loading of Rsn2 on different substrates could be due to difference in the method used for measuring it. In the case of measurement of fluorescence, auto-fluorescence was not taken into account. This auto-fluorescence might have added to the initial loading of Rsn2 and therefore, the reading between CA and persistence experiments vary. Hence it may be said that measurement of fluorescence alone may not be reliable for concluding the initial loading of Rsn2 on different substrates.

Thus contact angle measurement shows that presence of Rsn2 makes the surfaces more hydrophilic for range of hydrophobic materials.

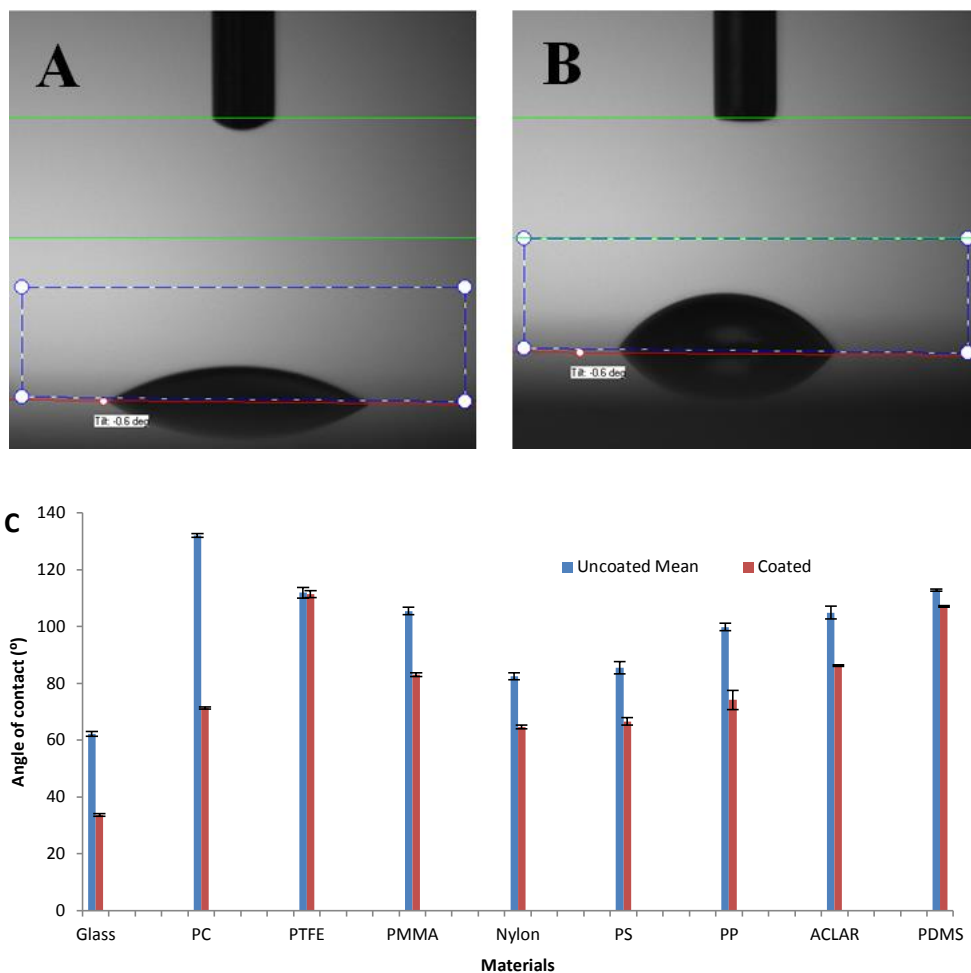


Figure 2-5 The contact angle of water on Rsn2 coated and non-coated regions after dip coating with the Rsn2 protein solution (1mg/ml). A typical example of a water droplet on coated surface (A) and non-coated surface (B) is shown. (C) Graphical representation of the contact angle of water measured on the range of hydrophobic materials. Mean values were used to plot graph with bars representing the standard deviation ($n=3$).

2.4.5 Persistence

The three dimensional structure of Rsn2 in solution reveals that it has a hydrophobic interior and hydrophilic exterior (Mackenzie et al., 2009). Here the authors also discuss that once Rsn2 comes to the air water interface, it is believed to open up to expose its hydrophobic core to the air leaving the hydrophilic exterior to interact with water. By the same principle it is expected that, when applied to hydrophobic surfaces, Rsn2 should unfold to make hydrophobic interactions with hydrophobic surfaces, thus resulting in coating the hydrophobic surface with Rsn2 protein. Investigations were made to test whether Rsn2 adheres to a surface and how long it stays there, using a fusion protein construct of Rsn2 with a small fluorescent protein fusion partner (improved Light Oxygen Voltage, iLOV, developed by Prof Christie of University of Glasgow (Christie et al., 2012)). This will impart fluorescence to the Rsn2 coating and the presence or absence

of coating can be detected using fluorescence microscopy. Controls, as mentioned in section 2.3.5 were used to increase the quality and reliability of quantification of fluorescence intensity, which directly correlates to the loading of iLOVRsn2 protein. It is worth noting that Flavin mononucleotide (FMN), the molecule imparting fluorescence, is not covalently bound to iLOV and therefore it is possibility that FMN could slowly leach out with longer lasting experiments.

Results after 1 day of initial coating show that the initial loading of iLOVRsn2 is highest on Nylon followed by PDMS and ACLAR, while the least loading is observed for Nescofilm. After 5 and 10 days of coating, the initial loading of iLOVRsn2 is gradually lost from Nylon, while it remains stable on PDMS and ACLAR. Results show that fluorescence intensity of iLOVRsn2 coating remains stable over the 10 days of incubation for ACLAR, Glass, Nescofilm, PC, PDMS, PP and PS types of material, while the intensity gradually decreases for Nylon and PMMA. Although the intensity of fluorescence measured on Nylon coating decreases after 10 days, it is still higher compared to the intensities of other material. This shows that PDMS and ACLAR are good choices of material for Rsn2 based application from the perspective of high and stable levels of loading.

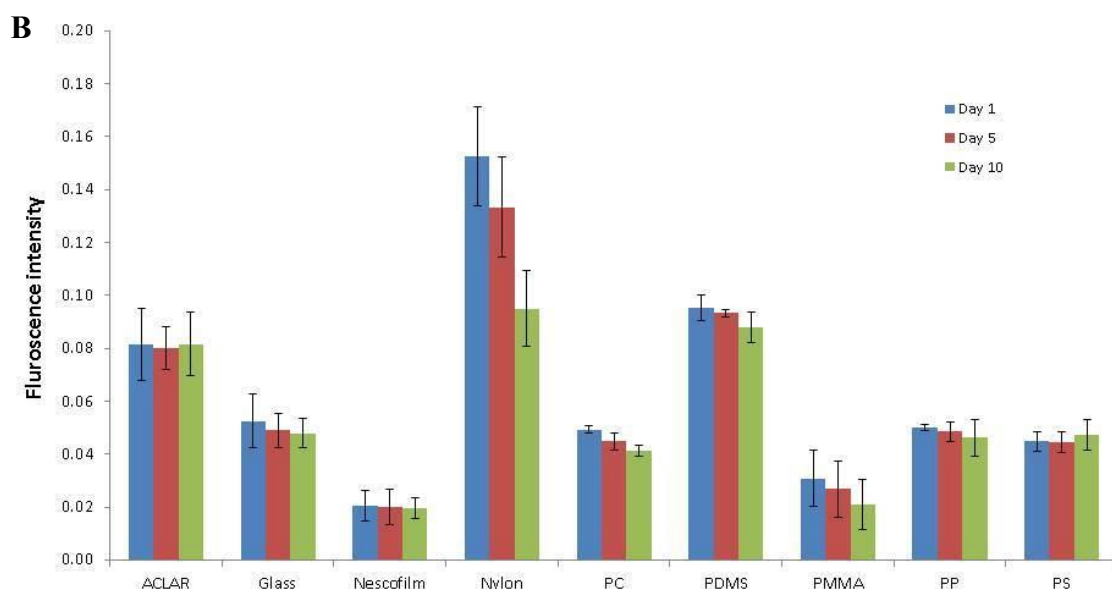
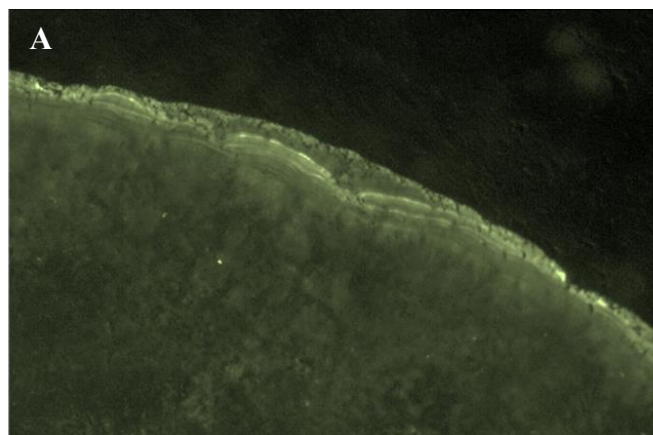


Figure 2-6 The persistence of Rsn2 coating on hydrophobic material. Persistence was measured by quantifying intensity of fluorescence from iLOVRsn2 (1mg/ml) coated protein. (A) A typical fluorescent image of the edge of Rsn2 droplet on PCL (B) Graphical representation of the persistence of Rsn2 coating on the range of hydrophobic materials tested. Measurements were recorded after 1, 5 and 10 days of incubation in PBS at 37°C. Mean values were used to plot graph with bars representing the standard deviation (n=3).

2.4.6 Cell patterning

In order to discover whether Rsn2 coated surfaces have the potential to pattern cells, PS substrates were dip coated with Rsn2 and seeded with fibroblasts. After 24 hours in culture, cells preferentially adhered to Rsn2 coated regions and exhibited a well-spread morphology compared to those cells adhered to the non-coated region. Bare PS substrates did not support cell growth and development with only a few undeveloped somata observed after 24 hours. Cells remained pattern compliant on Rsn2 treated PS surface after 72 hours in culture. Cells on Rsn2 treated PS surface exhibited cell growth and division compared to non-coated regions for the observed period of 72 hours as seen

in Figure 2-7. Cells cultured on Rsn2 coated PS shows significantly higher cell density compared to uncoated surfaces.

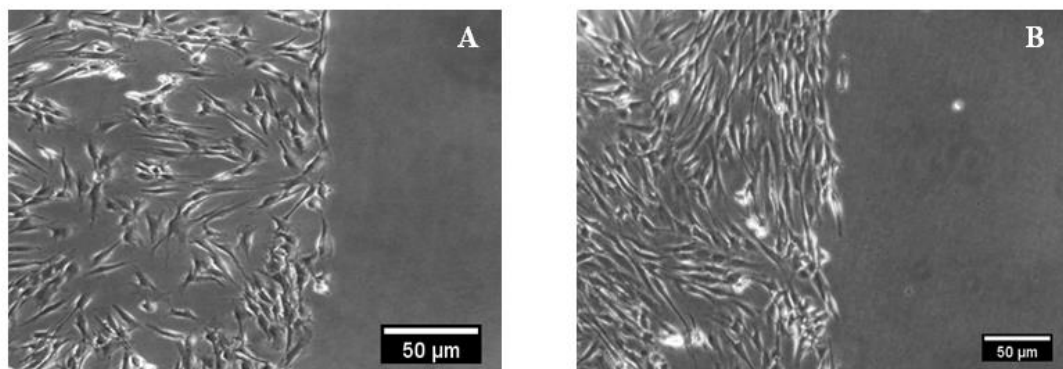
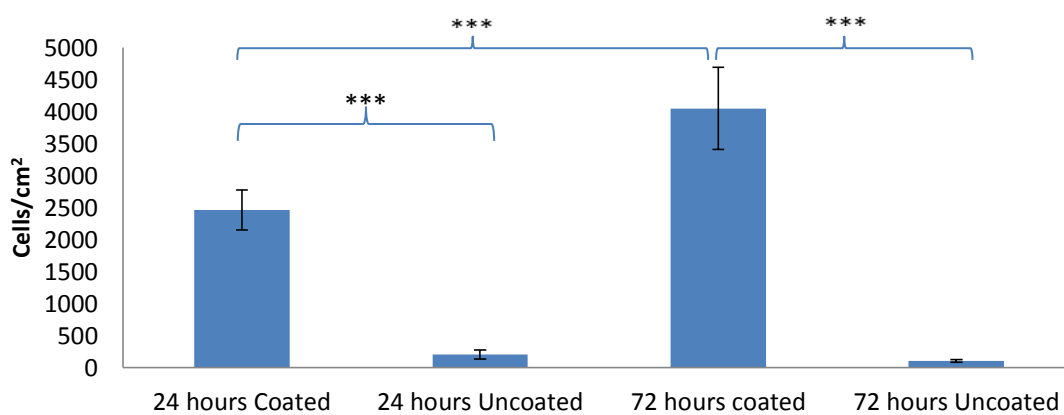


Figure 2-7 Representative light microscopy image taken at the boundary between Rsn2 coated and non-coated regions of the patterned h-Terts cells cultured on PS after (A) 24 hrs and (B) 72 hrs

A



B

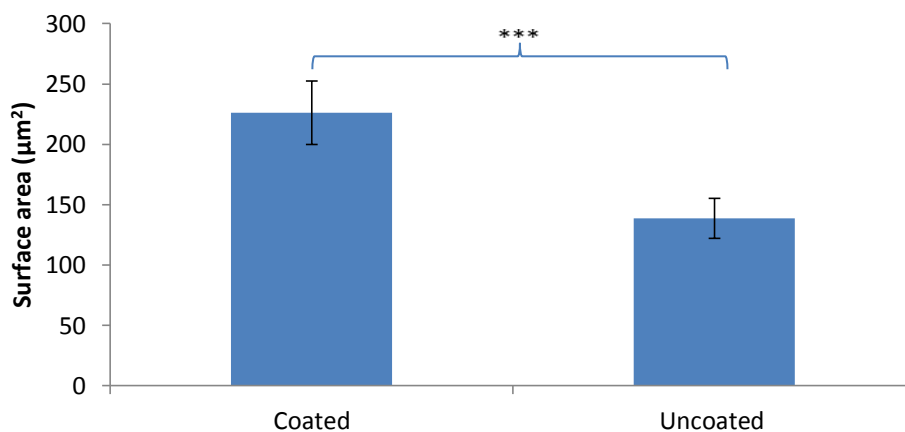


Figure 2-8 Comparison of coated and non-coted regions of h-Terts cells cultured on Rsn2 coated PS for (A) Cell density after 24 hours & 72 hours of incubation and (B) surface area per cell after 24 hours of incubation.

From the contact angle and persistence experiments, it was known that Rsn2 can coat a range of surfaces and from cell patterning experiments it was known that Rsn2 coating can support cell adhesion and cell patterning. The next step was to investigate the possibility of obtaining patterned cells on a range of material surfaces. For this PDMS, silanized glass and PS materials were used along with hTert cell lines. Even though Rsn2 can adsorb on a range of surfaces, only PDMS, glass and PS were selected for cell pattern screening because PDMS, PS and glass are extensively used for culturing different types of cells because of their optical transparency, low cost and easy availability or easy fabrication. Even though PS and glass are traditionally used for cell culture, PDMS gives an added advantage of biocompatibility, low toxicity and compatibility with soft lithography for making finer patterns (Lee et al., 2004). So PDMS was also selected.

Silanized glass and PDMS were used along with untreated hydrophobic PS to investigate the possibility of obtaining cell patterning on different types of substrates. Pattern compliant cells were obtained on all the three types of substrates as seen in the Figure 2-9.

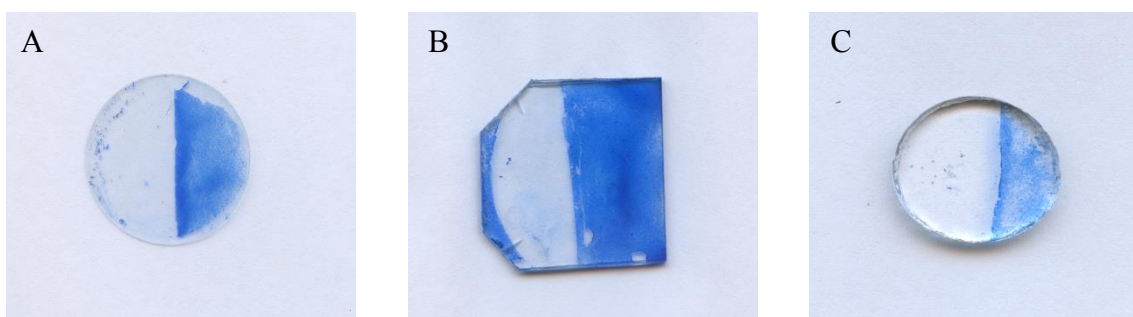


Figure 2-9 Scanned image of coomassie blue stained pattern compliant h-Tert cells cultured on Rsn2 coated and non-coated regions of (A) silanized glass, (B) PS & (C) PDMS after 72 hours of incubation.

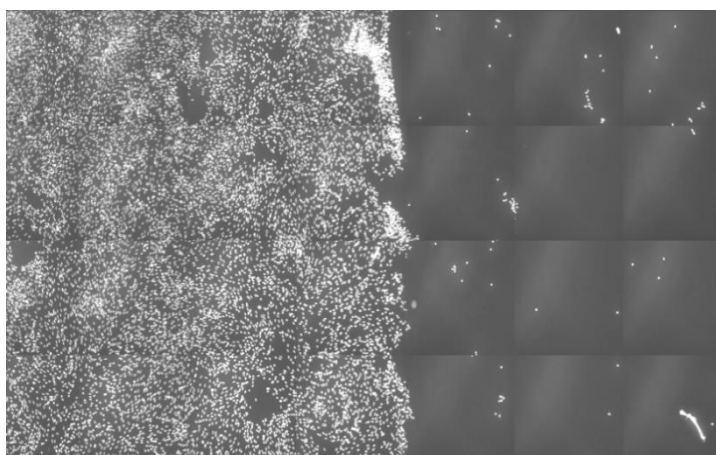


Figure 2-10 A montage fluorescence image taken on the edge of the Rsn2 coated and non-coated region seeded with h-Tert cells and stained with dapi, for the nucleus of cells. The image clearly shows that cells preferentially adhered to the Rsn2 coated region.

2.5 Discussion

From previous studies it was already known that Rsn2 is a surfactant protein, this work has reinforced those findings using the water contact angle; ESEM & pendent drop method and has shown that Rsn2 can be very effective for cell patterning on a range of hydrophobic surfaces. Literature reveals that most of the cell patterning technique developed have material dependency and is only suitable for limited number of surfaces, for example photolithography can only be used for SiO₂ based materials (Hughes et al., 2014). The obtained results of cell patterning Figure 2-7 experiment suggest that Rsn2 has material independency and can be used to modify a range of material surface to generate patterned cells. Thus the use of Rsn2 provides an important advantage of not limiting the cell patterning application to the type of substrate.

In the study conducted by Lussi et al., where the comparison is made on the long-term stability of cellular patterns developed with the PEG-graft patterning techniques. The conclusion was that the differences in the pattern compliancy of cells were due to the different interactions between the patterned substrate, the PEG graft and the serum containing cellular medium (Lussi et al., 2006). In contrast to the finding of Lussi et al., Rsn2 based patterned cells were pattern compliant in all three different substrates tested for 72 hours Figure 2-9.

Rsn2 only coats the surface and that coating does not require any specific surface chemistry but rely on physical parameter, thereby widening the scale of application (Straley and Heilshorn, 2009, Janssen et al., 2002b). The surface application of Rsn2 can be achieved by a simple dip coating technique. Most cell patterning methodologies require specialised instruments and facilities to pattern cells. For example, special/specific chemical and/or physical treatment is needed for soft lithography to develop PDMS mould (Qin et al., 2010b). This study has shown that obtaining pattern compliant cell using Rsn2 is not complicated, as it involves adsorption of protein onto material surfaces at normal room temperature and there is no need of specialised instrumental set up required for its application.

The use of Rsn2 gives an added advantage of retaining the mechanical properties of the selected material and being a protein it can be degraded into non-cytotoxic fragments (Straley and Heilshorn, 2009). Additionally, the requirement of specialized instruments and chemicals needed for direct patterning methods, like bioprinting, can incur higher cost and time compared to using Rsn2 for cell patterning (Gesellchen et al., 2014). More over Rsn2 production requires minimal protein expression facilities and its production

can be easily scaled up for achieving high yield. The surplus Rsn2 can also be easily and safely stored for long term use. To summarise, Rsn2 offers many advantages for its application in cell patterning.

One potential hurdle of using Rsn2 in therapeutic application is that Rsn2 being a foreign protein may trigger an immune response and therefore it may be a challenge to use Rsn2 protein for biomedical applications in future. Although other proteins, like hydrophobins (Scholtmeijer et al., 2002) and polydopamine (Ku et al., 2010), used in cell patterning may also be immunogenic. To counter this situation, there is a possibility of using SPLUNC1 protein, more information in section 1.6. SPLUNC1, a human surfactant protein, like Latherin is proposed to undergoes a conformational change at an interface and can be used to coat surfaces for cell patterning (Vance et al., 2013b).

Moreover, the method of applying Rsn2 by dip coating suited to generate total coverage of a substrate or large scale patterns with low precision. Finer patterning could be advantageous for controlling cell placement, which could be achieved by using Rsn2 as an ink for nano or micro contact printing. Prof Dalby of University of Glasgow have demonstrated the effects of nanotopography on stem cells (Dalby et al., 2014). Similarly, the nano-level features developed by coating Rsn2 using nano-contact printing can be used for co-culture patterning using specific integrin binding sequences (Table 3-1)

To conclude, the cell patterning method developed by using Rsn2 offers advantage of simple application technique, which will result in a persistent protein coat on a range of hydrophobic surfaces.

3 Functionalisation of PDMS with IBS-Rsn2

3.1 Introduction

Cell-based tissue engineering focuses on the restoration of a functional tissue in the hope of answering the currently unmet medical need of wound healing of complex tissues. For various tissue engineering approaches, cells are implanted into scaffolds capable of supporting three-dimensional (3D) tissue formation. The scaffold not only defines the 3D geometry of the tissue but also provides the microenvironment for cell attachment, proliferation and tissue neo-genesis.

The scaffolds currently used for cell attachment are typically made up of polymeric materials, and the behaviours of the attached cells are modulated by the surface properties of the polymeric material (Dalby et al., 2014). Modification of the surface properties of the material by presenting chemical and/or physical cues can significantly influence the interaction of the cell with the material surface (Ma, 2008, Qiu et al., 2014). Plasma treatment is routinely used to prepare the surfaces and facilitate protein immobilisation, either by covalent linkage or adsorption, so promoting cell adhesion (Nitschke et al., 2002).

Scaffold surface functionalization is routinely used for developing new tissue engineering strategies as it offers the advantage of making material surface cell friendly without changing the desirable material properties. The use of extracellular matrix (ECM) proteins, in particular, for surface modification could promote cell interaction and integration with the material surface (Higuchi et al., 2012). The work of this chapter focuses on making surface modifications to mimic the ECM in a facile manner by the application of ranaspumin-2 (Rsn2) fusion proteins.

ECM is mainly composed of glycosaminoglycans and proteins that include collagen, elastin, fibronectin and laminin, which have both structural and adhesive functions. Cells adhere to their environment with a wide array of membrane spanning cell adhesion molecules (CAM) that form the mechano-chemical link to the ECM (Shekaran and Garcia, 2011). Integrins are a prominent member of the CAMs.

Integrins are one of the principal animal cell membrane receptors used to bind to the extracellular matrix. They are heterodimeric in nature, each consisting of an α subunit and a β subunit (Hynes, 2002, Barczyk et al., 2010). Integrins function as transmembrane linkers between ECM and the actin cytoskeleton. Integrins and conventional signalling

receptors often cooperate to promote cell growth, cell survival, and cell proliferation (Takada et al., 2007, Hynes, 1999).

Integrins are known to operate as force dependent mechanotransducers attaching both to their ligands within the ECM and the actin cytoskeleton (Hynes, 2002). Activation allows bidirectional signalling between the two environs (Schoenwaelder and Burridge, 1999). Attachment of integrins to the ECM and aggregation into clusters known as focal adhesions sets off a number of intracellular signalling cascades such as the ERK1/2 mitogen activated protein kinase (MAPK) pathway. The MAPK pathway relies on integrin-dependent cell-surface interactions to trigger a chain reaction of kinase activation leading to changes in gene transcription and ultimately changes in gene expression (Zhu and Assoian, 1995).

Integrins bind a cell's surface to the ECM components such as fibronectin, vitronectin, collagen, and laminin by binding to specific peptide motifs.. In mammals, eighteen α and eight β subunits have been found and have been well characterised. Through different combinations of these α and β subunits, some 24 unique integrins are generated (Barczyk et al., 2010). Some integrin α subunits contain an I (interaction) domain and are closely related to each other. Also closely related to each other are the family of non-I-domain α subunits that recognise the RGD motif (Hynes, 2002). Each integrin dimer has distinct ligand-binding specificity and the list of various specific integrin-binding short peptide sequences that can be used to direct cell adhesion is given in Table 3-1 and Table 3-2.

Integrin subunits	Distribution/ cell type	Receptor/Binding Site /Ligand
$\alpha_1\beta_1$	Dorsal Root Ganglion (DRG), fibroblasts, vascular smooth muscle, liver, microvascular endothelium	Laminin, collagen
$\alpha_2\beta_1$	Fibroblasts	Laminin, collagen, thrombospondin, E-cadherin, tenascin
$\alpha_3\beta_1$	Fibroblasts, DRG	Collagen, Laminin, thrombospondin, fibronectin
$\alpha_4\beta_1$	Hematopoietic cells	Thrombospondin, VCAM-1, fibronectin, osteopontin, ICAM-4
$\alpha_5\beta_1$	DRG, human umbilical vein endothelia (HUVEC)	Fibronectin, osteopontin, fibrillin, thrombospondin,.
$\alpha_6\beta_1$	DRG (Low expression)	Laminin, thrombospondin
$\alpha_7\beta_1$	Skeletal and smooth muscle cells	Laminin
$\alpha_8\beta_1$	crypt cell, alveolar interstitial cells	Tenascin, fibronectin, osteopontin, vitronectin, TGF- β , nephronectin
$\alpha_9\beta_1$	T-cells	Tenascin, VCAM-1, osteopontin, plasmin, angiostatin, VEGF.
$\alpha_{10}\beta_1$	Chondrocytes	Laminin, collagen
$\alpha_{11}\beta_1$	Dermal cells, Periodontal ligament cells	Collagen
$\alpha V\beta_1$	Oligodendrocytes, astrocytes, pancreatic β cells	TGF- β , fibronectin, Vitronectin, osteopontin
$\alpha L\beta_2$	T-lymphocytes	ICAM, ICAM-4
$\alpha M\beta_2$	Neutrophils and Monocytes	ICAM, fibrinogen, ICAM-4, heparin
$\alpha X\beta_2$	Myeloid cells and activated B, NK and some cytotoxic T cells	ICAM, fibrinogen, ICAM-4, heparin, collagen
$\alpha D\beta_2$	Inflamed Macrophages, Eosinophils	ICAM, VCAM-1, fibrinogen, fibronectin, vitronectin, plasminogen
$\alpha IIb\beta_3$	Platelets	Fibrinogen, thrombospondin, fibronectin, vitronectin, collagens, ICAM-4
$\alpha V\beta_3$	Osteocytes, HUVEC, melanoma	Fibrinogen, vitronectin, thrombospondin, fibrillin, tenascin, fibronectin, osteopontin, Bone Sialoprotein (BSP), TGF- β .
$\alpha 6\beta_4$	DRG, Epithelial cells	Fibronectin, Laminin
$\alpha V\beta_5$	Fibroblasts, epithelial cells	Osteopontin, BSP, vitronectin, TGF- β
$\alpha V\beta_6$	Epithelial cells (proliferating)	TGF- β , fibronectin, Tenascin, Osteopontin
$\alpha 4\beta_7$	T-cells, Intestinal Mast progenitor cells	MAdCAM-1, VCAM-1, fibronectin, osteopontin
$\alpha E\beta_7$	Tcells (memory)	E-cadherin
$\alpha V\beta_8$	Dendritic cells, Langerhans cells	Collagens, Laminins, Fibronectin, TGF- β

Table 3-1 Integrins and their binding partners. List of different integrin subunits with their protein binding ligands found in various types of tissue. Each integrin can bind to more than one protein binding ligand. (Anselme, 2000, Plow et al., 2000, Higuchi et al., 2012, Takada et al., 2007, Orla Protein technologies, Bennett et al., 2001a, Siebers et al., 2005)

NOTE: Cells express more than one type of integrin at a time, and expression varies according to the stage of cell cycle stage and during development.

<i>Integrin binding sequence</i>		<i>Integrin</i>	<i>Reference</i>
<i>RGD</i>	<i>collagen I, vitronectin, fibronectin, Bone sialoprotein</i>	$\alpha_3\beta_1$, $\alpha_5\beta_1$, $\alpha_8\beta_1$, $\alpha_v\beta_1$, $\alpha_v\beta_3$, $\alpha_v\beta_5$, $\alpha_v\beta_6$, $\alpha_{11b}\beta_3$	(Pytela et al., 1987, Ruoslahti, 1996b)
<i>PHSRN</i>	<i>Fibronectin</i>	$\alpha_5\beta_1$	(Aota et al., 1994)
<i>IKVAV</i>	<i>Laminin</i>	$\alpha_3\beta_1$, <i>α1 chain</i>	(Saha et al., 2007, Caniggia et al., 1996, Nomizu et al., 1995)
<i>LDVP</i>	<i>Laminin</i>	$\alpha_4\beta_1$	(Komoriya et al., 1991, Bayless and Davis, 2001)
<i>FHRRIKA</i>	<i>BSP, collagen</i>	$\alpha_2\beta_1$	(Healy et al., 1999b, Schuler et al., 2009)
<i>REDV</i>	<i>Fibronectin</i>	$\alpha_4\beta_1$	(Humphries et al., 1986, Bayless and Davis, 2001)
<i>KRSR</i>	<i>BSP</i>		(Balasundaram and Webster, 2007)
<i>YIGSR</i>	<i>Laminin</i>	β_1 chain	(Frith et al., 2012)
<i>(GG)DGEA</i>	<i>collagen I</i>	$\alpha_2\beta_1$	(Hennessy et al., 2009, McCann et al., 1997)
<i>HHLGGAKQAGDV</i>	<i>Fibrinogen γ-chain</i>	$\alpha_{11b}\beta_3$	(Hagisawa et al., 2016)
<i>GPR</i>		$\alpha_2\beta_2$	(Graham et al., 2003)
<i>AEIDGIEL</i>	<i>Fibronectin</i>	$\alpha_9\beta_1$	(Yokosaki et al., 1998)
<i>QIDS</i>	<i>Fibronectin</i>	$\alpha_4\beta_1$	(Clements et al., 1994)
<i>PPRARI</i>	<i>Fibronectin (heparin II domain)</i>	$\alpha_4\beta_1$	(Gonzalez et al., 2009)
<i>GFOGER</i>	<i>Collagen</i>	$\alpha_1\beta_1$, $\alpha_2\beta_1$	(Hennessy et al., 2009)

Table 3-2 Integrin binding sequences (IBS), their molecule(s) of origin, their binding integrins and the citation, where the sequences have been described.

A series of studies where surfaces have been modified such that RGD tripeptide motifs are displayed to cells have shown that this can promote cell attachment and proliferation. Coating a scaffold material's surface with only the RGD peptide can limit cell type-specific adhesion, since all cells express RGD binding integrins. Moreover, binding by RGD-directed integrins is only optimal in the presence of other synergistic peptides. For instance, the presence of a PHSRN synergy peptide, on fibronectin domain 10, along with RGD can substantially enhance the adhesive activity of $\alpha_5\beta_1$ integrin (Redick et al., 2000). Some other peptide sequences, like the IKVAV, can mediate $\alpha_3\beta_1$ integrin-mediated neurite outgrowth (Tashiro et al., 1989). Thus it is hypothesised that to make a surface cell type specific, the availability of a combination of specific integrin binding sequence (IBS) might be needed.

The genetic engineering provides an opportunity to develop recombinant fusion proteins containing cell adhesive peptides, which can be used to generate biomimetic biomaterials interfaces (Hersel et al., 2003). The biomimetic substrates produced by presenting peptide sequences in this manner might then promote cell adhesion. The work described in this chapter is building on the cell patterning chapter and is focused on developing a functionalised scaffold specialised for osteoblasts, and DRG neurons, using IBS as a fusion partner with Rsn2. The selection of IBS was based on the information summarised

in Table 3-1 and Table 3-2, which suggests that DRG neurons express $\alpha_1\beta_1$, $\alpha_3\beta_1$ and $\alpha_5\beta_1$, while osteoblasts express $\alpha_3\beta_1$ and $\alpha_v\beta_3$ integrins. Five short biomimetic peptides were selected which would bind to these integrins, namely (in standard single letter code) RGD, PHSRN, IKVAV, LDVP and FHRIKKA. This was backed by literature that showed that use of FHRIKKA and RGD would promote osteoblasts differentiation (Rezania and Healy, 1999b), while IKVAV and LDVP would promote neuronal outgrowth (Tashiro et al., 1989). Thus we hypothesised that by presenting short peptide sequences, which bind to the expressed integrin receptors, like RGD; FHRIKKA and PHSRN on scaffold surface would promote osteoblasts adhesion while presenting RGD, PHSRN, IKVAV, and LDVP might improve DRG cell adhesion.

3.2 Aim

The aim of the work described in this chapter was to develop a tool that allows the functionalizing of a wide range of hydrophobic scaffolds with cell type selective IBS-Rsn2 fusion proteins that have been tailored to promote cell adhesion on otherwise non-selective surfaces.

3.3 Method and Materials

3.3.1 IBS-Rsn2 cloning and protein expression

The IBS-Rsn2 expression constructs were created by PCR subcloning. Primers were designed, one to anneal to the 5' end of the Rsn2 non-coding strand that incorporated each IBS preceded by a NdeI restriction site; whereas the 3' end primer would bind to the Rsn2 coding strand and contained a BamHI restriction site. Table 3-3 shows the primer sequences.

Rsn2_FL_3'Primer (3' → 5') : CTA-CTA-CTA-CTA-CTA-CCT-ATA-AT	
Rsn2_FL_5'Primer (5' → 3')	
<i>RGD</i>	CAT-ATG-CGT-GGC-GAT -TTA-ATA-TTA-GAT-GGG-GAC-CTA-CTA
<i>LDVP</i>	CAT-ATG-CTG-GAT-GTG-CCG -TTA-ATA-TTA-GAT-GGG-GAC-CTA-CTA
<i>IKVAV</i>	CAT-ATG-ATT-AAA-GTG-GCG-GTG -TTA-ATA-TTA-GAT-GGG-GAC-CTA-CTA
<i>PHSRN</i>	CAT-ATG-CCG-CAT-TCT-CGT-AAC -TTA-ATA-TTA-GAT-GGG-GAC-CTA-CTA
<i>FHRRIKA</i>	CAT-ATG-TTT-CAT-CGT-CGT-ATT-AAA-GCG -TTA-ATA-TTA-GAT-GGG-GAC-CTA-CTA

Table 3-3 Sequences of primers designed to generate IBS-Rsn2. **CAT-ATG** is the NdeI site, **C-CTA-GG** is the BamHI site and IBS coding nucleotides are coloured red.

PCR amplification was then carried out at an annealing temperature of 50⁰C with these primers, using the pET28-Rsn2 template to produce an IBS-Rsn2 PCR product. The PCR product was subjected to agarose gel electrophoresis, and the excised fragment was then subjected to gel purification (Wizard® SV Gel and PCR Clean-Up System) to avoid any contaminating template. 3' adenine overhangs were added to each insert using Taq polymerase (GoTaq® Flexi DNA Polymerase # M8301). The fragments were then ligated into the pCR4.0-TOPO vector with complementary 3' thymine overhangs which contain immobilised topoisomerase enzyme (Invitrogen). DNA sequencing of the transformed DH5 alpha (Invitrogen™) cells were carried out to investigate that the TA-cloned fragments had the correct sequence.

Each IBS-Rsn2 coding sequence was then subcloned. The restriction enzymes NdeI and BamHI were used to cut the insert out of the pCR4 vector producing sticky overhangs to subclone into the pET-28 expression plasmid (Novagen, #69864) cut with the same restriction enzymes. The ligated plasmids were then transformed into *E. coli* DH5 alpha, followed by the selection of clones using colony PCR and DNA sequencing. The recombinant plasmid DNA was then ready to be transformed into the expression cells of choice, BL21 (DE3) cells (Agilent).

All the expressed proteins will have his-tag and thrombin cleavage site before the IBS-Rsn2. The proteins Rsn2, RGD-Rsn2, FHRIKKA-Rsn2 and PHSRN-Rsn2, were expressed as described in section 2.2.1. IKVAV-Rsn2 and LDVPRsn2 were expressed

overnight at 15°C with all other conditions being the same as outlined in Section 2.2.1 and given to Dr Kredi for for her to investigate if these would promote axonal outgrowth.

3.3.2 Contact Angle

Contact angle measurements for IBS-Rsn2 coated PDMS surfaces were made using the protocol described in Chapter 2.

3.3.3 Silanisation

The Glass coverslips/slides were cleaned using piranha solution (a 3:1 mixture of sulphuric acid and hydrogen peroxide), rinsed with water, and air dried thoroughly. Then the glass coverslip/slides were briefly soaked in a minimal volume of silanizing reagent (Chlorodimethylsilane, Sigma-Aldrich) and the excess solution was allowed to evaporate in the fume hood before thoroughly rinsing with log flumes. Silanised glass coverslips/slides were then air dried.

3.3.4 Routine cell culture

Cell culture work was performed aseptically at room temperature using laminar flow hoods and cells were kept in an incubator at 37°C under humidified conditions with 5% CO₂. Cells were maintained in modified DMEM culture medium containing foetal bovine serum (FBS), antibiotic mixture and sodium pyruvate.

Fibroblast h-Tert cells were cultured and seeded, as mentioned in chapter two method and material section, onto IBS-Rsn2 coated PDMS surfaces for 24 hours. After which they were fixed and subjected to DAPI staining for nucleus and immunofluorescence microscopy as described later.

3.3.5 Isolation and culture of osteoblastic cells

Osteoblastic cells were isolated from neonatal rat calvaria by Dr M Riehle using explant culture as briefly described in the following. Firstly, the neonates were schedule 1 killed using an overdose of pentorbital and their DRG removed by another user. The same animals were collected in sterile plastic bags on ice and 1-4 hours later used to extract the calvariae. After cutting through the skin and soft connective tissue the calvariae were removed, and collected at room temperature in Hanks' Balanced Salt Solution (GIBCO® HBSS). Using a binocular microscope the periosteum and other adhering soft tissue was removed from the bone using scalpel blades and Dumont No 7 forceps. The collected, soft tissue free calvariae of two rats were then cut into small, ca. 1mm large pieces. The bone pieces were washed twice with HBSS and placed in a 25 cm² TCP flask with ca. 1-

2ml DMEM media (10%FBS, 5% ABS, 85% DMEM Sigma) such that the meniscus of the media would confine the bone pieces into contact with the substrate. The media would be carefully exchanged every three days. After 7-14 days *in vitro* a cell layer would surround the bone pieces. At this stage I would take over the cultures and treat these as follows.

The cell layer was then digested by giving a trypsin-collagenase proteolytic treatment. Rat calvaria cells obtained were seeded in a 25 cm² (T-25) (BD Biosciences, San Jose, CA, USA) tissue culture dish. The cells were grown until confluence in Dulbecco's Modified Eagle's Medium (DMEM) (PAA Laboratories) supplemented with 10% Foetal bovine serum (FBS, Invitrogen), 1% penicillin and streptomycin (Sigma) and sodium pyruvate (Sigma).

Isolated osteoblast cells were seeded into a 75 cm² (T-75) culture flask (BD Biosciences, San Jose, CA, USA) containing medium and incubated. After 48 hrs in culture, the non-adherent cells were discarded, and cells were fed with fresh medium. The medium was replaced twice a week. Cells were allowed to reach 70-80% confluence and then passaged as follows: Briefly, the culture medium was aspirated and the cells washed in HEPES-saline (4-(2-hydroxyethyl)-1-piperazineethanesulfonic acid) following which 5 ml trypsin (PAA Laboratories) was added and incubated at 37°C for 5 minutes. The action of trypsin was neutralised by adding 5 ml medium, and a cell count was performed using a Neubauer chamber. The cells were then seeded in a 150 cm² (T-150) culture flask (BD Biosciences, San Jose, CA, USA) at a concentration of 100 cells/cm².

3.3.6 PDMS fabrication

PDMS 184 polymer solution (Sylgard® 184 Silicone Elastomer, Dow Corning, UK) was added to curing agent at a ratio of 9:1 (w:w). The polymer and curing agent were mixed very thoroughly in a disposable cup and then degassed for 20 minutes. The degassed PDMS was poured into a petri dish or a silicon wafer mould and cured in an 80°C oven for 2 hours before being left to cool and cut into individual 11 mm diameter devices with a 13mm diameter cork borer.

The unreacted component of the crosslinked PDMS was extracted by three cycles of swelling the polymer in n-hexane (Riedel-de Haën), and shrinking of the samples in ethanol.

3.3.7 Sample preparation

Samples were sterilised before seeding by immersing them in 70% ethanol for 30 mins, after which each sample was rinsed twice in sterilised water followed by drying with a flow of 0.22µm filtered compressed air in a laminar flow cabinet.

For Rsn2, RGD-Rsn2, PHSRN-Rsn2, FHRIKKA-Rsn2, RGD-Rsn2:PHSRN-Rsn2 (1:1), RGD-Rsn2:FHRIKKA-Rsn2 (1:1), FHRIKKA-Rsn2:PHSRN-Rsn2 (1:1) and RGD-Rsn2:PHSRN-Rsn2:FHRIKKA-Rsn2 (1:1:1) coatings, protein solution (1 mg/ml total concentration) was added to each surface and left to incubate for 30 mins. After this, the excess protein solution was removed, and the samples were rinsed in water before seeding with cells.

3.3.8 Differentiation assay

The osteoblast cells, when about 70% confluent, were used at passage 3 and 4. Cells were plated into 12-well tissue culture dishes at a cell seeding density of 1000 cells/cm². Cells were fed thrice in a week.

For all experiments, coverslips and PDMS used were rinsed in 70% ethanol three times followed by further rinsing in sterile PBS saline solution and then cell culture medium. Cells were seeded onto ten different surfaces: plain glass coverslips (positive control), untreated PDMS (negative controls), Rsn2, RGD-Rsn2, PHSRN-Rsn2, FHRIKKA-Rsn2, RGD-Rsn2: PHSRN-Rsn2 (1:1), RGD-Rsn2:FHRIKKA-Rsn2 (1:1), FHRIKKA-Rsn2:PHSRN-Rsn2 (1:1) and RGD-Rsn2:PHSRN-Rsn2:FHRIKKA-Rsn2 (1:1:1).

Samples were fixed after 0, 1, 7 or 28 days in culture.

3.3.9 Immunofluorescence staining

After various times after seeding, cultured osteoblast cells were washed three times with phosphate buffered saline (PBS) and fixed with 4% formaldehyde/PBS for 15 minutes at 37°C. Cells were then permeabilized for 5 minutes at 4°C with a permeabilizing solution of 0.1% w/v sucrose, 50 mM NaCl, 3 mM MgCl₂.6H₂O, 20 mM HEPES (4-(2-hydroxyethyl)-1-piperazine-ethanesulphonic acid) and 0.5% v/v Triton X-100 in 100 ml H₂O (pH 7.2). Non-specific binding sites were blocked with 1% bovine serum albumin (BSA) in PBS for 15 minutes at 37°C. To visualise the actin cytoskeleton a 1% BSA/PBS solution of rhodamine-conjugated phalloidin ((1:200), Molecular Probes USA) was used. Along with phalloidin, either mouse anti-vinculin(1:150), mouse monoclonal anti-osteopontin (OPN) Ig (1:50) or mouse monoclonal anti-osteocalcin (OCN) Ig (1:50)

were made with 1% BSA in PBS . Each stain was added to its respective sample and incubated at 37°C. After 1 hr, samples were washed with 0.5% Tween 20 in PBS 3 times for 5 minutes to reduce background labelling. After incubation, secondary antibodies made in 1% BSA/PBS were added to the respective samples. Horse biotinylated anti-mouse IgG (1:150) was added to anti- vinculin, anti-OPN and anti-OCN containing samples and were further incubated for 1 hr at 37°C. Samples were washed with Tween 20/PBS as previously described and incubated at 4°C for 30 minutes in a 1% BSA/PBS solution of fluorescein isothiocyanate (FITC) conjugated streptavidin ((1:50), Vector Laboratories UK). A final washing step was carried out to remove any excess stain. Samples were mounted on glass slides using mountant containing 4'6- diamidino-2-phenylindole (DAPI, Vector Laboratories UK) and cells were observed using a Zeiss Axiophot fluorescence microscope at 20X magnification (0.40 NA). Images were captured using an Evolution QEi digital monochromatic CCD camera (Media Cybernetics USA) with QCapture imaging software.

3.3.10 Quantification

The fluorescence microscopy images were analysed using FIJI software (Schindelin et al., 2012) to assess cell density and to quantify the number of focal adhesions per cell. The fluorescence images of DAPI stained samples were exported to FIJI, to calculate number of particles Figure 3-1. To quantify the number of focal adhesion formed, the fluorescence images of vinculing stained samples were exported to FIJI and the threshold tool was used to trace the focal cell adhesions formed Figure 3-2. A paired sample T-test was used to test statistical significance between the quantitative data obtained from cells cultured on different IBS-Rsn2 coated PDMS substrates. The null hypothesis of the paired sample T-test assumes that the true mean difference between the paired samples is zero and all differences are by random chance.

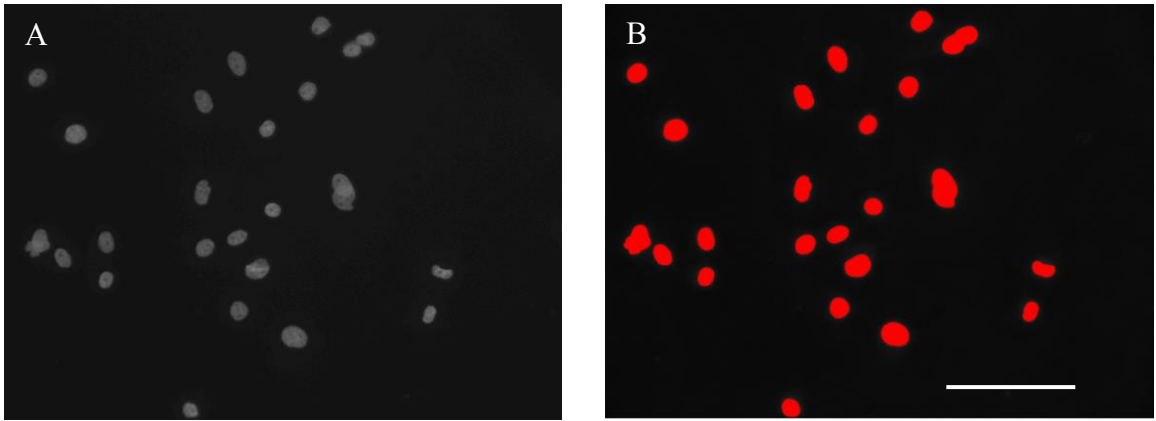


Figure 3-1 A representative fluorescent image of the osteoblast cells cultured on IBS-Rsn2 coated PDMS, fixed and stained with DAPI (A), which was used for adjusting threshold (B) for nucleus quantification. The red colour indicates the area identified by FIJI after thresholding.

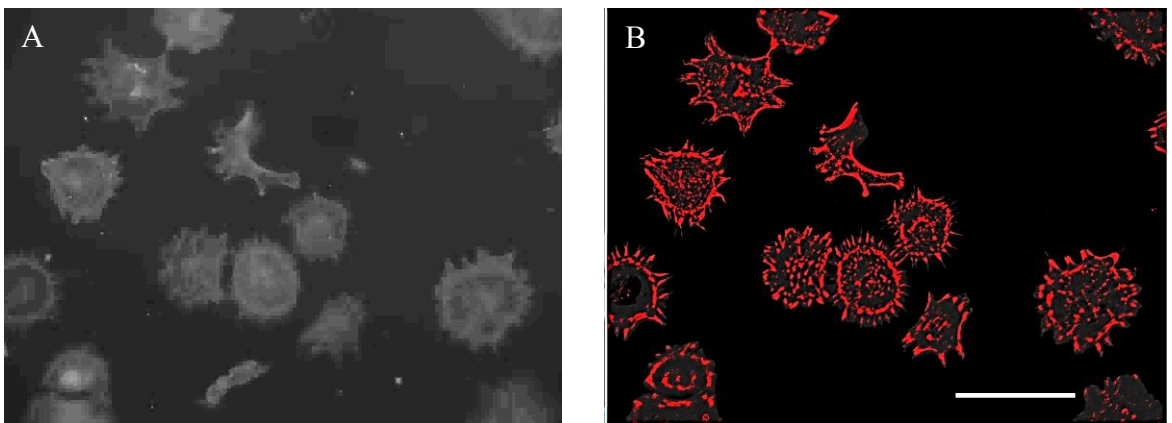


Figure 3-2 A representative fluorescence image of the osteoblast cells cultured on IBS-Rsn2 coated PDMS, fixed and stained with vinculin (A), which was used for adjusting threshold (B) for quantification of focal adhesions formed. The red colour indicates the area identified by FIJI after thresholding. Scale bar is for 100 μm .

3.4 Results

3.4.1 IBS-Rsn2 fusion construct cloning

For tissue engineering applications it is important to develop a functional scaffold capable of supporting a functional tissue. For the formation of a functional tissue, the adhesion of particular cell types should be directed onto a three-dimensional scaffold. This cell type specificity may be achieved by presenting a fusion construct of specific integrin binding sequences with Rsn2 on the surface of the scaffold. To test this, five IBS sequences were selected and were cloned with Rsn2 to develop recombinant IBS-Rsn2 proteins. Specially designed primers for 5'Rsn2 incorporating the IBS coding region were used for amplification of each IBS-Rsn2 construct as shown in Figure 3-3.

The solution structure of Rsn2 determined by NMR revealed that the N-terminal peptide of the protein, first 16 residues, was disordered in bulk solution. Previous work by Dr. Vance had shown that the presence of the thrombin-cleavable affinity tag in the recombinant protein did not affect the protein's surfactant properties (Vance, 2012). Indeed, a fusion protein incorporating the small fluorescent domain iLOV (Chapman et al., 2008) N-terminal to Rsn2 also retained surface activity (Vance, 2012). Thus it was hypothesised that the introduction of an additional peptide sequence at the N-terminus would be unlikely to disrupt surface activity. Moreover, the disordered, 16 residue N-terminal peptide might help in presenting the IBS for cell attachment at a distance from the Rsn2-coated surface. Thus a site immediately preceding the N-terminal leucine residue of the natural, mature Rsn2 sequence was chosen for the addition of the IBS peptide.

The PCR products obtained were gel purified and used for TOPO TA cloning into the pCR4.0 vector. Competent cells were then transformed with the vector carrying IBS Rsn2 gene generating many colonies.

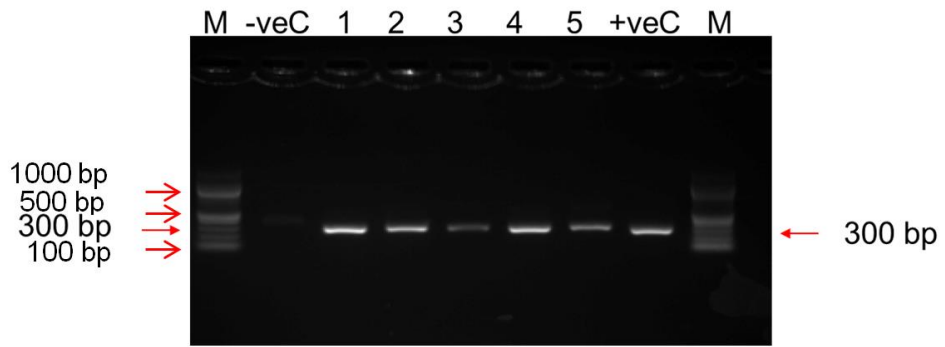


Figure 3-3 PCR amplification of IBS-Rsn2 product using primers incorporating IBS, where (1) no template negative control; (2) RGD-Rsn2; (3) LDVP-Rsn2; (4) PHSRN-Rsn2; (5) IKVAV-Rsn2; (6) FHRRIKA-Rsn2, (7) Rsn2 as a positive control; (M) 100bp ladder. The red arrow points to the amplified IBS-Rsn2 fragments of almost 300bp.

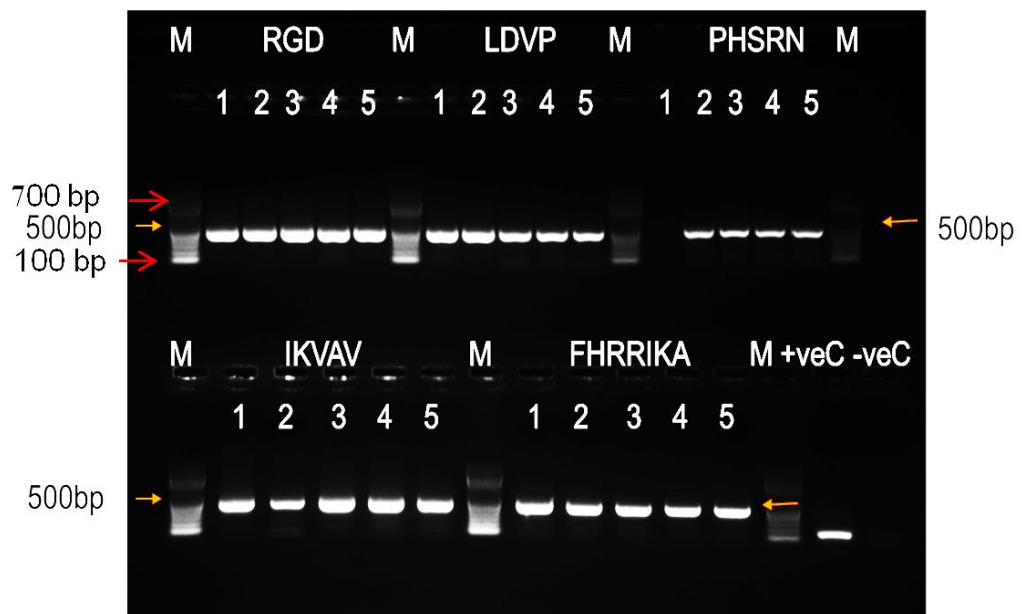


Figure 3-4 Colony PCR. Screening of colonies for the correct insert using PCR for all five IBS-Rsn2 fusion construct (1-5) colonies selected for colony PCR and (M) 100bp ladder. The orange arrows indicate the amplified IBS-Rsn2 fragments of almost 500bp.

Colony PCR was performed using M13 primers to screen for the presence of the insert in the pCR4.0 vector. The expected sizes of the colony PCR products are for RGD: 474bp, LDVP is 477bp, PHSRN is 480bp, IKVAV is 480bp, FHRRIKA is 486bp and positive control is 165bp. Agarose gel electrophoresis Figure 3-4 revealed that all selected colonies gave rise to a PCR product of the expected size insert except PHSRN 1. Plasmid DNA was extracted from each positive clones and sequenced (University of Dundee). The sequencing results confirmed that the positive clones carried the right sequences.

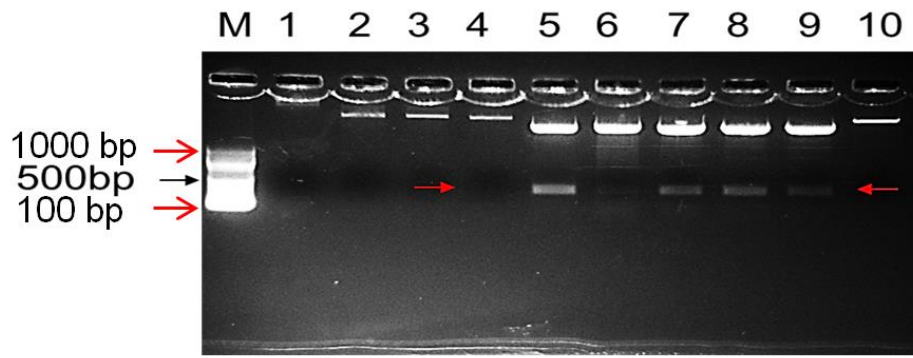


Figure 3-5 A 1% agarose gel for double digested vector and insert with *NdeI* and *BamHI*, where M is 100 bp Ladder, 1 is *Rsn2* uncut, 2 is *BamHI* control, 3 is *NdeI* control, 4;5;6;7;8;9;10 are double digests for *Rsn2*; *RGD*; *LDVP*; *PHSRN*; *IKVAV*; *FHRRIKA*; *pET28* vector (followed by Alkaline Phosphatase treatment) The red arrow points to the *IBS-Rsn2* fragments generated after double digestion.

Once confirmed, each pCR4.0 vector carrying an insert was subjected to double digestion with *NdeI* and *BamHI* to produce the desired insert flanked with the respective restriction sites. In parallel, the destination vector, pET28, was double digested and subjected to alkaline phosphatase treatment to prevent self-ligation. The double digest was subjected to agarose gel electrophoresis Figure 3-5, and each band of the correct size was excised and gel extracted followed by overnight ligation into the pET28 vector.

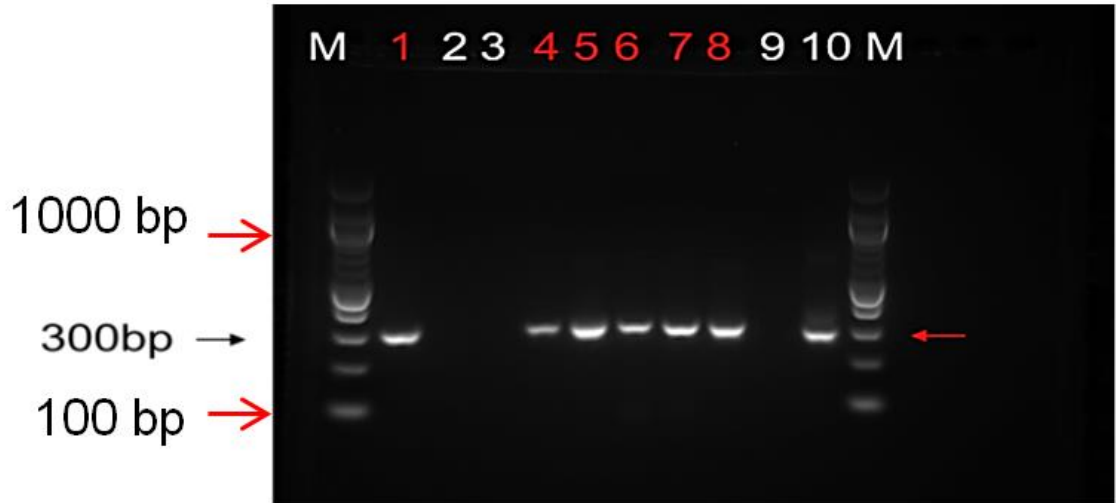


Figure 3-6 An example of agarose gel electrophoresis of colony PCR products from selected *IBS-Rsn2* constructs ligated into pET28 and transformed into *DH5alpha* cells, where M is 100bp ladder, 1-5 are *RGD* colonies, 6 and 7 *PHSRN*, 8 *IKVAV*, 9 no plasmid negative control and 10 *Rsn2* as a positive control. Colonies labelled in red are positive clones. The red arrow points to the amplified *IBS-Rsn2* products.

The ligated construct was then transformed into competent cells and the clones obtained were screened by colony PCR Figure 3-6, positive clones were sequenced (Figure 3-7).

The sequencing result allowed the identification of plasmids that had the correct sequence for each IBS-Rsn2.

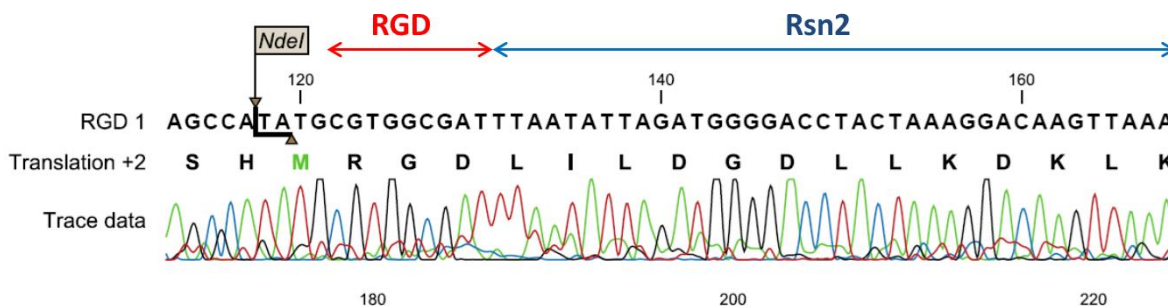


Figure 3-7 An example of the sequencing result for IBS-Rsn2 in pET28 vector confirmed the insertion of RGD (IBS) between the start codon and Rsn2 gene.

3.4.2 IBS-Rsn2 fusion protein expression

Following successful construction of each expression vector, each IBS-Rsn2 vector was transformed into BL21 (DE3) cells and expression of the individual proteins tested. SDS-PAGE analysis of RGD-Rsn2; LDVP-Rsn2; PHSRN-Rsn2 and FHRRIKA-Rsn2 revealed their presence in both soluble and insoluble fractions whereas the majority of the IKVAV-Rsn2 was in the insoluble fraction.

Since significant proportions of each IBS-Rsn2, Rsn2 was found in the insoluble fraction in the small scale test expressions, large-scale expression tests were set up to investigate whether sufficient IBS-Rsn2 could be expressed and purified successfully. Following purification of each IBS-Rsn2, they were subjected to SDS-PAGE to check the purity and integrity of each protein. The yield of purified protein obtained for RGD-Rsn2 and PHSRN-Rsn2 was more than 10 milligrammes per litre of culture (mg/L) (Figure 3-8), and for FHRRIKA-Rsn2 it was nearly 8 mg/L, whereas LDVP-Rsn2 gave 4 mg/L and IKVAV-Rsn2 2.5 mg/L. Since LDVP-Rsn2 and IKVAV-Rsn2 gave low yields of soluble protein (Figure 3-9), steps were taken to optimise their expression conditions.

Optimisations were carried out by reducing the incubation temperature and extending the time of induction from 37⁰C for 3 hours to 15⁰C overnight, and by reducing the IPTG concentration from 1mM to 0.4mM or 0.1mM. Test expressions carried out using these conditions showed that reducing the temperature to 15⁰C with 1 mM IPTG induction resulted in most of the protein being found in the soluble fraction. The results of the test expression were assessed on a larger scale culture which gave yields above 10 mg/L for both LDVP-Rsn2 and IKVAV-Rsn2 (Figure 3-10).

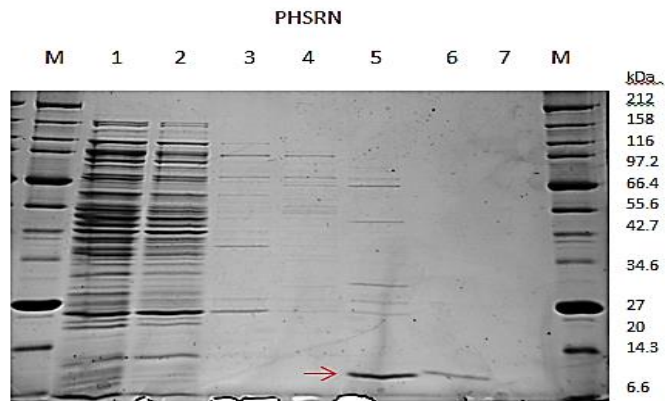


Figure 3-8 SDS-PAGE of PHSRN-Rsn2 affinity purification, where (1) Cell lysate flow through; (2) Binding buffer1; (3) Binding buffer2; (4) Wash buffer1; (5) Elution buffer1; (6) Elution buffer2; (7) 1M immidazole and (M) Marker. The red arrow points to the right sized expressed protein almost 14 kDa.

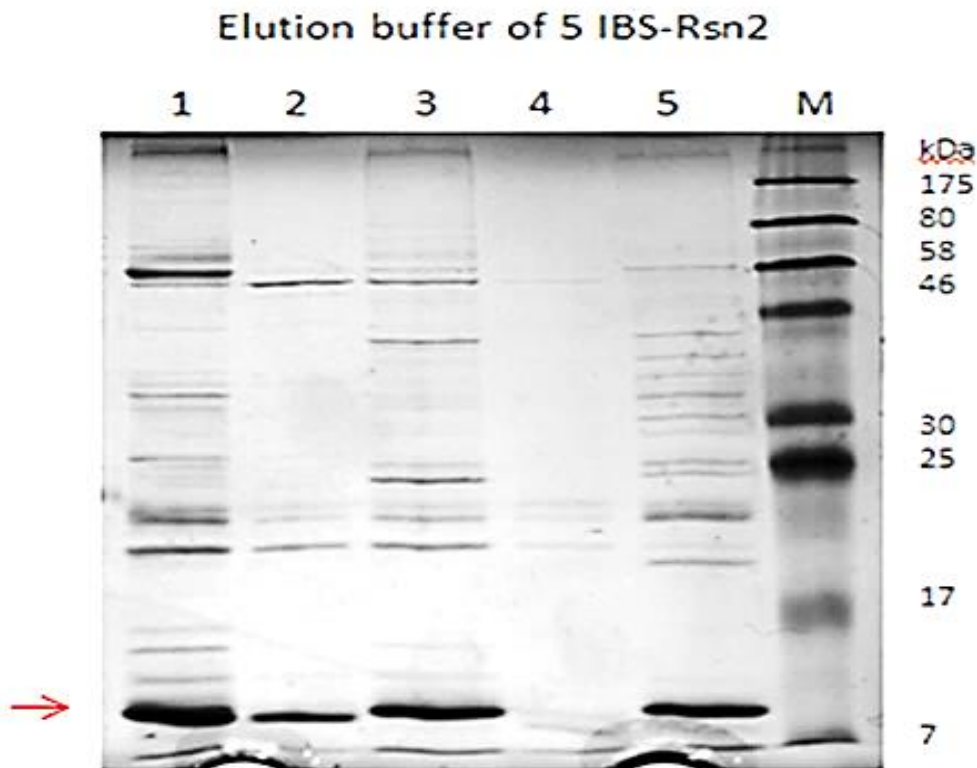


Figure 3-9 SDS-PAGE of the five IBS-Rsn2 samples after Ni²⁺-affinity purification, where (1) RGD-Rsn2; (2) LDVP-Rsn2; (3) PHSRN-Rsn2; (4) IKVAV-Rsn2; (5) FHRRIKA-Rsn2 and (M) Marker. The red arrow points to the expected size for the expressed proteins of almost 14 kDa.

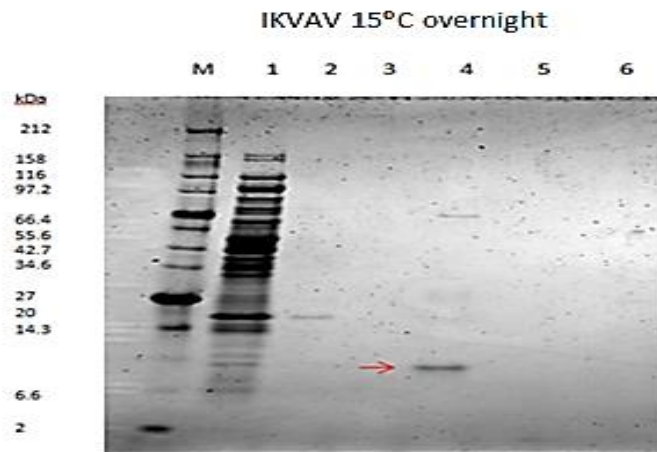


Figure 3-10 SDS-PAGE of IKVAV-Rsn2 affinity purification.(1) Cell lysate flow through; (2) Binding buffer1; (3) Wash buffer1; (4) Elution buffer1; (5) Elution buffer2; (6) 1M imidazole and (M) Marker. The red arrow points to the right sized expressed protein of almost 14 kDa.

3.4.3 Contact angle measurements

Following successful expression and purification of each of the IBS-Rsn2, their effects on the surface modification of PDMS was assessed using contact angle measurements to confirm that their surface activity is not hindered by the addition of short peptide the N-terminus of the protein. For this, each IBS-Rsn2 was used to coat PDMS and the water contact angle of these coated surfaces measured. Rsn2, uncoated PDMS and silanized glass were used as positive and negative controls. The results obtained showed that all the IBS-Rsn2 proteins could reduce the surface tension by coating a hydrophobic surface.

The contact angle measurement is there to show that the IBS-Rsn2s all stick to the surface, but approximately equal loading is only assumed, but not measured. The results of the contact angle measurements suggests that the angle of contact could be changed by the different natures of the IBSs themselves.

For future work, it would be better to quantitatively measure the coverage of different Rsn2 mutants at the surface. For achieving this, specially designed antibodies should be used against specific IBS-Rsn2 coated surface, to prove the presence of IBS-Rsn2 on surface. Upon confirmation of the presence of IBS-Rsn2, it would be seeded with cells and if the cells adhesion is restricted on the conjugated antibody-IBS-Rsn2 surface compared to IBS-Rsn2 surface, then it would suggest that IBS-Rsn2 is available for cell attachment.

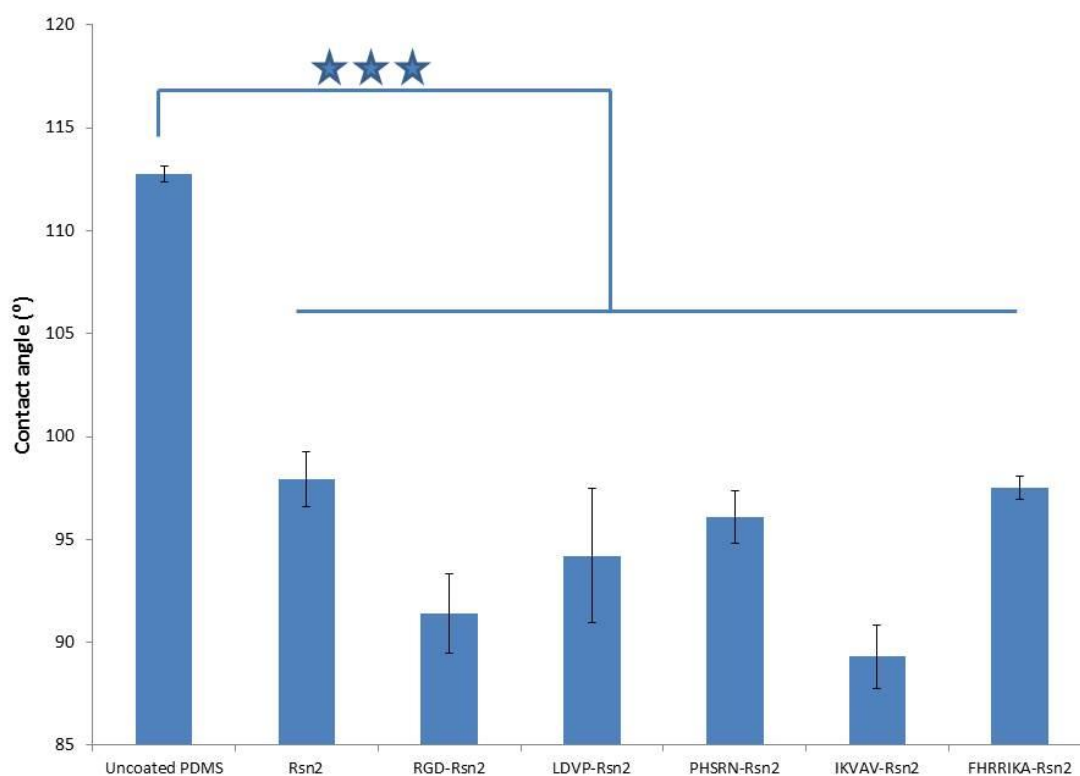


Figure 3-11 Graphical representation of the contact angle measurement of the droplet of water on various IBS-Rsn2 coated PDMS surface. The average water contact angle was used along with \pm SD on different IBS-Rsn2 coated PDMS surfaces. Measurements were made immediately after coating a PDMS surface with the proteins. (n=3 repeats).

3.4.4 Fibroblast cell culture on different IBS-Rsn2 coated PDMS

Once it was confirmed that the IBS-Rsn2 proteins coat PDMS substrates, as judged by the reductions in surface tension seen, the next step was to check whether the IBS were available to bind to cells or were concealed in the protein surface structure. To investigate this, IBS-Rsn2 coated PDMS samples were seeded with fibroblast (hTert) cells, cultured for 24 hours and the cell density calculated. A striking difference in cell density was seen between uncoated PDMS and Rsn2-coated samples, as seen earlier in cell patterning chapter. The cell densities on each of the IBS-Rsn2 were also higher than on the uncoated coated PDMS and even exceeded the densities seen with Rsn2 (Figure 3-12) Thus, since the cell densities seen were higher for all the IBS-Rsn2 coated samples than for Rsn2 alone, it seems likely that the IBS are available for cell binding and exert a positive effect.

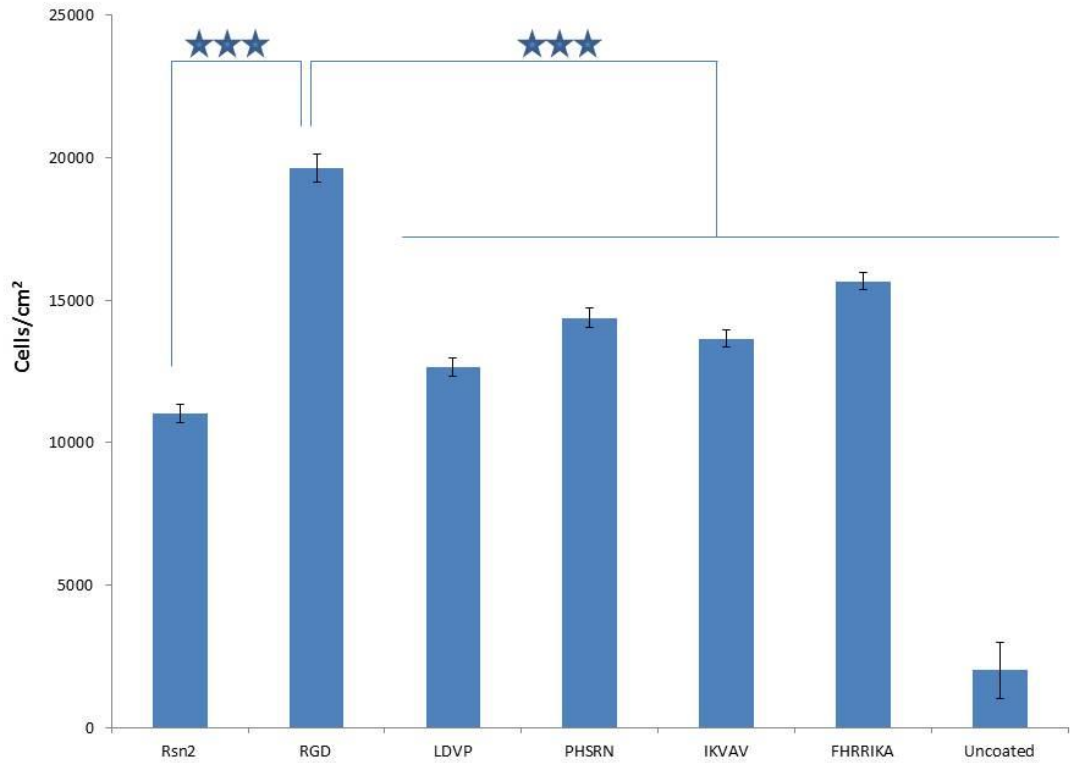
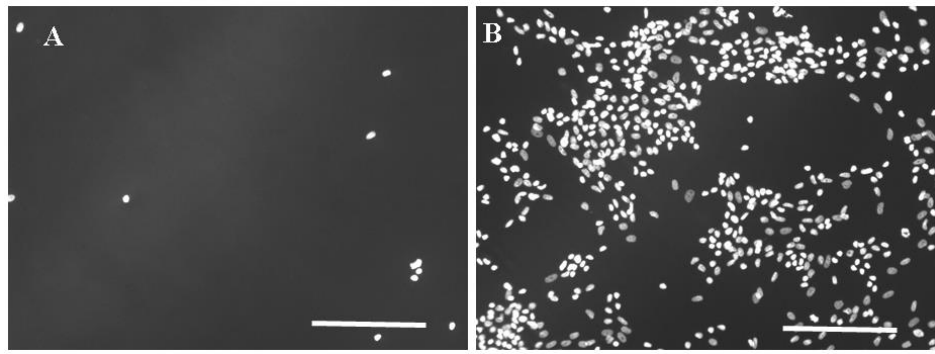


Figure 3-12 Cell density of fibroblast cells cultured on various IBS-Rsn2. Fibroblast cells were cultured on protein coated PDMS surface for 24 hours and cell density calculated following immunofluorescence microscopy for nucleus staining. (A) A representative image of nucleus staining on un-coated PDMS surface. (B) A representative image of nucleus staining on RGD-Rsn2 coated PDMS surface. (C) A graphical representation of cell density obtained in different IBS-Rsn2. RGD-Rsn2 is significantly different from all the other samples. Stars indicate significant differences between the different coatings as determined by paired sample T-test, Where $***p < 0.001$. The bars indicate standard deviation (n=3 repeats)

3.4.5 Osteoblast cell culture on IBS-Rsn2 coated PDMS

Having established that all the IBS-Rsn2 proteins could promote fibroblast cell adhesion on PDMS, coated PDMS substrates were cultured with primary calvaria bone cells.

As the IBS-Rsn2 were designed to support nerve and osteoblast cells, IBS-Rsn2 proteins expected to promote nerve cell outgrowth by binding neuron specific integrin ($\alpha_1\beta_1$, $\alpha_3\beta_1$ and $\alpha_5\beta_1$) were passed to a co-worker, Dr Kredi, who showed that IKVAV-Rsn2 improved nerve outgrowth from rat dorsal root ganglion explants (Kredi, 2015). For the osteoblast cell culture work, IBS-Rsn2 incorporating either RGD, or the PHSRN and FHRRIKA sequences that are ligands for the osteoblast specific integrins ($\alpha_3\beta_1$ and $\alpha_v\beta_3$) were used to investigate their effects on osteoblast adhesion and differentiation.

3.4.5.1 Osteoblasts after 4 hrs in culture

After 4 hrs (day 0) in culture, cells seeded on RGD-Rsn2, RGD-Rsn2:PHSRN-Rsn2 (1:1), and RGD-Rsn2:PHSRN-Rsn2: FHRRIKA-Rsn2 (1:1:1) had adhered to the surface and displayed extended morphologies compared to the control coatings (glass and Rsn2). In contrast, Rsn2, PHSRN-Rsn2, FHRRIKA-Rsn2, RGD-Rsn2:FHRRIKA-Rsn2 (1:1) and PHSRN-Rsn2:FHRRIKA-Rsn2 (1:1) did not promote osteoblasts spreading at this time point (Figure 3-13).

This qualitative analysis is supported by comparing the cell densities and the average number of focal adhesions per cell (Figure 3-14 and Figure 3-15). The number of focal adhesions seen per cell was assessed to establish which of the surfaces tested provided the best environment to support cell attachment. The highest number of focal cell adhesions per cell formed on RGD-Rsn2 and RGD-Rsn2: PHSRN-Rsn2: FHRRIKA-Rsn2 (1:1:1) coated surfaces. This was followed by the RGD-Rsn2:PHSRN-Rsn2 (1:1) and the other coatings did not support the formation of focal adhesions by osteoblasts.

The results can only enlighten about the osteoblast's preferences for the formation of the initial cell attachments. The next step was to see which coating provided the best surface for osteoblast development after longer time in culture.

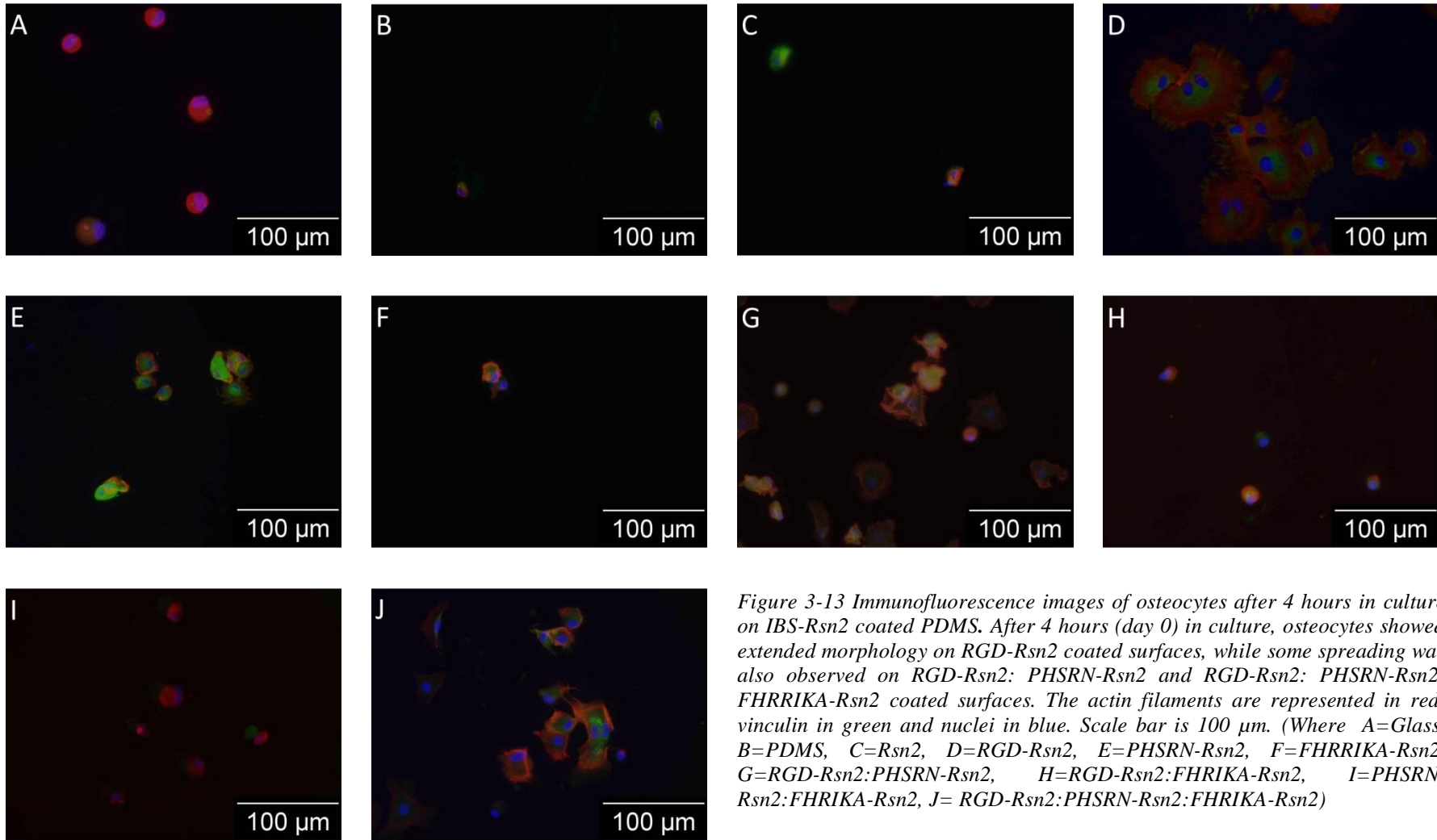


Figure 3-13 Immunofluorescence images of osteocytes after 4 hours in culture on IBS-Rsn2 coated PDMS. After 4 hours (day 0) in culture, osteocytes showed extended morphology on RGD-Rsn2 coated surfaces, while some spreading was also observed on RGD-Rsn2: PHSRN-Rsn2 and RGD-Rsn2: PHSRN-Rsn2: FHRIKA-Rsn2 coated surfaces. The actin filaments are represented in red, vinculin in green and nuclei in blue. Scale bar is 100 μ m. (Where A=Glass, B=PDMS, C=Rsn2, D=RGD-Rsn2, E=PHSRN-Rsn2, F=FHRIKA-Rsn2, G=RGD-Rsn2:PHSRN-Rsn2, H=RGD-Rsn2:FHRIKA-Rsn2, I=PHSRN-Rsn2:FHRIKA-Rsn2, J= RGD-Rsn2:PHSRN-Rsn2:FHRIKA-Rsn2)

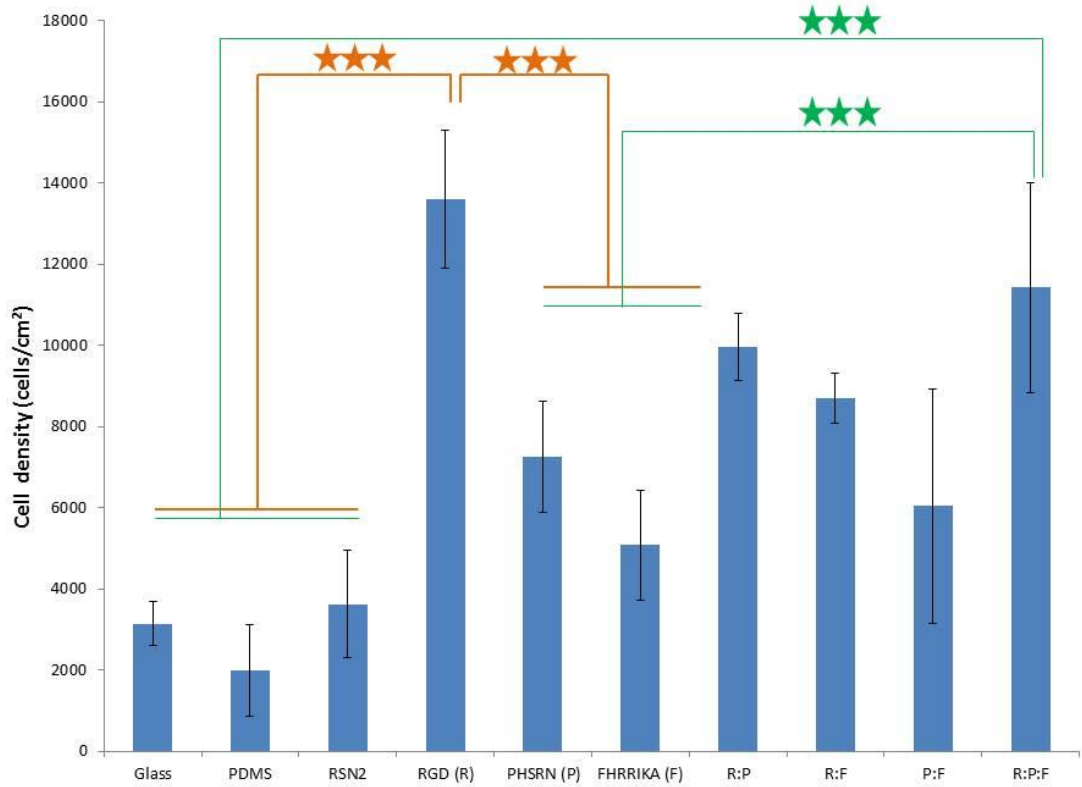


Figure 3-14 Density of cells on various IBS-Rsn2 coated surface after 4 hours in culture. The graph represents the average number of osteoblasts cells/cm² after 4 hours in culture on Glass and Rsn2 - positive control, PDMS - negative control, and test - RGD-Rsn2 (R) coated PDMS, PHSRN-Rsn2 (P) coated PDMS, FHRIKA-Rsn2 (F) coated PDMS, R:P (RGD-Rsn2:PHSRN-Rsn2) coated PDMS, R:F (RGD-Rsn2:FHRIKA-Rsn2) coated PDMS, P:F (PHSRN-Rsn2: FHRIKA-Rsn2) coated PDMS and R:P:F (RGD-Rsn2:PHSRN-Rsn2:FHRIKA-Rsn2) coated PDMS. RGD-Rsn2 and R:P:F-Rsn2 are significantly different from all the other samples. Stars indicate significant differences between the different coatings as determined by paired sample T-test, Where ***p<0.001. The bars indicate standard deviation (n=3 biological repeats).

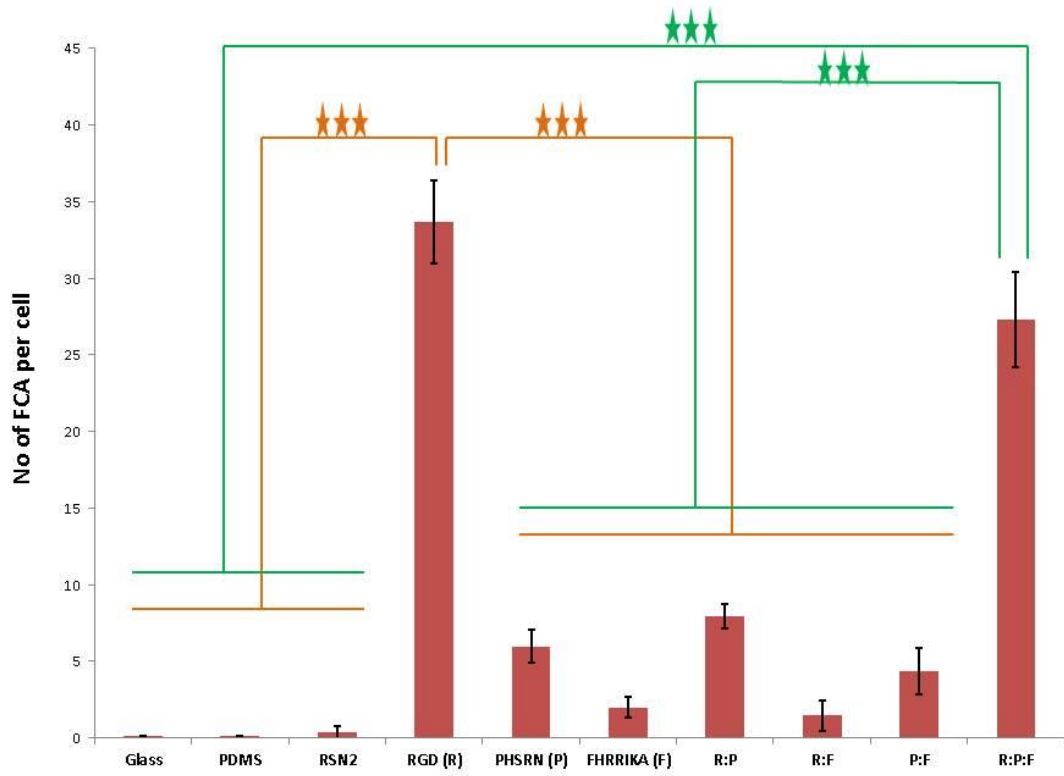


Figure 3-15 Graphical representation of the quantified number of focal adhesion formed per cells on various IBS-Rsn2 coated surfaces after 4 hours in culture. The graph represents the number of FCA per cells after 4 hours in culture on Glass and Rsn2 - positive control, PDMS - negative control, and test - RGD-Rsn2 (R) coated PDMS, PHSRN-Rsn2 (P) coated PDMS, FHRIKA-Rsn2 (F) coated PDMS, R:P (RGD-Rsn2:PHSRN-Rsn2) coated PDMS, R:F (RGD-Rsn2:FHRIKA-Rsn2) coated PDMS, P:F (PHSRN-Rsn2: FHRIKA-Rsn2) coated PDMS and R:P:F (RGD-Rsn2:PHSRN-Rsn2:FHRIKA-Rsn2) coated PDMS. RGD-Rsn2 and R:P:F-Rsn2 are significantly different from all the other samples. Stars indicate significant differences between the different coatings as determined by paired sample T-test, Where *** $p < 0.001$. The bars indicate standard deviation ($n=3$ biological repeats).

3.4.5.2 Osteoblasts after 1 and 7 days in culture

All osteoblast cells were cultured on different IBS-Rsn2 coated PDMS for either one or seven days and compared with bare glass, PDMS and Rsn2-coated PDMS controls. The cell density, formation of focal adhesions, and morphology of the osteoblasts varied considerably on the different coatings.

At the 1 day time point, the highest cell density, most extended morphology, and highest number of focal adhesions per cell were observed on RGD-Rsn2 and RGD-Rsn2:PHSRN-Rsn2:FHRRIKA-Rsn2 (1:1:1) coated surfaces. Higher cell density with some cell spreading and formation of focal cell adhesions was also observed on RGD-Rsn2:PHSRN-Rsn2 (1:1) and RGD-Rsn2:FHRRIKA-Rsn2 (1:1), compared to the glass and Rsn2 controls. In contrast, lower cell density; focal cell adhesions and cell spreading were observed on PHSRN-Rsn2, FHRRIKA-Rsn2, and PHSRN-Rsn2: FHRRIKA-Rsn2 (1:1) coated surfaces (Figure 3-16 to Figure 3-18).

After 7 days in culture, the highest cell densities were observed in RGD-Rsn2 and RGD-Rsn2: PHSRN-Rsn2: FHRRIKA-Rsn2 (1:1:1), followed by RGD-Rsn2: FHRRIKA-Rsn2 (1:1). Quantification of focal cell adhesions were not made as two samples had such a high cell density that cells had become confluent on the surface and even overgrown each other. Vinculin staining revealed the formation of focal cell adhesions on RGD-Rsn2: PHSRN-Rsn2 (1:1); RGD-Rsn2: FHRRIKA-Rsn2 (1:1); PHSRN-Rsn2: FHRRIKA-Rsn2 (1:1) as well as FHRRIKA-Rsn2 coated samples (Figure 3-19 and Figure 3-20).

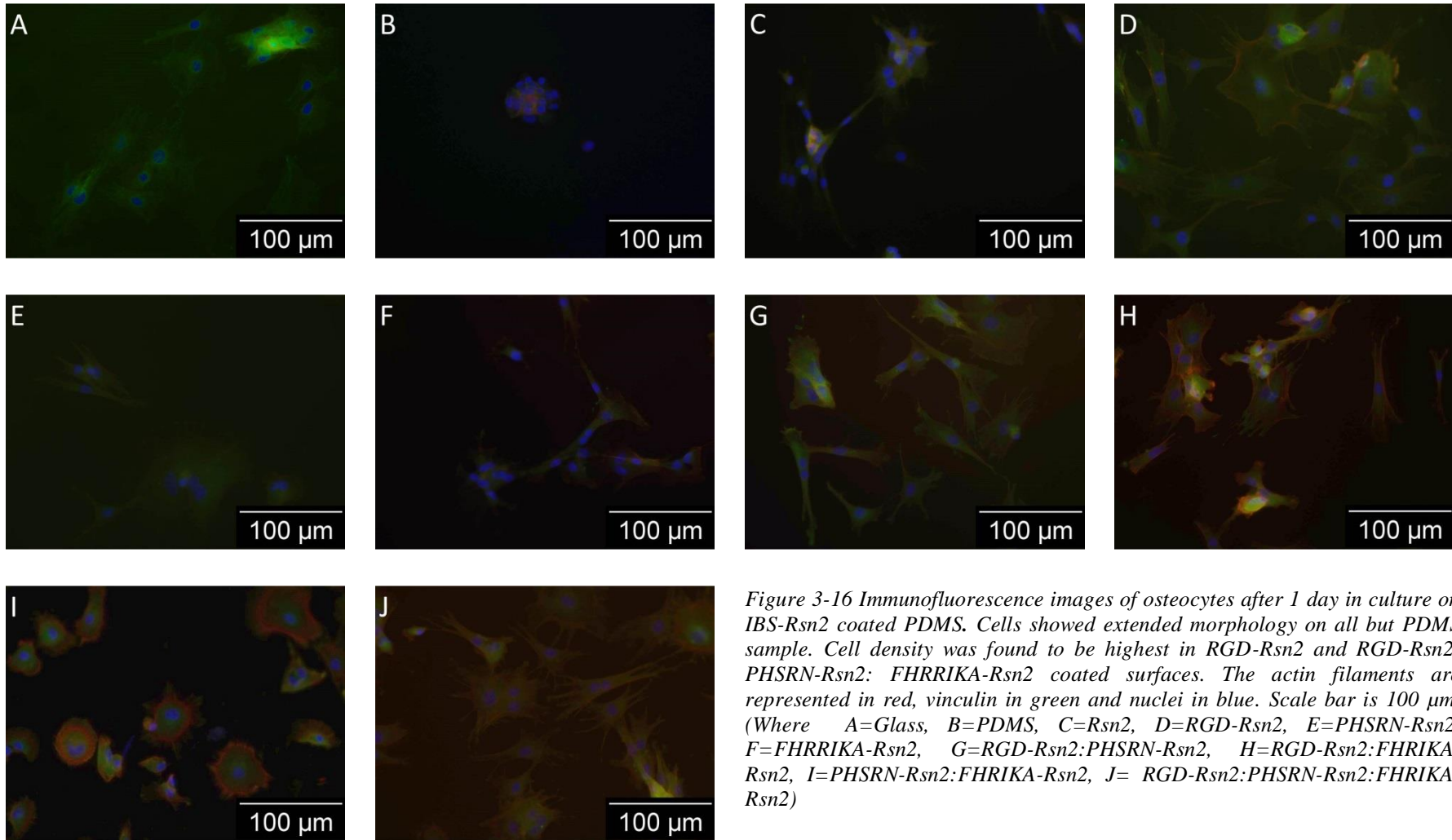


Figure 3-16 Immunofluorescence images of osteocytes after 1 day in culture on IBS-Rsn2 coated PDMS. Cells showed extended morphology on all but PDMS sample. Cell density was found to be highest in RGD-Rsn2 and RGD-Rsn2:PHSRN-Rsn2: FHRRIKA-Rsn2 coated surfaces. The actin filaments are represented in red, vinculin in green and nuclei in blue. Scale bar is 100 μm . (Where A=Glass, B=PDMS, C=Rsn2, D=RGD-Rsn2, E=PHSRN-Rsn2, F=FHRRIKA-Rsn2, G=RGD-Rsn2:PHSRN-Rsn2, H=RGD-Rsn2:FHRIKA-Rsn2, I=PHSRN-Rsn2:FHRIKA-Rsn2, J= RGD-Rsn2:PHSRN-Rsn2:FHRIKA-Rsn2)

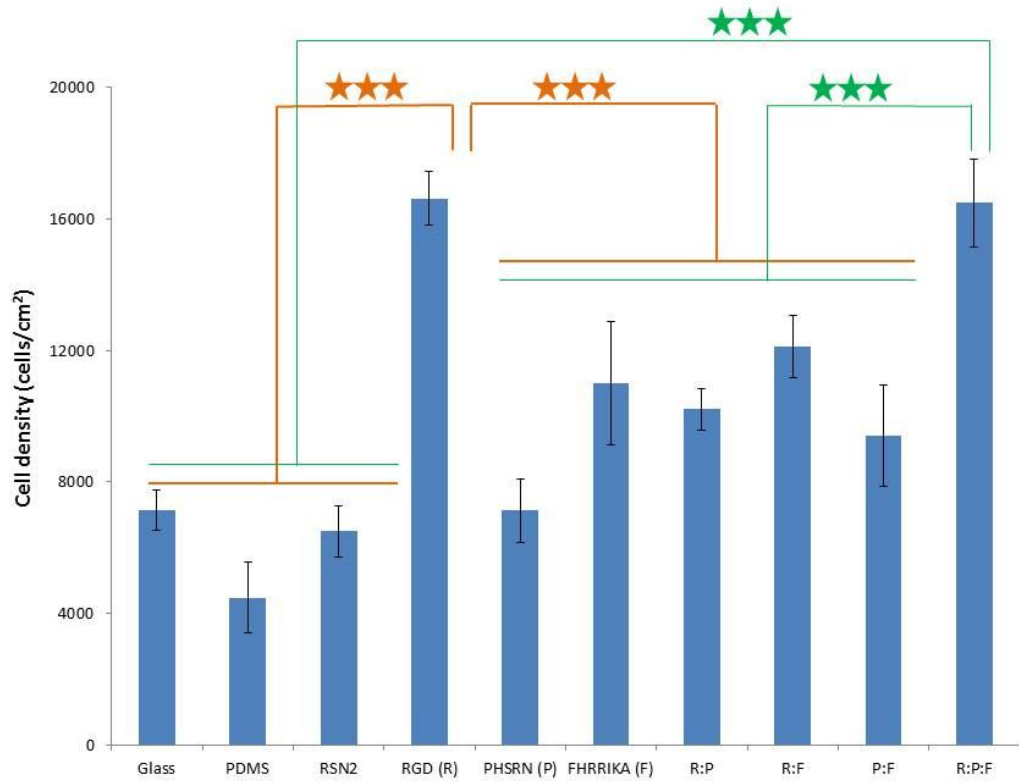


Figure 3-17 Density of cells on various IBS-Rsn2 coated surface after 1 day in culture. The graph represents the average number of osteoblasts cells/cm² after 1 days in culture on Glass and Rsn2 - positive control, PDMS - negative control, and test - RGD-Rsn2 (R) coated PDMS, PHSRN-Rsn2 (P) coated PDMS, FHRRIKA-Rsn2 (F) coated PDMS, R:P (RGD-Rsn2:PHSRN-Rsn2) coated PDMS, R:F (RGD-Rsn2:FHRRIKA-Rsn2) coated PDMS, P:F (PHSRN-Rsn2: FHRRIKA-Rsn2) coated PDMS and R:P:F (RGD-Rsn2:PHSRN-Rsn2:FHRRIKA-Rsn2) coated PDMS. RGD-Rsn2 and R:P:F-Rsn2 are significantly different from all the other samples. Stars indicate significant differences between the different coatings as determined by paired sample T-test, Where *** $p < 0.001$. The bars indicate standard deviation ($n=3$ biological repeats).

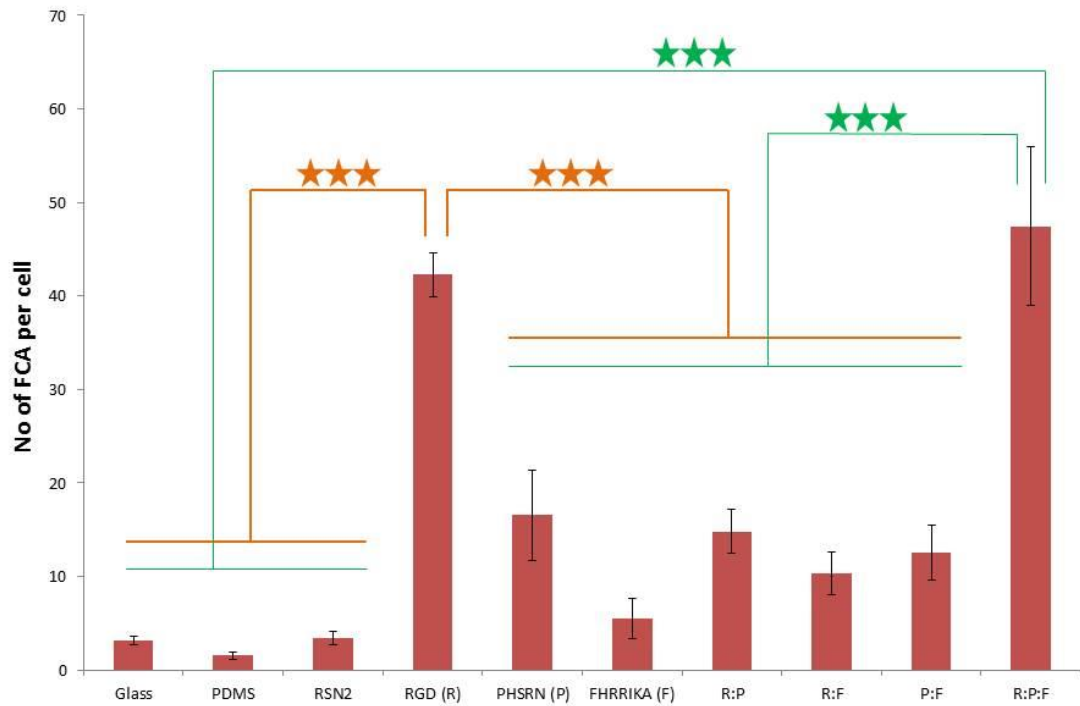


Figure 3-18 Graphical representation of the quantified number of FCA per cells on various IBS-Rsn2 coated surfaces after 1 day in culture. The graph represents the number of FCA per cells after 1 day in culture on Glass and Rsn2 - positive control, PDMS - negative control, and test - RGD-Rsn2 (R) coated PDMS, PHSRN-Rsn2 (P) coated PDMS, FHRRIKA-Rsn2 (F) coated PDMS, R:P (RGD-Rsn2:PHSRN-Rsn2) coated PDMS, R:F (RGD-Rsn2:FHRRIKA-Rsn2) coated PDMS, P:F (PHSRN-Rsn2: FHRRIKA-Rsn2) coated PDMS and R:P:F (RGD-Rsn2:PHSRN-Rsn2:FHRRIKA-Rsn2) coated PDMS RGD-Rsn2 and R:P:F-Rsn2 are significantly different from all the other samples. Stars indicate significant differences between the different coatings as determined by paired sample T-test, Where *** $p < 0.001$. The bars indicate standard deviation ($n=3$ biological repeats).

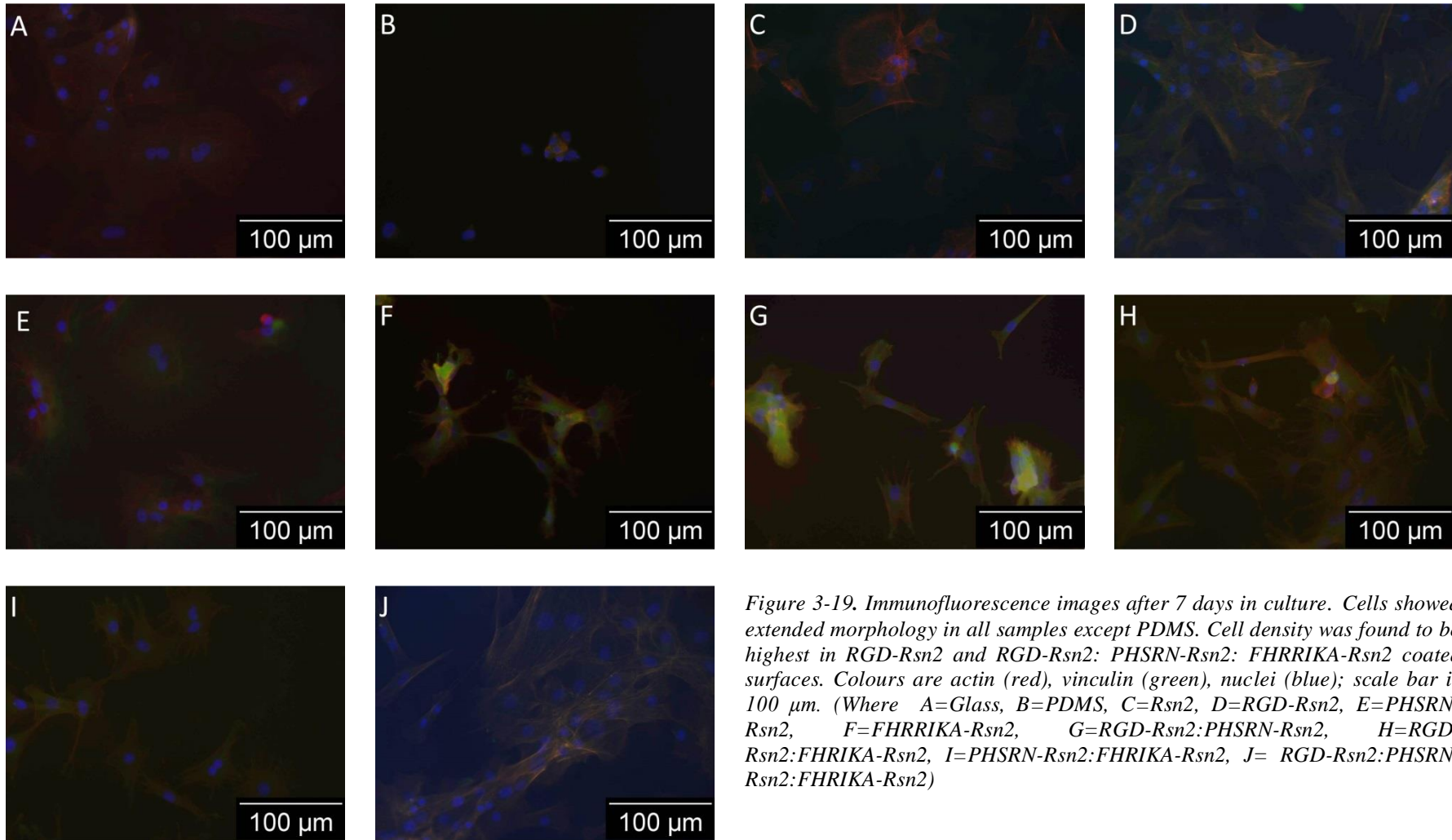


Figure 3-19. Immunofluorescence images after 7 days in culture. Cells showed extended morphology in all samples except PDMS. Cell density was found to be highest in RGD-Rsn2 and RGD-Rsn2: PHSRN-Rsn2: FHRRIKA-Rsn2 coated surfaces. Colours are actin (red), vinculin (green), nuclei (blue); scale bar is 100 μm . (Where A=Glass, B=PDMS, C=Rsn2, D=RGD-Rsn2, E=PHSRN-Rsn2, F=FHRRIKA-Rsn2, G=RGD-Rsn2:PHSRN-Rsn2, H=RGD-Rsn2:FHRIKA-Rsn2, I=PHSRN-Rsn2:FHRIKA-Rsn2, J= RGD-Rsn2:PHSRN-Rsn2:FHRIKA-Rsn2)

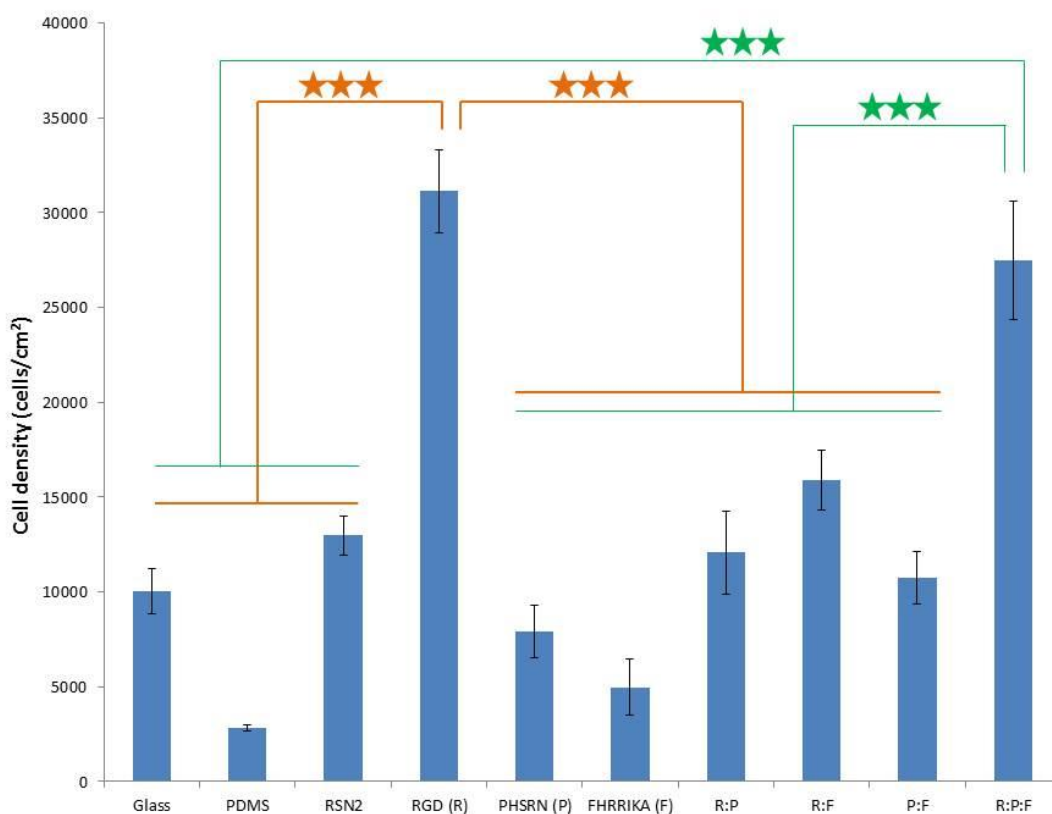


Figure 3-20 Density of cells on various IBS-Rsn2 coated surface after 7 days in culture. The graph represents the average number of osteoblasts cells/cm² after 7days in culture on Glass and Rsn2 - positive controls, PDMS - negative control, and test - RGD-Rsn2 (R) coated PDMS, PHSRN-Rsn2 (P) coated PDMS, FHRRIKA-Rsn2 (F) coated PDMS, R:P (RGD-Rsn2:PHSRN-Rsn2) coated PDMS, R:F (RGD-Rsn2:FHRRIKA-Rsn2) coated PDMS, P:F (PHSRN-Rsn2: FHRRIKA-Rsn2) coated PDMS and R:P:F (RGD-Rsn2:PHSRN-Rsn2:FHRRIKA-Rsn2) coated PDMS. RGD-Rsn2 and R:P:F-Rsn2 are significantly different from all the other samples. Stars indicate significant differences between the different coatings as determined by paired sample T-test, Where *** $p < 0.001$. The bars indicate standard deviation ($n=3$ biological repeats)

3.4.6 Comparison of the cell density of osteoblasts at various time points

The cell densities of the osteoblasts on different IBS-Rsn2 coated PDMS were compared at the different time points assessed and the data are shown in Figure 3-21. When compared to bare PDMS, PDMS coated with Rsn2 alone and with all the IBS-Rsn2 proteins tested promoted cell adhesion at all the time points. The initial densities of attached cells (after 4 hours in culture) were substantially higher on RGD-Rsn2 coated surfaces than for most of the other IBS, except for the mixed RGD-Rsn2:PHSRN-Rsn2:FHRRIKA-Rsn2 (1:1:1) surface. This early time point was used to establish which IBS is best situated for osteocyte adhesion. The more prolonged cultures, after 1 day and

7 days, also showed the same trend in cell density, suggesting osteoblasts preference to form attachment on the RGD-Rsn2 and RGD-Rsn2:PHSRN-Rsn2:FHRRRIKA-Rsn2 (1:1:1) coated surface compared to other IBS-Rsn2.

The RGD-Rsn2 and RGD-Rsn2:PHSRN-Rsn2:FHRRRIKA-Rsn2 coated surfaces were not only preferred by osteoblasts for cell adhesion, but also promoted growth and cell division compared to other IBS-Rsn2 coated surfaces as can be seen by comparing the cell densities in Figure 3-17 and Figure 3-20. In contrast, on the PHSRN-Rsn2, FHRRRIKA-Rsn2 and PHSRN-Rsn2:FHRRRIKA-Rsn2 coated surfaces the cell density did not increase.

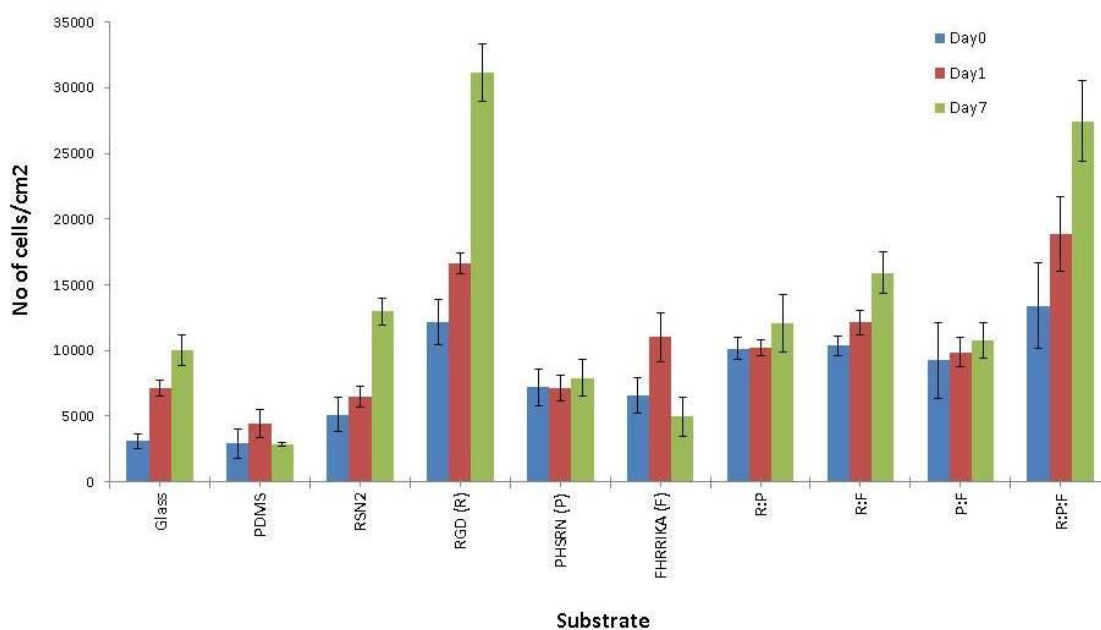


Figure 3-21 Density of cells on day0, day1 and day7. The graph represents the average number of osteoblasts cells/cm² after 0, 1 and 7days of culture on Glass and Rsn2 combining the data from figures 23, 25 and 27. In sequence the data is plotted for positive controls, PDMS - negative control, and test - RGD-Rsn2 (R) coated PDMS, PHSRN-Rsn2 (P) coated PDMS, FHRRRIKA-Rsn2 (F) coated PDMS, R:P (RGD-Rsn2:PHSRN-Rsn2) coated PDMS, R:F (RGD-Rsn2:FHRRRIKA-Rsn2) coated PDMS, P:F (PHSRN-Rsn2: FHRRRIKA-Rsn2) coated PDMS and R:P:F (RGD-Rsn2:PHSRN-Rsn2:FHRRRIKA-Rsn2) coated PDMS. The bars indicate standard deviation.

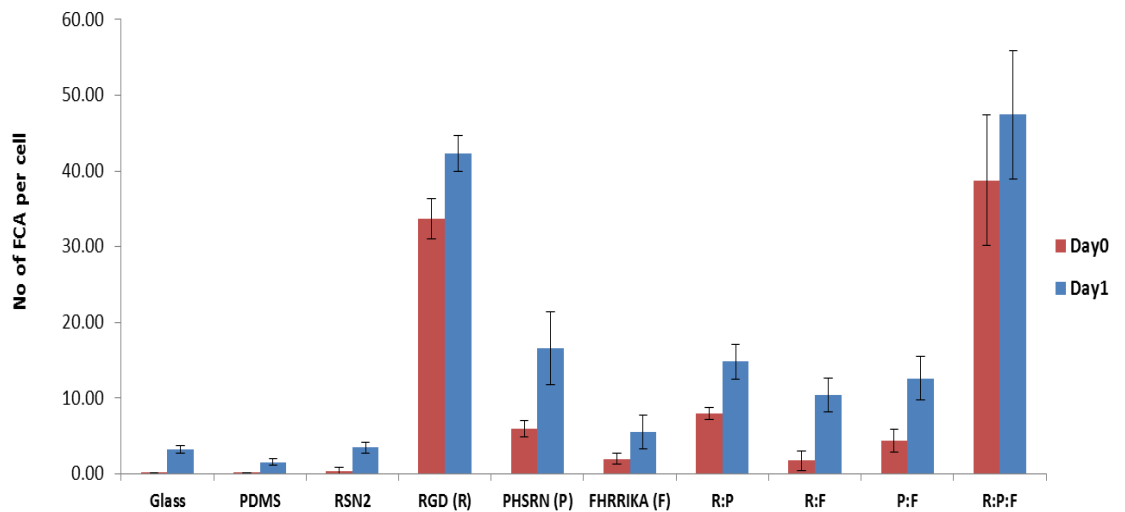


Figure 3-22. Quantification of the average number of focal cell adhesions per cell on day0 and day1. The graph represents the average number of focal cell adhesions per cell after 0 and 1 days of culture on Glass and Rsn2- positive controls, PDMS - negative control, and test - RGD-Rsn2 (R) coated PDMS, PHSRN-Rsn2 (P) coated PDMS, FHRRIKA-Rsn2 (F) coated PDMS, R:P (RGD-Rsn2:PHSRN-Rsn2) coated PDMS, R:F (RGD-Rsn2:FHRRIKA-Rsn2) coated PDMS, P:F (PHSRN-Rsn2: FHRRIKA-Rsn2) coated PDMS and R:P:F (RGD-Rsn2:PHSRN-Rsn2:FHRRIKA-Rsn2) coated PDMS. The bars indicate standard deviation.

3.4.7 Osteopontin and Osteocalcin expression

All the protein coated samples were cultured for 28 days and were immunolabelled to visualise the expression of the bone cell marker proteins OPN and OCN. Although cells grown on all the IBS-Rsn2 coated samples showed expression of OPN, RGD-Rsn2:PHSRN-Rsn2: FHRRIKA-Rsn2 (1:1:1) coated sample showed the most prominent expression over all the other coatings (Figure 3-23).

Similarly, the determination of expression of OCN in all samples showed varying levels of expression across all the samples. OCN expressions level was also most prominent in RGD-Rsn2: PHSRN-Rsn2: FHRRIKA-Rsn2 coated samples compared to all the other coatings. The immunofluorescence images of all the samples stained for OCN are shown in Figure 3-24.

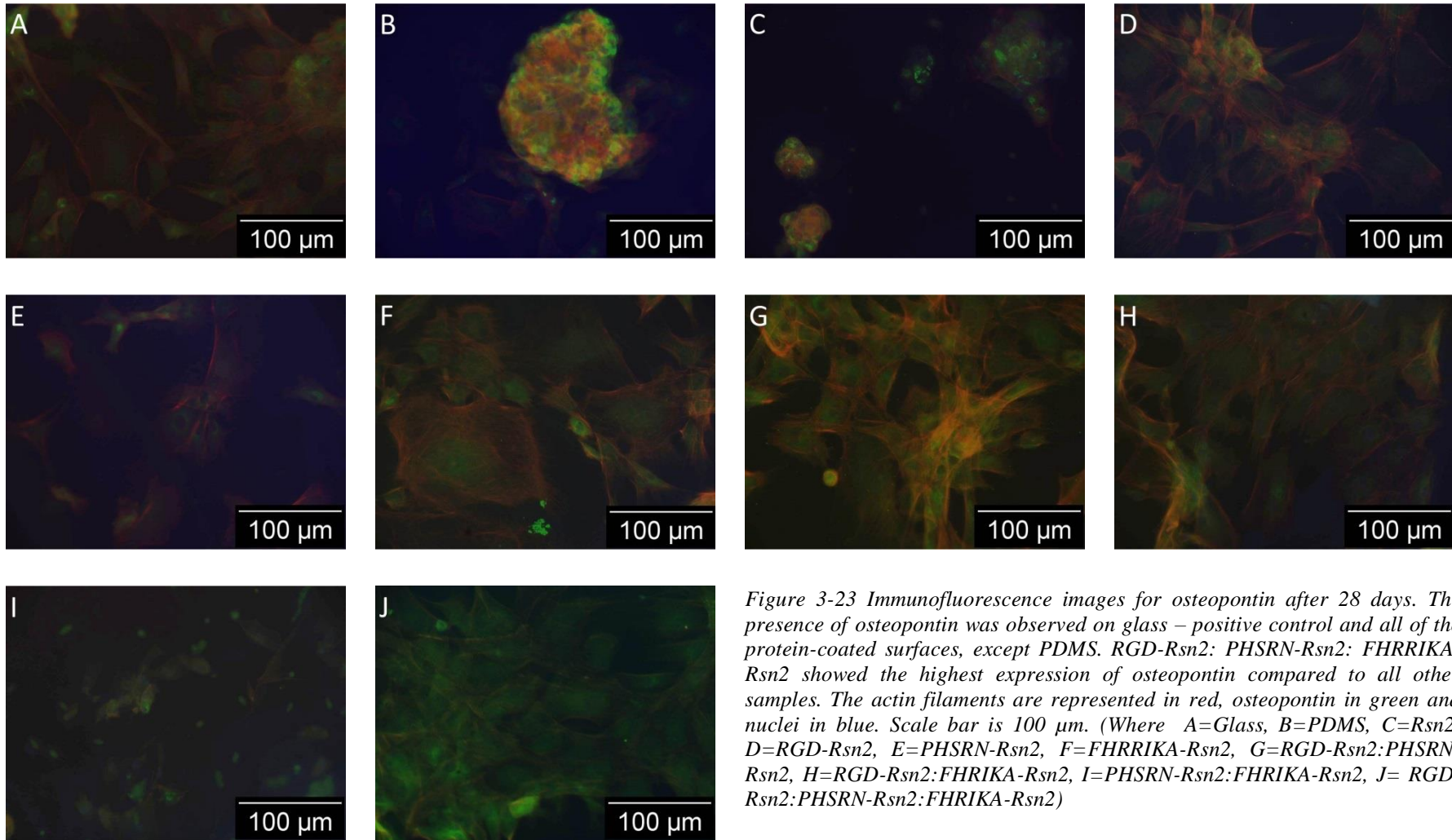


Figure 3-23 Immunofluorescence images for osteopontin after 28 days. The presence of osteopontin was observed on glass – positive control and all of the protein-coated surfaces, except PDMS. RGD-Rsn2: PHSRN-Rsn2: FHRIKA-Rsn2 showed the highest expression of osteopontin compared to all other samples. The actin filaments are represented in red, osteopontin in green and nuclei in blue. Scale bar is 100 μm. (Where A=Glass, B=PDMS, C=Rsn2, D=RGD-Rsn2, E=PHSRN-Rsn2, F=FHRIKA-Rsn2, G=RGD-Rsn2:PHSRN-Rsn2, H=RGD-Rsn2:FHRIKA-Rsn2, I=PHSRN-Rsn2:FHRIKA-Rsn2, J= RGD-Rsn2:PHSRN-Rsn2:FHRIKA-Rsn2)

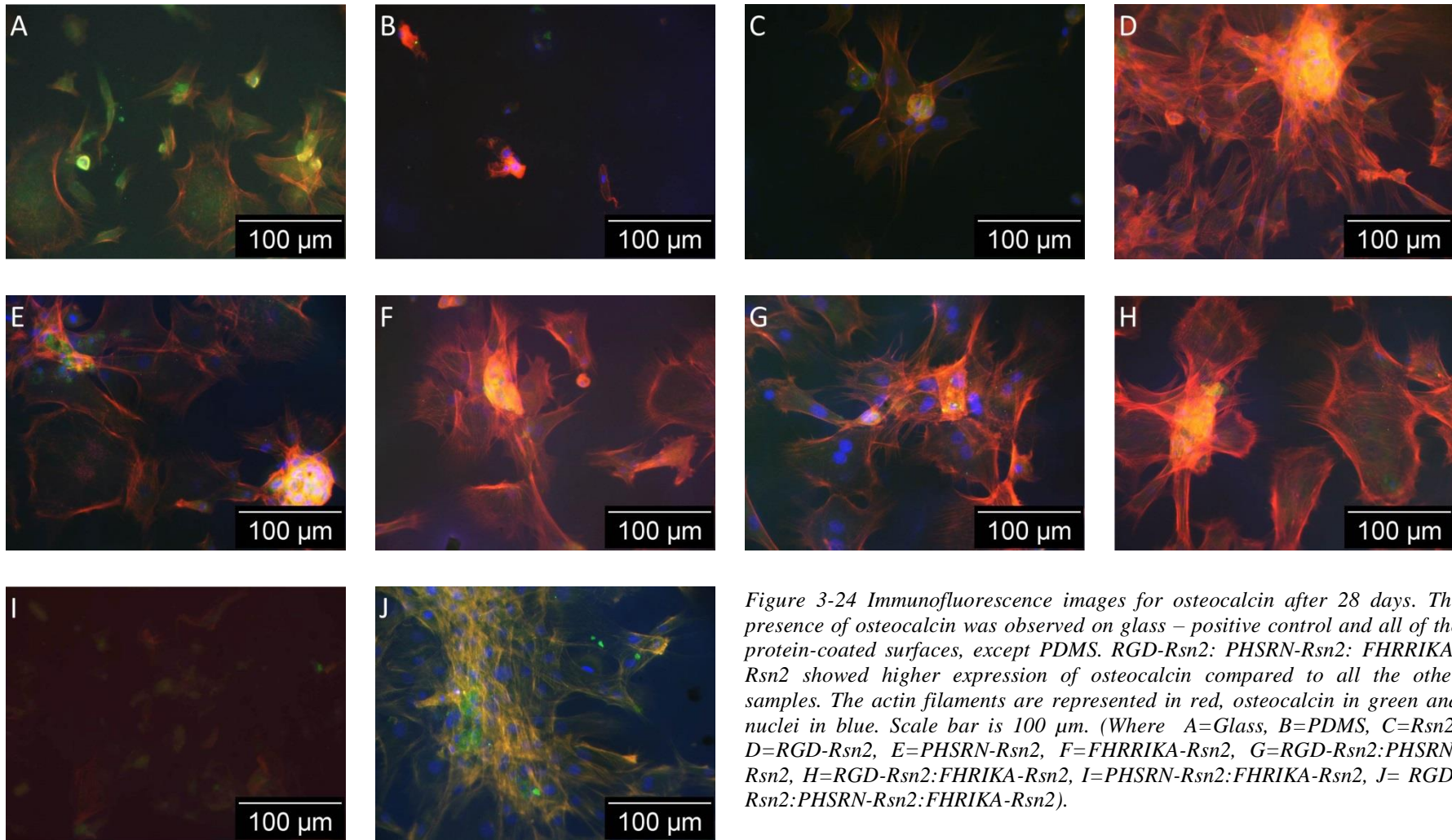


Figure 3-24 Immunofluorescence images for osteocalcin after 28 days. The presence of osteocalcin was observed on glass – positive control and all of the protein-coated surfaces, except PDMS. RGD-Rsn2: PHSRN-Rsn2: FHRIKA-Rsn2 showed higher expression of osteocalcin compared to all the other samples. The actin filaments are represented in red, osteocalcin in green and nuclei in blue. Scale bar is 100 μm . (Where A=Glass, B=PDMS, C=Rsn2, D=RGD-Rsn2, E=PHSRN-Rsn2, F=FHRIKA-Rsn2, G=RGD-Rsn2:PHSRN-Rsn2, H=RGD-Rsn2:FHRIKA-Rsn2, I=PHSRN-Rsn2:FHRIKA-Rsn2, J= RGD-Rsn2:PHSRN-Rsn2:FHRIKA-Rsn2).

3.5 Discussion

Biomaterials have a vital role in tissue engineering as they provide a surface where cells can attach, develop and proliferate. Surface modifications are routinely made to augment the biocompatibility of scaffolds (Chan and Leong, 2008b). For this, usually various bioactive molecules or growth factors are introduced to control and enhance cell interactions, proliferation, differentiation and generation of ECM (Chan and Leong, 2008b).

Bioactive molecules can be presented on the surface by adsorption or via covalent modifications, made after plasma treatment. The bioactive molecules used can either be whole ECM protein or short cell adhesive peptide sequences. Moreover, during the modification process, short peptides tend to be more stable and can be easily mass-produced in laboratories (Tallawi et al., 2015). Thus short biomimetic peptides were selected for making fusion constructs with Rsn2 using recombinant protein technology.

Rsn2 through its surface activity adsorbs to scaffold surfaces (as shown and discussed in chapter 2) allowing the establishment of a simple and easy to replicate method to bio-functionalize a surface with accessible active sites. IBS-Rsn2 constructs were designed, successfully expressed, and the proteins isolated and purified. These IBS-Rsn2 proteins all proved to be surface active as judged by contact angle measurements and the addition of short peptides to the N-terminus of Rsn2 did not significantly affect its functionality.

Having confirmed that all of the IBS-Rsn2 were surface active, they were used to coat PDMS substrates and seeded with h-Tert cells, and then cultured for 24 hours discover whether the IBS presented on Rsn2 were available for cell attachment. The literature reveal that not all the proteins containing RGD sequence can mediate cell attachment, and only a few of them can do so (Ruoslahti, 1996a). This is because the RGD sequence might not be presented on the surface of protein and so be available for integrin binding (Pierschbacher and Ruoslahti, 1987). The h-Tert cell results confirmed that all the IBS presented on Rsn2 were available for attachment as the cell density on all of the IBS-Rsn2 coated substrates came out to be higher than the cell densities observed on Rsn2 alone coated surfaces (Figure 3-21) suggesting that the N-terminus of Rsn2 remains flexible and tolerates the addition of short peptides (Vance, 2012, Mackenzie et al., 2009). Thus the designed constructs were functional and were then used to study which IBS promoted osteoblast adhesion, proliferation and differentiation in a manner similar to Dalby et al (Dalby et al., 2007).

Interactions between osteoblasts and the ECM of bone that are mediated by integrin receptors are important determinants of the cells proliferation, differentiation and expression of osteocalcin (OCN) and osteopontin (OPN) (Bennett et al., 2001b)

To test the ability of different IBS-Rsn2 coated surfaces to influence the differentiation of cells cultured on them, primary bone cells were used since they are both more differentiable than fibroblasts and express a different subset of integrins. Out of several IBS-Rsn2 tested, RGD-Rsn2 and the mixture of RGD-Rsn2:PHSRN-Rsn2:FHRRIKA-Rsn2 (1:1:1) outperformed others in initial cell adhesion, cell spreading and proliferation.

The work presented in this chapter agrees with other studies using RGD, the fibronectin-derived IBS, favoured cell attachment from day 0 and also showed enhanced cell spreading and proliferation, along with OPN and OCN expression after day 28. These observations are in line with observations made by Fraioli et al., who used peptidomimetic ligands to functionalise surfaces to promote $\alpha v \beta 3$ or $\alpha 5 \beta 1$ integrin mediated osteoblast adhesion. They observed enhanced cell attachment and spreading along with cell proliferation and higher mineralization on the surfaces coated with the ligands (Fraoli et al., 2015). Similarly, Wang et al observed that $\alpha 5 \beta 1$ integrin is the dominant integrin that initiates the osteoblasts attachment with the RGD-cell binding site on fibronectin. (Wang et al., 2010). A similar observation has been made by Dr. Roberts in our lab, who showed that upon interaction of mesenchymal stem cells with RGD-immobilised surface, favoured bone cell differentiation, and enhanced OPN and OCN expression (Roberts, 2013).

The obtained results of RGD as a cell adhesive peptide are in agreement with some other studies, where chemically attached RGD has been shown to favour initial cell attachment, spreading and mineralisation of osteoblast cells (Beuvelot et al., 2009, Bell et al., 2011, Hu et al., 2003).

All this observation made earlier and in this thesis proves that functionalising surface with RGD will promote bone cell attachment and mineralisation.

The results obtained in this thesis also suggest that mimicking ECM by presenting more than one type of IBS (e.g. sample 10 R:P:F) resulted in enhanced focal adhesion formation, along with expression of OCN and OPN. These results are in agreement with the results of cell binding assays conducted by Gronthos et al. who showed that osteoblasts have the ability to adhere to different ECM proteins with a preference to fibronectin over collagen, vitronectin and laminin (Gronthos et al., 1997). The findings

presented by Healy et al. also showed that by presenting more than one type of IBS together promoted cell spreading and mineralization, mediated by the collagen and vitronectin receptors (Healy et al., 1999a)

Many studies have been conducted using RGD in combination with other peptides, to mimic the ECM, and have found to have positively affected osteoblasts' development and mineralisation. One such study used cell-binding peptide RGD along with the synergistic peptide PHSRN, found in fibronectin, and saw enhanced differentiation of, and calcium deposition by the cultured osteoblasts (Nakaoka et al., 2013, García et al., 2002, Petrie et al., 2006).

Another study showed that rat calvaria cells cultured on immobilised biomimetic peptide surfaces had a preference for RGD:FHRRIKA. In that study RGD alone showed the highest number of focal adhesions per cell formed after 4 hours in culture, while RGD:FHRRIKA surface showed mineralisation of the matrix after 24 days in culture (Rezania and Healy, 1999a). A similar study used bio-mimetic peptide sequence RGD in combination with KRSR or FHRRIKA, heparin-binding peptide sequences, for promoting osteoblast outgrowths. They found out that when RGD is used along with other peptides, osteoblast migration and outgrowth was stimulated (Schuler et al., 2009). Both these studies suggest that RGD if used in combination with PHSRN and /or FHRRIKA, to mimic ECM, will enhance osteoblastic development (Mrksich, 2009).

To summarise, all of the IBS-Rsn2 coated PDMS were biocompatible for 28 days in culture, suggesting that the protein coating is stable for that long, or that cells once attached and differentiation initiated, the ECM they deposit interacts sufficiently well with the substrate to keep them attached. Also, that IBS-Rsn2 can be successfully used to mimic ECM, which in this case up to three fusion constructs were used. Result successfully show that osteoblast cells preferred RGD-Rsn2 and RGD-Rsn2: PHSRN-Rsn2: FHRRIKA-Rsn2 (1:1:1) over the other Rsn2 constructs; and that these coatings promoted initial cell attachment, osteoblast differentiation and matrix mineralisation. RGD-Rsn2: PHSRN-Rsn2 (1:1) and RGD-Rsn2: FHRRIKA-Rsn2 (1:1) also positively influenced osteoblast differentiation as compared to the controls.

To conclude, RGD-Rsn2 alone, or in combination with PHSRN-Rsn2 and/or FHRRIKA-Rsn2, favour the adhesion and spreading of osteoblast cells to PDMS surfaces that have been simply coated with them and support differentiation of the cells as judged by the expression of protein markers of mature osteoblasts.

4 Stabilisation of micro-emulsions droplets

4.1 Introduction

This chapter describes work undertaken in an effort to demonstrate the use of EP protein to direct biomineralisation onto surfaces that do not naturally support this process. Specifically, the aim was to make mineralised droplets stabilised by surfactant Rsn2 protein and mineralising it with biomineralising EP protein. The rationale was that Rsn2 being a surfactant protein will act on air-water interface and will stabilise the droplets, while the EP protein being a biomineralising protein will mineralise the droplets when subjected to calcium containing solution. The obtained the mineralised droplets could be used for drug delivery, cosmetics, fabricating microcapsules, and other applications.

4.1.1 Biomineralisation

Living organisms deposit minerals to form skeletal architecture to perform a range of functions including support, mobility and protection (Veis, 2010). Minerals comprising carbonate, silica and phosphates are combined with proteins, carbohydrates and lipids, generating a staggering range of skeletal architecture featuring intricate details (Cusack and Freer, 2008). This phenomenon of skeletal formation through mineral deposition is termed biomineralisation.

The fossil record indicates that the process of biomineralisation has been occurring for more than 550 million years (Veis, 2010). The process of biomineralisation is often precisely controlled by a set of extracellular macromolecules including proteins, glycoproteins and polysaccharides, collectively called the shell matrix (Addadi and Weiner, 1992). Even though the shell matrix accounts for less than 5% of weight of the total shell weight, it controls several different aspects of shell formation including size, shape, the calcium carbonate polymorph (calcite vs aragonite), crystal organisation and crystal orientation (Marin et al., 2008, Arakaki et al., 2015).

The extracellular matrix proteins in particular are responsible for crystal nucleation, encouraging crystal growth and stopping of crystal growth (Veis, 1990). Incorporation of macromolecules into the shell matrix protects the crystal lattice against fracture by creating defects, which will absorb stress and stop the progression of cracks (Aizenberg et al., 1995). These matrix proteins are highly acidic, phosphorylated, and have motifs such as Asp repeats and Ser-Ser repeats (Weiner and Hood, 1975). The highly acidic and negatively charged nature of these proteins may act as a template for mineralisation by providing calcium-binding sites (Alvares, 2014).

In vitro crystallisation experiments using shell matrix acidic proteins confirmed that they play a role in controlling crystal morphology and crystal polymorph (Feng, 2009). Many molluscan biomineralising proteins have been found so far and they can be grouped either based on pI values, 44 biomineralising protein are grouped according to pI values (Marin et al., 2008), or based on their osteogenic properties, 77 invertebrate skeletal nacre proteins are grouped together based on their osteogenic properties (Sarashina and Endo, 2006), or location (Kobayashi and Samata, 2006).

4.1.2. Molluscan Shell Formation and Extrapallial Fluid

Most mussel shells are made up of calcium carbonate. In contrast, the bivalves like the common blue mussel, *Mytilus edulis*, have shells of made up of outer prismatic calcite layer and inner nacreous aragonite layer (Figure 4-1) (Yin et al., 2005).

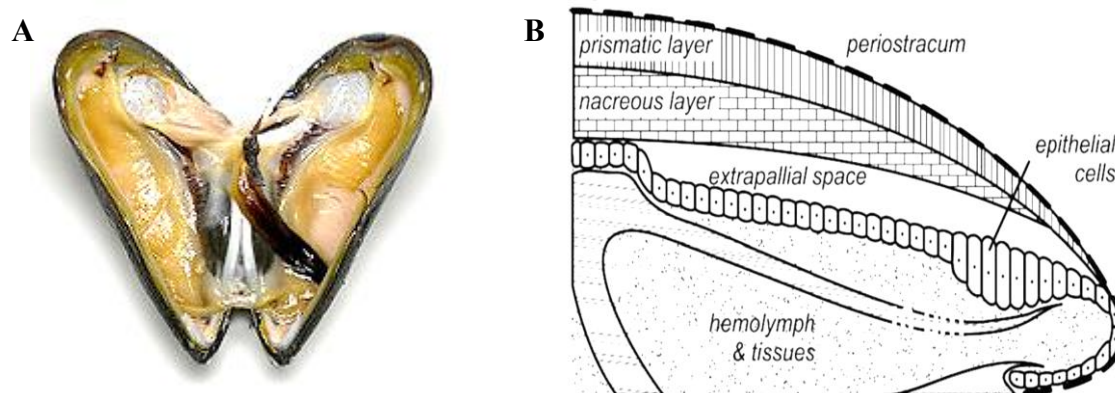


Figure 4-1 The common blue mussel *M. edulis*. (A) An extrapallial space between mantle and shell of the *M. edulis*. (B) Schematic diagram of transverse section of the mantle edge of a bivalve (Behrens, 2007).

In the common blue mussel, *Mytilus edulis*, the extrapallial (EP) fluid is secreted into the extrapallial space formed between the mantle and the shell (Figure 4-1 B). EP fluid has a higher concentration of Ca^{2+} ions compared to their blood, suggesting that the extrapallial fluid has a role in shell formation (Crenshaw, 1972). Subsequent chemical analysis of EP fluid using SDS-PAGE showed that EP fluid contains five different proteins (Misogianes and Chasteen, 1979). Hattan *et al.* identified the most abundant protein in extrapallial fluid, a 28 kDa protein, and named it extrapallial (EP) protein (Hattan et al., 2001a). Further work on the primary structure of this protein showed that the EP protein is made up of 213 amino acids in total, of which the first 23 amino acids constitute a secretion signal peptide (Yin et al., 2005). EP protein is highly glycosylated

and usually exists in disulphide linked dimeric form (Yin et al., 2005). The protein's secondary structure is stabilised by calcium binding (Hattan et al., 2001a).

EP protein has many Glu and Asp acidic residues; which will further facilitate calcium binding; and make EP protein an ideal candidate for the development of synthetic biomineralising strategies to mimic nature.

4.1.2 Rsn2 Protein

Rsn2, a surfactant protein, is isolated from the foam nest of Túngara frog. The surfactant properties of this protein are described and proven, in section 2.5. .

4.2 Aims & Objectives

Exploiting the role that EP protein plays in biomineral formation, combined with the surfactant properties of Rsn2, the strategy of stabilising droplets with Rsn2 and mineralising the droplets using EP protein aimed to direct mineral formation on surfaces that would otherwise not support mineral formation.

Work describe by Ji.B et al (Ji et al., 2010) was the precedent for this work about exploring the possibility of use of EP biomineralising protein with the aim of generating hybrid mineralised capsules as shown by Schulz.A et al (Schulz et al., 2011).

The rationale was that Rsn2 being a surfactant protein will act on air-water interface and will stabilise the droplets, while the EP protein being a biomineralising protein will mineralise the droplets when subjected to calcium containing solution. Idea was to develop Ep-Rsn2 fusion protein, which would have the ability to stabilise and mineralise oil droplets. To ensure control of all parameters, a microfluidic on-chip approach was used to generate uniform bubbles. The mineralised droplets could be used for drug delivery, cosmetics, fabricating microcapsules, and other applications.

4.3 Method and Materials

4.3.1 Rsn2 stabilised bubbles and droplets

A microfluidics system was used to make bubbles and droplets of uniform size. The microfluidic chip used was designed and fabricated by Dr Jonathan McKendry.

4.3.1.1 Fabrication of microfluidic chip

The microfluidic chip was generated by casting polydimethylsiloxane (PDMS) elastomer on a Pyrex glass substrate (Li et al., 2014). The PDMS oligomer and curing agent (Sylgard 184, Dow Corning) were mixed in a ratio of 10:1, poured into a silicon master mould, and cured at 70°C overnight (Yin et al., 2009). The silicon master was fabricated by optical lithography, while the electrodes were configured by depositing a thick platinum film on the silicon master. The photoresist was deposited onto the silicon master, which protected the substrate against irradiation, such that it then makes the features that will template the channels when the PDMS is cast onto it (Hua and Pennell, 2009).

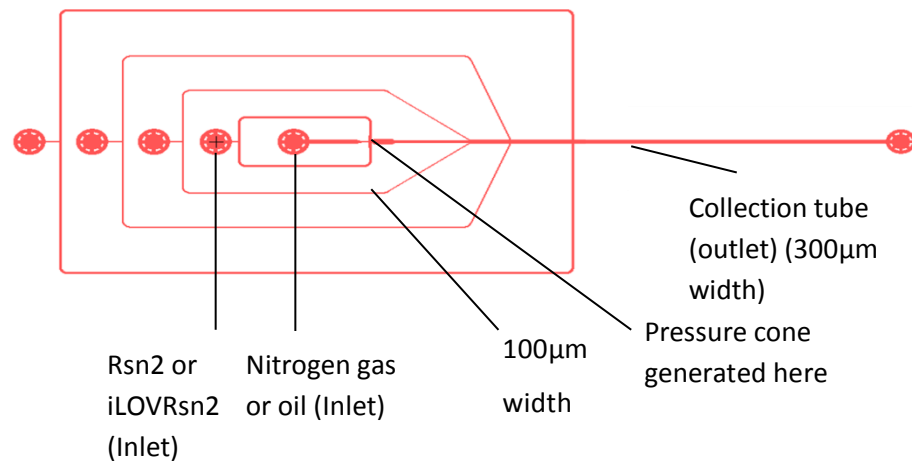


Figure 4-2 Schematic diagram of the microfluidics chip design used to form bubbles and oil droplets. Where the dimensions mentioned are channels' widths, while the circles represents the inlet and outlet channels.

4.3.1.2 Making droplets and bubbles

The microfluidic chip (Figure 4-2) consists of parallel inlet flow channels separated by a distance of 1 mm. Each channel has uniform cross section dimensions of 100 µm width x 50 µm height. The single outlet channel is wider with a cross section of 300µm wide x 50 µm height. Polytetrafluoroethylene (PTFE) tubing (Cole Palmer, Hanwell, UK) of 100 µm internal diameter and 300 µm outer diameter was inserted carefully into the outlet

reservoir to extend the reaction channel and allow collection of the product (Yashina et al., 2012). Optimisations of flow rate were carried out to reduce the size of bubbles to below 100 μm by changing flow rate from 1 $\mu\text{l}/\text{minutes}$ to 10 $\mu\text{l}/\text{minutes}$ in the flow cells. For further experiments a flow rate of 5 $\mu\text{l}/\text{minutes}$ was used. Reagents (Rsn2, Nitrogen gas or per-fluorinated oil) were delivered through the inlets at flow rates of 5 $\mu\text{l}/\text{minutes}$ using precision syringe pumps (KD Scientific). The supply pressures (250 mbar for Rsn2 and 212 mbar for nitrogen gas) were kept constant and bubbles of nitrogen gas or droplets of per-fluorinated oil were made at room temperature (22⁰C). A high-speed camera was used to capture images of the droplets/bubbles formed. The bubbles or droplets were transferred to a microscope slide for analysis by a Zeiss Axiovert light inverted microscope or Zeiss Axiophot fluorescence microscope. The images from microscopy were processed using ImageJ to facilitate measurement of the dimensions of the droplets/bubbles.

4.3.2 EP-Rsn2 – cloning and protein production

Unless otherwise stated, the method of protein production for developing EP-Rsn2 recombinant protein was as described for IBS-Rsn2 in section 3.3.

4.3.3 Inclusion body preparation

Inclusion bodies containing insoluble protein are part of the pellet along with cell debris after centrifugation of the cell lysate. The cell pellet was resuspended in wash solution (5 g l⁻¹ methionine and 1 mM EDTA) and pelleted by spinning at 11,000 rpm for 20 minutes. The wash step was performed three times. The pellet was resuspended and incubated on a magnetic stirrer at 4⁰C overnight in acetonitrile-water (1:1) solution with 0.1% TFA.

4.4 Results

4.4.1 EP-Rsn2 cloning

4.4.1.1 Primer design

An EP cDNA codon optimised for high level expression in *E. coli* and carried in a pET 15 based expression vector was obtained from Prof Maggie Cusack. The EP gene was flanked by NdeI and XhoI restriction sites. Primers were designed to amplify the whole EP gene and fragments flanked with NdeI and AseI restriction sites that could be cloned into the NdeI site of existing pET28-Rsn2 vector to generate EP-Rsn2 fusion proteins. XhoI had to be replaced by AseI because XhoI has stop codon in its sequence and there were no directly available XhoI sites in pET28 to be used (the XhoI site is at the 3' end of the EP coding sequence). AseI was selected because it has compatible cohesive ends with NdeI. Thus the AseI digested sticky end can be ligated to the NdeI half site, the 5' end of the pET28-Rsn2 expression cassette, to generate EP-Rsn2 construct. The EP-Rsn2 construct were flanked by NdeI on 5' end and BamHI on the 3' end.

Full length EP protein was also expressed from the pET15 construct, but most of it was not folded and was found in inclusion bodies (Figure 4-3). Thus three sets of primers were designed to amplify different EP fragments to incorporate into Rsn2 fusions, all containing the N-terminal calcium binding domain (Figure 4-3). Shorter fragment lengths were made so that if full length (FL) FL EP-Rsn2 does not fold then a shorter fragment such as 76E EP-Rsn2 and 82S EP-Rsn2 might work. The first 76 (as in 76E) and 82 (as in 82S) amino acids were selected as they are followed by C1q sequence. This C1q sequence also plays an important role in biomineralisation of bones, but it is the highly charged and has glycosylation sites, and therefore might be difficult to fold (Kishore and Reid, 2000). Thus primers were designed to amplify the first 76 and 82 amino acid long fragment, which has better prospects of being folded when expressed as an Rsn2 fusion construct. Table 4-1 below shows the primer sequences.

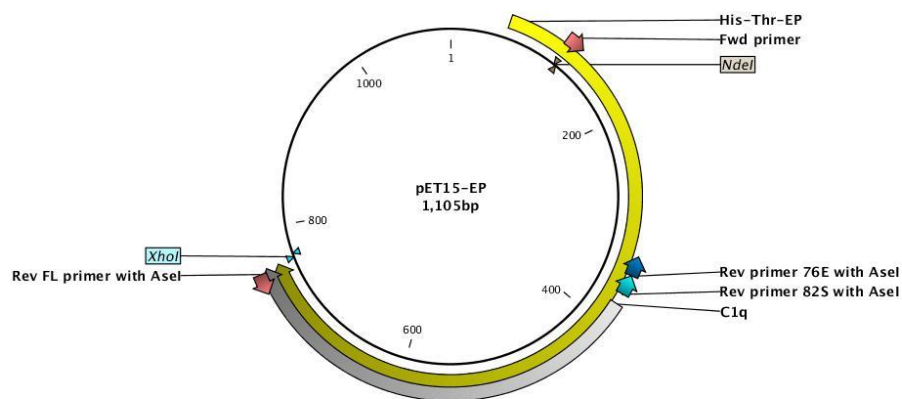


Figure 4-3 The binding sites of the three sets of primers design for pET15 EP, which each result in amplification of a different size EP fragment.

	Sequence Fwd (5'-3')	Rev Primer Sequence For N-terminal EP (5'-3')	Ann Tem
FL (218 AAs)	AGCCATATGAACCCGGTG	ATTAAT GTGCAGCATAAAAGCCGGT	53.7
76E (76 AAs)	AGCCATATGAACCCGGTG	ATTAAT TTCTTCGTGCAGATGTTT	48.1
82S (82 AAs)	AGCCATATGAACCCGGTG	ATTAAT GCTTTTGAAATATTCAAC	41.9

Table 4-1 The EP fusion protein primer sequences, where **ATTAAT** is the restriction site for AseI, which has compatible ends with NdeI. Here AAs stand for amino acids.

4.4.1.2 PCR

PCR amplification was carried out at the annealing temperature specific to each primer pair, many times dictated by 3' primer annealing temperature is shown in Table 4-1. pET15-EP was used as a template to produce three different fragments of the EP coding sequence as PCR products. The first primer pair was used to amplify 654 bp coding for the full length EP gene, second primer pair was to amplify 228 bp coding for the N terminal 76 amino acids and third primer pair was for 246bp coding for the N terminal 82 amino acids. The PCR products were purified by agarose gel electrophoresis and each excised fragment was then purified using gel purification (Wizard® SV Gel and PCR Clean-Up System) to remove any contaminating product.

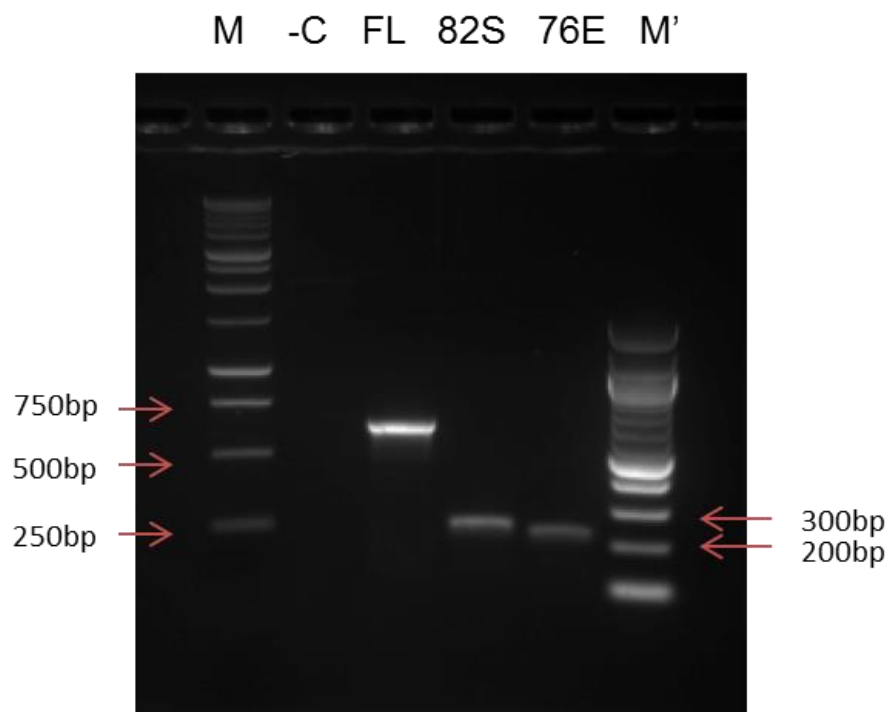


Figure 4-4 PCR amplification from EP pET15 using primers incorporating *AseI* restriction site to generate a fragment flanked with *AseI* and *NdeI*, (1) no plasmid as a negative control; (2) EP-FL; (3) EP-82S; (4) EP-76E; (M) 1kb ladder promega and (M') is 100bp Promega marker.

4.4.1.3 *Topo TA cloning and transformation*

3' adenosine overhangs were added to each insert using Taq polymerase (GoTaq® Flexi DNA Polymerase # M8301). The gene was then recombined into pCR4.0-TOPO vector with complementary 3' thymine overhangs which contains immobilised topoisomerase enzyme (Invitrogen). The Topo-TA cloned mixture was then transformed into One shot TOPO cells (using the manufacturer's protocol), miniprep and DNA sequencing carried out to check that the TA-cloned fragments had the correct sequence.

4.4.1.4 *Subcloning*

Each EP coding sequence was then subcloned into the Rsn2 containing pET28 vector. The restriction enzymes *NdeI* (NEB) and *AseI* (NEB) were used to cut the insert out of the pCR4 vector producing sticky overhangs. In parallel, Rsn2 containing pET28 expression plasmid was linearized with *NdeI* restriction enzyme (NEB) and dephosphorylated using alkaline phosphatase (NEB) to generate sticky overhangs compatible with the EP fragments.

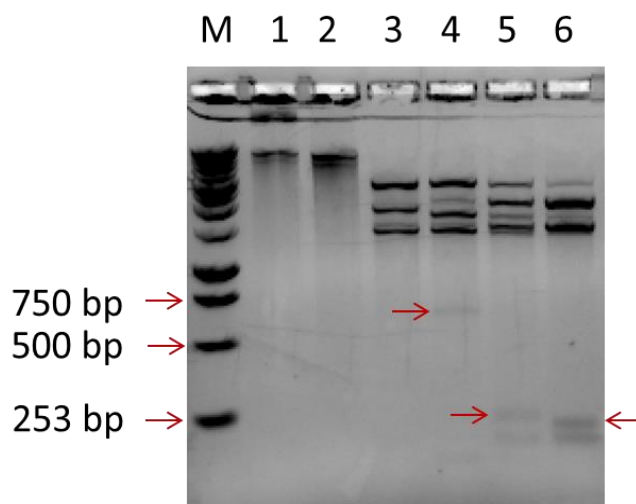


Figure 4-5 Agarose gel electrophoresis of restriction digests of all three EP fragments in pCR4.0 TOPO generated using primers incorporating *NdeI* and *AseI* sites. (1) plasmid alone; (2) *NdeI* single digest; (3) *AseI* single digest; (4) EP-FL double digest; (5) EP-82S double digest; (6) EP-76E double digest; (M) 1kb ladder promega. Red arrows shows the linearised inserts of the correct size.

The gel-purified EP fragments were ligated into Rsn2 containing pET-28 expression plasmid using T4 DNA ligase enzyme (NEB). Ligation reactions were incubated at 16^oC overnight and were then transformed into chemically competent DH5 alpha (Subcloning Efficiency™ DH5α™ Competent Cells # 18265-017) using the manufacturer's protocol.

4.4.1.5 Orientation Screening

Plasmid DNA was purified from transformed colonies and screened for the presence of the correct insert by subjecting it to *NdeI* and *BamHI* restriction digest. For this, several colonies were grown, miniprep, and the plasmids were used for restriction double digest. If the insert is in the correct orientation, carrying 5' *NdeI* and 3' *AseI*, then a band of the correct size will appear. If the insert is in the wrong orientation, a band corresponding to the Rsn2 cDNA alone will be visible. Thus double digest with *NdeI* and *BamHI* is an effective way of screening colonies.

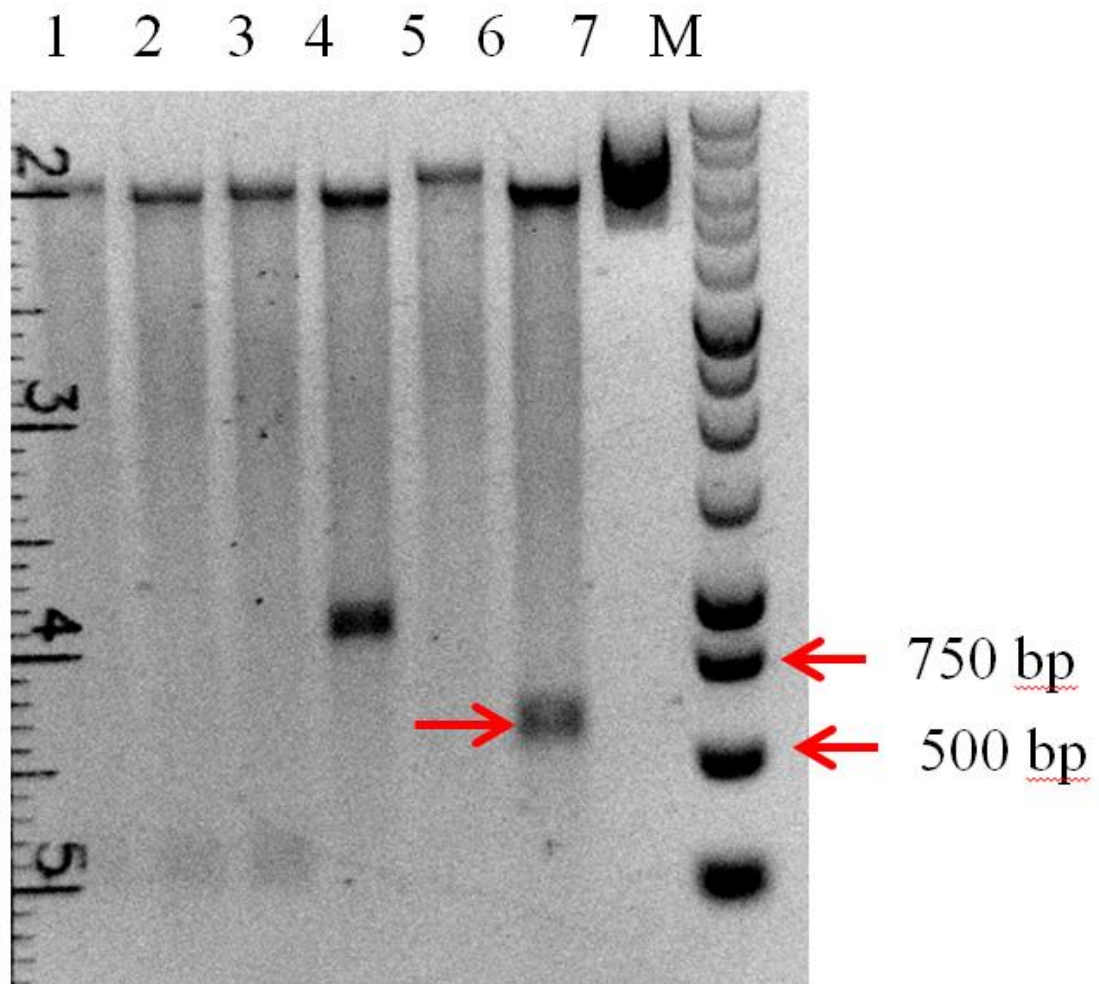


Figure 4-6 Agarose gel electrophoresis results showing screening of plasmid from six EP82S-Rsn2 colonies by restriction double digest. (1 to 6) plasmid double digest using *NdeI* and *BamHI*; (7) Uncut plasmid; (M) 1kb ladder Promega. Red arrows indicate the excised bands of the correct size, suggesting that the colony has the correct orientation of the insert.

Colonies were screened and those which contained inserts of the correct size e.g. colony 6 in Figure 4-6 were sequenced. The verified plasmids were then transformed into the Tuner (DE3) pLysS expression cells.

4.4.2 Test expression

Test expression was carried out to check for expression and solubility of the EP82S-Rsn2 fusion protein, using a representative for all three EP-Rsn2 proteins. SDS-PAGE analysis suggested that the soluble protein expression is low for all EP-Rsn2 constructs at all IPTG concentrations (0.1mM, 0.4mM or 1 mM) tested. Further optimisations were carried out in an attempt to improve the yield of protein by decreasing the incubation temperature to 4°C post induction, and increasing incubation from 3 hours to overnight, but this did not result in any improvement in protein yield.

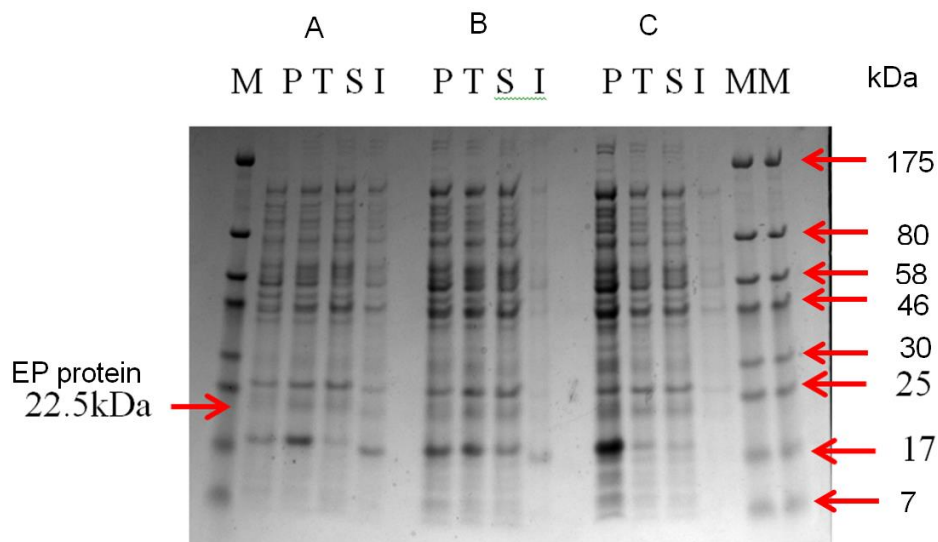


Figure 4-7 SDS-PAGE of EP82S-Rsn2 test expressions induced at different IPTG concentrations, (A) 0.1mM; (B)0.4mM and (C) 1 mM IPTG ; (P) Pre-induced fraction; (T) Total post-induced fraction; (S) Soluble fraction; (I) Insoluble fraction and (M) Marker (7-175kD, NEB).

4.4.3 EP pET15 protein expression and purification

Upon successful transformation, test expression was carried out for all three EP-Rsn2 fusion constructs. For all the three test expression, samples were incubated at 37°C after inducing with 1 mM IPTG. Post induced samples were then subjected to SDS-PAGE. SDS-PAGE analysis suggests that the soluble protein expression was low for all the three EP-Rsn2 constructs. Thus optimisations were made in order to get the protein insoluble fraction. For this, IPTG concentration was decreased to 0.4 mM from 1mM and the rest of the parameters constant. Post-induced samples were obtained at the end of 3 hours incubation at 37°C and were subjected to SDS-PAGE, which showed that the expressed protein is going in the insoluble fraction. Further trials were made by further reducing the IPTG concentration to 0.1mM and conducting SDS-PAGE analysis of the post induced samples, which also showed presence of expressed protein in insoluble fraction.

Further optimisations were carried out by increasing the time of incubation after inducing the samples with 1 mM IPTG. The post induced samples were harvested after incubating them overnight at 37°C and subjected to SDS-PAGE analysis. The obtained results showed that the proteins were still insoluble.

In order to give chaperons enough time for folding the expressed EP-Rsn2 proteins, the post induced incubation time was increased and simultaneously the induction was decreased by lowering the concentration of IPTG, so that proteins gets enough time to be folded and thereby they remain in the desired soluble fraction. With this logic, the IPTG

concentration was decreased to 0.4mM and increased the time of incubation simultaneously. The post induced samples were subjected to SDS-PAGE, which revealed that the expressed protein was going in the insoluble fraction. So the next step was to further decrease IPTG concentration to 0.1mM and post induced samples were incubated overnight. The SDS-PAGE gel showed that the expressed protein was still going in the insoluble fraction.

After unsuccessful protein expression by reducing the IPTG concentration and increasing the time of incubation, the next step tried was to decrease the temperature of post induced incubation from 37⁰C to 4⁰C. The decrease in incubation temperature will result in lowering of basal metabolic rate and thereby reducing the kinetics of protein expression. Thus the chance of protein being folded and in the soluble fraction increases. To achieve this, samples were induced with IPTG (0.1mM, 0.4mM, 1mM) and incubated at 4⁰C overnight. The resultant samples were run on the SDS-PAGE for analysis, which showed that protein was still going in the insoluble fraction.

Further optimisations were carried out in an attempt to improve the yield of protein by trying a different type of expression cells like BL21(DE3), and trying out all of the above mentioned combination of decreasing IPTG concentration along with the incubation temperature to 4⁰C and increasing the time of incubation from 3 hours to overnight, but this did not result in any improvement in protein yield.

4.4.4 Inclusion body preparation

Samples from all three wash steps and the acetonitrile-water sample were analysed by SDS-PAGE alongside the nickel affinity purification samples. The gel revealed that EP protein was well expressed (Figure 4-8), but mostly present in the insoluble fraction and was mostly solubilized by the acetonitrile-water extraction.

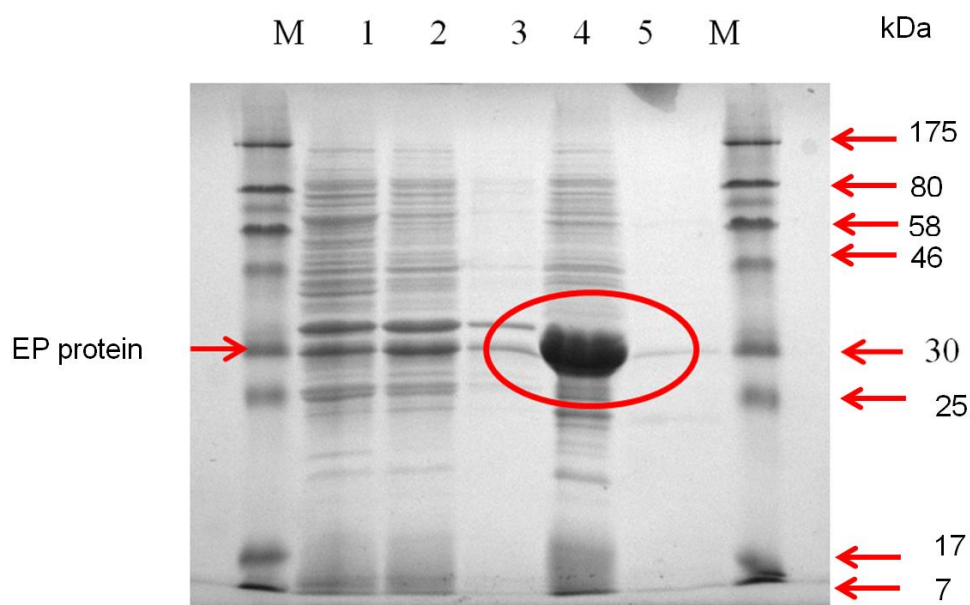


Figure 4-8 SDS-PAGE of large scale expression of EP from pET15 (1) Methionine wash 1 of the cell pellet; (2) Methionine wash 2 of the cell pellet; (3) Methionine wash 3 of the cell pellet; (4) After overnight extraction of protein from inclusion bodies using acetonitrile-water (50:50); (5) Elution fraction of the cell lysate supernatant subjected to Ni affinity chromatography and (M) Marker (7-175kD, NEB).

Since the EP protein was already of reasonable purity, it was lyophilised without further purification. Attempts were then made to solubilise lyophilised EP into pure water or buffers. However, the EP lyophilizate was not soluble in water or buffers at a range of pH 3-10.

4.4.5 Formation of Rsn2 stabilised bubbles

As a proof of principle that Rsn2 could stabilise the formation of micro-scale bubbles, nitrogen gas bubbles were made in an aqueous solution of Rsn2. Nitrogen gas and Rsn2 solution were passed through inlet flow cells on a microfluidic chip (Figure 4-9A). At the pressure cone that is generated at the meeting point of aqueous phase and nitrogen gas, bubbles are formed. The bubbles then pass through the collection tube and can be collected in an eppendorf tube. Being less dense than the aqueous phase, the bubbles tend to float on the liquid in the eppendorf.

At a flow rate of 5 μ l/minutes bubbles of 118.5 ± 7.8 μ m diameter were generated. Figure 4-9 shows bubble formation, and a representative view of the bubbles formed. These bubbles were stable for more than 24 hours but upon incubation at 4^oC for more than 48 hours they started to coalesce giving a population of heterogeneous sized bubbles. No bubbles were formed in control sample, where buffer was used in place of Rsn2. A range of concentrations from 0.1-1 mg/ml Rsn2 were used to make bubbles, but

no bubbles were formed at a lower concentrations showing that at least 1 mg/ml Rsn2 was required for bubble formation.

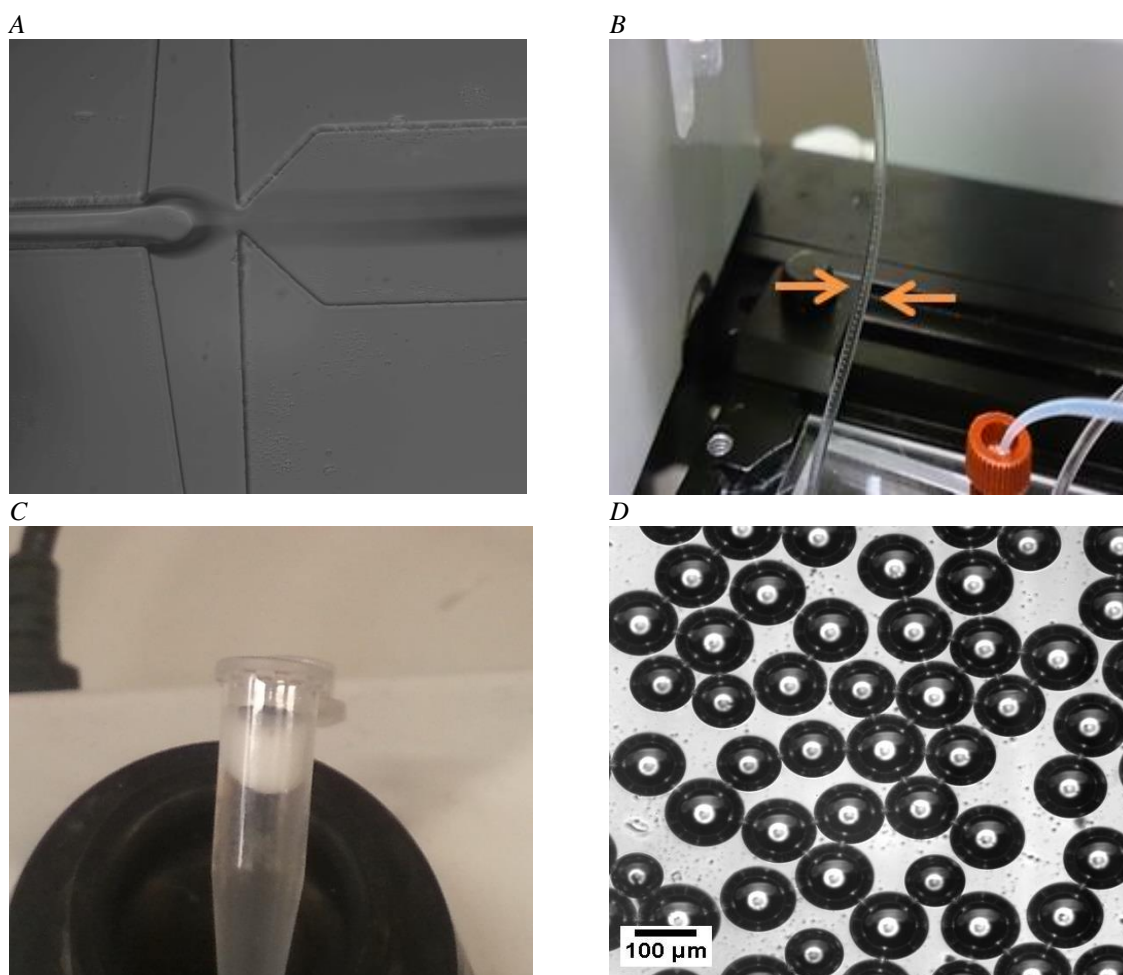


Figure 4-9 illustrates the process of Rsn2-stabilized N_2 bubble formation. Where (A) is the image of the pressure cone formed at the microfluidic junction where Rsn2 solution and nitrogen gas meet, resulting in formation of bubbles, (B) shows bubbles passing through the collection tube, (C) shows a mass of bubbles floating in an eppendorf tube, and (D) shows the bubbles viewed by light microscopy.

4.4.6 Formation of Rsn2 stabilised droplets

Rsn2-stabilised bubbles of nitrogen gas were made in a microfluidic device as a prelude to using Rsn2 in the device to form stable droplets of immiscible liquids that can be mineralised to generate nanoparticles. Perfluorinated oil was passed through one microfluidic inlet channel instead of nitrogen gas to generate Rsn2 stabilised oil droplets. The Rsn2 stabilised droplets were examined using light microscopy (Figure 4-10A). In subsequent experiments Rsn2 was replaced with iLOVRsn2, a fluorescent tagged Rsn2 protein (section-2.4.1), to produce iLOVRsn2 stabilised fluorescent oil droplets. Perfluorinated oil was selected as it is neutral in buoyancy which will allow droplet emulsion to remain suspended in solution. If the droplets are neutral in buoyancy, there will be less tendency for them to phase separate, which will also be important for

mineralisation. While, iLOVRsn2 facilitates monitoring of the localisation of partition between droplet (surface) and bulk aqueous phase formed. Droplets of $49.48 \pm 0.96 \mu\text{m}$ diameter were formed at a constant flow rate of $5 \mu\text{l}/\text{minutes}$ for both solutions. The droplets were examined by fluorescence microscopy, where the intrinsic fluorescence of the iLOV fusion partner was used for tracing Rsn2. Figure 4-10 shows a representative view of the droplets formed. Fluorescence was only found outside of the droplets, confirming that Rsn2 is working at the oil buffer interface to stabilise the oil droplets formed. These droplets were stable for more than 6 months upon subsequent incubation at 4°C . In contrast, the control sample, where only buffer was used in place of Rsn2 solution, immiscible layers of oil and buffer were found. The obtained droplets were washed to confirm that Rsn2 was at the surface, but upon washing the droplets disintegrated suggesting Rsn2 is required in solution for droplet stabilisation.

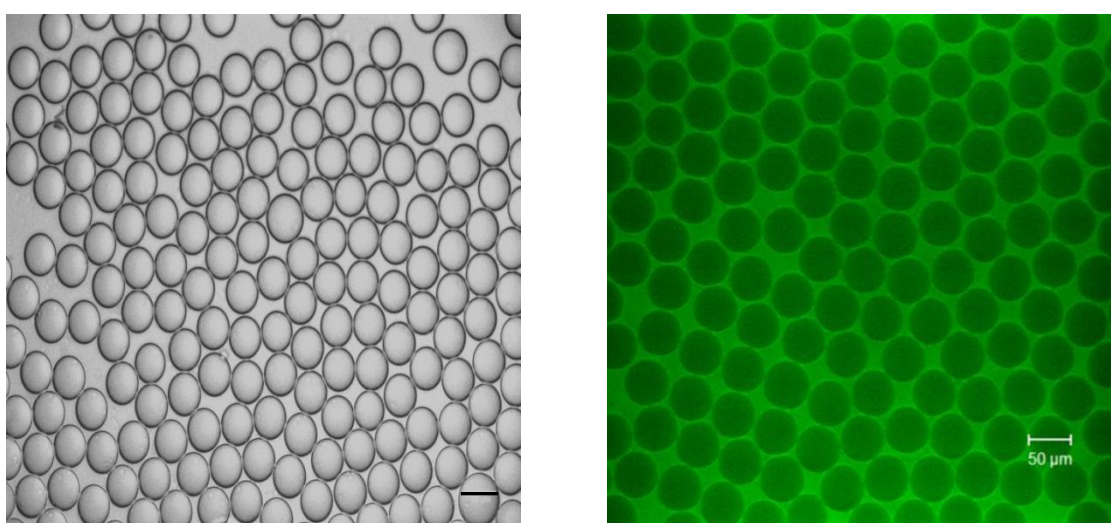


Figure 4-10 Representative image of (A) Rsn2 stabilised oil droplets captured using light microscope and (B) iLOVRsn2 stabilised oil droplets captured using fluorescence microscope. Scale bar = $50 \mu\text{m}$

After producing droplets with iLOVRsn2 on the surface, the aim was to biomineralise the droplets using EP-Rsn2 fusion construct by incubating them with the mineralising solution. EP protein being a biomineralising protein would bind to calcium and would biomineralise the droplets to generate hybrid biomineralised capsules.

In order to achieve this, attempts were made for generating Ep-Rsn2 fusion constructs, which were then used for protein production.

4.5 Discussion and future work

This chapter describes work undertaken in an effort to demonstrate the use of EP protein to direct biomineralisation onto surfaces that do not naturally support this process. Specifically, the aim was to make mineralised droplets stabilised by surfactant Rsn2 protein and mineralising them with biomineralising EP protein functionality.

Further, the aim was to develop a mineralised material mimicking nacre or bone-like tissue. To achieve this, the material surface would be coated with EP-Rsn2 and then it would be allowed to mineralise by dipping in calcium carbonate solution. This coating and mineralising steps might result in a layer of mineral crystal, which would resemble a nacre or a de-cellularised bone. A de-cellularised bone is made up of mineralised calcium and protein; the only difference will be in the type of protein and mineral formed (Hydroxylapatite in bone vs calcite if EP is used).

For this, EP protein was recombinantly over-expressed in *E. coli* as a His-tagged fusion protein, or as a tagged fusion with Rsn2 proved to be largely insoluble, most likely forming inclusion bodies. Native EP protein is secreted into the extra pallial space by the epithelial cells of the mollusc's mantle. This might have an impact on the folding and solubility of the EP protein *in vivo*. To address this challenge, it might be advantageous to produce EP containing proteins using prokaryotic secreting, or eukaryotic systems, like *Pichia pastoris*, for protein expression (Rosano and Ceccarelli, 2014).

Bacterial protein expression systems are commonly used as the cells are easy to culture, grow fast and generate good yields of recombinant protein (Khow and Suntrarachun, 2012). However, eukaryotic protein expression systems offer advantages including more native-like post translational modification. This may be important for EP which is normally glycosylated (Yin et al., 2005). If a secreting expression system were used for recombinant EP-Rsn2 expression, there is a high chance of excessive foaming of the culture medium due to the surfactant nature of Rsn2 component in the recombinant fusion protein and this may complicate cell culture. Other possibilities include exploring the use of insect cell or *Pichia pastoris* expression systems for the EP-Rsn2 protein expression, but these also typically require some aeration or agitation.

Native EP protein has a low pI and calcium ions are needed for its stabilisation in its native form (Feng, 2009). Thus addition of calcium ions in the buffer used for re-suspending the powdered lyophilised EP might prove to be beneficial. The other

possibility is that the protein needs to be purified better first, e.g. by RP-HPLC or denatured with a chaotrope and refolded from that denatured state.

The N-terminus of EP protein has a short calcium-binding peptide with repeat sequence of histidine and aspartate residues ‘DDHHDDHHD’ (Hattan et al., 2001b), one can use this short calcium-binding peptide to make EP-Rsn2 recombinant fusion construct. This shorter recombinant protein might help in protein folding and result in protein solubilisation. Another possibility is to try different biomineralising proteins as fusion partners with Rsn2. For example a 23-kD silicatein- α protein, this protein has been used for the formation of synthetic siliceous spicules (Morse, 2005). Osteopontin derived short peptides like FHRRIKA (Table 3-2) found in extracellular matrix of human bone could be used for biomineralisation.

In summary, attempts were made to obtain soluble recombinant EP-Rsn2 protein but were unsuccessful. The low solubility could perhaps be attributed to native EP protein having glycosylation sites, and glycosylation may be needed for its solubility and function in its native form. More work is needed to explore the possible options for production of soluble EP-Rsn2 protein. Upon successful expression of EP-Rsn2 protein, production of mineralised droplet should be possible.

In parallel, microfluidics was selected for making monodispersed droplets, as it gives a precise control over the production conditions, including the volume of droplet and mixing of their contents, along with the reproducibility and scalability (Ralf et al., 2012). Many have used microfluidics to make droplet emulsions and have managed to get them of varying sizes (1 μm to 100's of μm) (Ralf et al., 2012, Baret, 2012). Although the use of surfactant in emulsion formation is inevitable, none have used natural protein surfactants for droplet emulsion stabilisation. Saito et al. and Van Dijke et al. reported successful preparation of emulsions using protein from milk, egg white or soya bean flour in combination with various oils, but none of these proteins are classed as biosurfactants (Sahin et al., 2016, van Dijke et al., 2010, Saito et al., 2005). Schulz et al. have used hydrophobins for stabilising oil droplet, which were then used to mineralise but did not use microfluidics for making the emulsions (Schulz et al., 2011).

5 General discussion

General discussion

The work described in this thesis is about using the biophysical properties of Rsn2 for applications in cell patterning, functionalising scaffolds and stabilising oil droplets emulsion.

Rsn2, a protein with intrinsic surfactant activity, adsorbs to hydrophobic surfaces using non-covalent interactions, and makes the material surface hydrophilic. The Rsn2 surface coat forms rapidly and can be applied by simply dip coating with the Rsn2 solution. The Rsn2 surface coating method developed is reproducible and does not require any chemical or physical pre-treatment. Moreover, Rsn2 has demonstrated its ability to coat a range of hydrophobic polymeric surfaces, as shown by water contact angle and persistence experiments (section- 2.4). The resulting Rsn2 coating proved to be stable and persistent, and Rsn2 coated surfaces were then able to be used to promote cell adhesion, develop functionalised polymeric scaffolds and stabilise oil droplet emulsions.

The ability to produce recombinant Rsn2 fusion proteins without interfering with the proteins' surface activity was exploited. The results from section 3.4.1 showed that Rsn2 can successfully act as a fusion partner for several integrin binding sequence (IBS) peptides, and are relatively easy to express and purify. Given the experience with IBS peptide and iLOV domain fusions, it is highly likely that Rsn2 can be used to produce surface active fusions for other peptides or proteins of interest. In the recombinant Rsn2 fusion proteins developed, the Rsn2 acts as the anchor to the surface leaving the fusion partner accessible, active and solvent exposed.

Rsn2 also provides a distinct advantage for creating mixed protein surfaces, which can be applied for mimicking extracellular matrix (ECM) or by presenting growth factors, with application in tissue engineering. Rsn2 coatings could find their applications in number of places, such as coating cell culture surfaces; for immobilising enzymes; for diagnostics biosensor application; or for studying protein-protein interactions.

Although hydrophobin reduces interfacial surface tension to a greater extent, as discussed in section 1.4, and has demonstrated equally good application possibilities when compared to Rsn2 (Wösten and Scholtmeijer, 2015, Hou et al., 2009, Linder et al., 2002). For hydrophobin, in order to form assembly on solid materials, aqueous solution of protein is added onto the cleaned material surface and incubated overnight at 25°C in the presence of 0.02% NaN₃. This is followed by harsh extraction steps, which needs to

be carried out using 2% SDS at 100°C, in order to form sheets of hydrophobins (Wösten et al., 1995, Wösten et al., 1994). Thus Rsn2 was selected as it provides an easy method to develop a coating technique as compared to hydrophobin, which requires comparatively harsh and prolonged treatment to form a coat.

Moreover, fungal spores are well-known to cause respiratory allergies. A study conducted by Weichel M et al showed that hydrophobins, which coats the fungal spores, can also trigger allergic response (Weichel et al., 2003). In addition, hydrophobins aggregates at the interface to make amyloid like film, which can uptake the congo-red staining (Kwan et al., 2006). However, in the histology world congo-red is used to stain amyloid plaques of patients with Alzheimer's disease (Wu et al., 2012). Thus the ability of hydrophobin to trigger allergenic response and uptake the congo-red stain, will limit its applicability in cell based therapy.

A potentially productive avenue is to explore the idea of using SPLUNC1 for applications in humans. SPLUNC1 is a surfactant protein isolated from the upper respiratory tract of humans, more information in section-1.6. In comparison with Rsn2, SPLUNC1 is difficult to express and purify from the constructs so far tested, requiring carefully optimised culture temperature, IPTG levels and specialized E. coli strains. If allergenicity did not prove to be a problem, Rsn2 production could be more easily scaled up and economic in production. The insight of the mechanisms of Rsn2 and SPLUNC1 could be perhaps used to produce humanised Rsn2 sequences. Moreover, Rsn2 was selected as a candidate to develop a model system for future replication with SPLUNC1.

To conclude, the surfactant properties of Rsn2 can be used for many potential biomedical applications and can act as a model system for developing SPLUNC1 application

6 References

- ADDADI, L. & WEINER, S. 1992. Control and Design Principles in Biological Mineralization. *Angewandte Chemie International Edition in English*, 31, 153-169.
- AIZENBERG, J., HANSON, J., ILAN, M., LEISEROWITZ, L., KOETZLE, T. F., ADDADI, L. & WEINER, S. 1995. Morphogenesis of calcitic sponge spicules: a role for specialized proteins interacting with growing crystals. *FASEB J*, 9, 262-8.
- ALEXANDROV, N. A., MARINOVA, K. G., GURKOV, T. D., DANOV, K. D., KRALCHEVSKY, P. A., STOYANOV, S. D., BLIJDENSTEIN, T. B., ARNAUDOV, L. N., PELAN, E. G. & LIPS, A. 2012. Interfacial layers from the protein HFBII hydrophobin: dynamic surface tension, dilatational elasticity and relaxation times. *J Colloid Interface Sci*, 376, 296-306.
- ALVARES, K. 2014. The role of acidic phosphoproteins in biomineralization. *Connect Tissue Res*, 55, 34-40.
- ANSELME, K. 2000. Osteoblast adhesion on biomaterials. *Biomaterials*, 21, 667-81.
- AOTA, S., NOMIZU, M. & YAMADA, K. M. 1994. The short amino acid sequence Pro-His-Ser-Arg-Asn in human fibronectin enhances cell-adhesive function. *J Biol Chem*, 269, 24756-61.
- ARAKAKI, A., SHIMIZU, K., ODA, M., SAKAMOTO, T., NISHIMURA, T. & KATO, T. 2015. Biomineralization-inspired synthesis of functional organic/inorganic hybrid materials: organic molecular control of self-organization of hybrids. *Org Biomol Chem*, 13, 974-89.
- ARIMA, K., KAKINUMA, A. & TAMURA, G. 1968. Surfactin, a crystalline peptidelipid surfactant produced by *Bacillus subtilis*: Isolation, characterization and its inhibition of fibrin clot formation. *Biochem Biophys Res Commun*, 31, 488-494.
- ASSELINEAU, C. & ASSELINEAU, J. 1978. Trehalose-containing glycolipids. *Progress in the Chemistry of Fats and other Lipids*, 16, 59-99.
- BALASUNDARAM, G. & WEBSTER, T. J. 2007. Increased osteoblast adhesion on nanograined Ti modified with KRSR. *J Biomed Mater Res A*, 80, 602-11.
- BANAT, I. M., FRANZETTI, A., GANDOLFI, I., BESTETTI, G., MARTINOTTI, M. G., FRACCHIA, L., SMYTH, T. J. & MARCHANT, R. 2010. Microbial biosurfactants production, applications and future potential. *Appl Microbiol Biotechnol*, 87, 427-44.
- BARCZYK, M., CARRACEDO, S. & GULLBERG, D. 2010. Integrins. *Cell and Tissue Research*, 339, 269-280.
- BARET, J.-C. 2012. Surfactants in droplet-based microfluidics. *Lab Chip*, 12, 422-433.
- BAYLESS, K. J. & DAVIS, G. E. 2001. Identification of Dual $\alpha 4\beta 1$ Integrin Binding Sites within a 38 Amino Acid Domain in the N-terminal Thrombin Fragment of Human Osteopontin. *Journal of Biological Chemistry*, 276, 13483-13489.
- BEHRENS, P. B., E. (EDS.) 2007. *Handbook of Biomineralization - Biomimetic and Bioinspired Chemistry*, Weinheim: WILEY-VCH Verlag GmbH & Co.
- BELL, B. F., SCHULER, M., TOSATTI, S., TEXTOR, M., SCHWARTZ, Z. & BOYAN, B. D. 2011. Osteoblast response to titanium surfaces functionalized with extracellular matrix peptide biomimetics. *Clin Oral Implants Res*, 22, 865-72.

- BENNETT, J. H., CARTER, D. H., ALAVI, A. L., BERESFORD, J. N. & WALSH, S. 2001a. Patterns of integrin expression in a human mandibular explant model of osteoblast differentiation. *Arch Oral Biol*, 46, 229-38.
- BENNETT, J. H., MOFFATT, S. & HORTON, M. 2001b. Cell adhesion molecules in human osteoblasts: structure and function. *Histol Histopathol*, 16, 603-11.
- BERNARD, A., PHILIPPE RENAULT, J., MICHEL, B., RUDOLF BOSSHARD, H. & DELAMARCHE, E. 2000. *Microcontact Printing of Proteins*.
- BERRY, J. D., NEESON, M. J., DAGASTINE, R. R., CHAN, D. Y. C. & TABOR, R. F. 2015. Measurement of surface and interfacial tension using pendant drop tensiometry. *J Colloid Interface Sci*, 454, 226-237.
- BEUVELOT, J., PORTET, D., LECOLLINET, G., MOREAU, M. F., BASLE, M. F., CHAPPARD, D. & LIBOUBAN, H. 2009. In vitro kinetic study of growth and mineralization of osteoblast-like cells (Saos-2) on titanium surface coated with a RGD functionalized bisphosphonate. *J Biomed Mater Res B Appl Biomater*, 90, 873-81.
- BINGLE, C. D., LECLAIR, E. E., HAVARD, S., BINGLE, L., GILLINGHAM, P. & CRAVEN, C. J. 2004. Phylogenetic and evolutionary analysis of the PLUNC gene family. *Protein Sci*, 13, 422-30.
- BONAZZA, K., GADERER, R., NEUDL, S., PRZYLUCKA, A., ALLMAIER, G., DRUZHININA, I. S., GROTHE, H., FRIEDBACHER, G. & SEIDL-SEIBOTH, V. 2015. The fungal cerato-platanin protein EPL1 forms highly ordered layers at hydrophobic/hydrophilic interfaces. *Soft Matter*, 11, 1723-32.
- BONMATIN, J. M., GENEST, M., LABBE, H. & PTAK, M. 1994. Solution three-dimensional structure of surfactin: a cyclic lipopeptide studied by ¹H-NMR, distance geometry, and molecular dynamics. *Biopolymers*, 34, 975-86.
- BORNHORST, J. A. & FALKE, J. J. 2000. [16] Purification of Proteins Using Polyhistidine Affinity Tags. *Methods Enzymol*, 326, 245-254.
- BRANDANI, G. B., SCHOR, M., MORRIS, R., STANLEY-WALL, N., MACPHEE, C. E., MARENDUZZO, D. & ZACHARIAE, U. 2015. The Bacterial Hydrophobin BslA is a Switchable Ellipsoidal Janus Nanocolloid. *Langmuir*, 31, 11558-11563.
- BRITTO, C. J. & COHN, L. 2015. Bactericidal/Permeability-increasing protein fold-containing family member A1 in airway host protection and respiratory disease. *Am J Respir Cell Mol Biol*, 52, 525-34.
- BROMLEY, K. M., MORRIS, R. J., HOBLEY, L., BRANDANI, G., GILLESPIE, R. M. C., MCCLUSKEY, M., ZACHARIAE, U., MARENDUZZO, D., STANLEY-WALL, N. R. & MACPHEE, C. E. 2015. Interfacial self-assembly of a bacterial hydrophobin. *Proceedings of the National Academy of Sciences*, 112, 5419-5424.
- CANIGGIA, I., LIU, J., HAN, R., WANG, J., TANSWELL, A. K., LAURIE, G. & POST, M. 1996. Identification of receptors binding fibronectin and laminin on fetal rat lung cells. *Am J Physiol*, 270, L459-68.
- CHAN, B. P. & LEONG, K. W. 2008a. Scaffolding in tissue engineering: general approaches and tissue-specific considerations. *Eur Spine J*, 17 Suppl 4, 467-79.
- CHAN, B. P. & LEONG, K. W. 2008b. Scaffolding in tissue engineering: general approaches and tissue-specific considerations. *European Spine Journal*, 17, 467-479.
- CHAPMAN, S., FAULKNER, C., KAISERLI, E., GARCIA-MATA, C., SAVENKOV, E. I., ROBERTS, A. G., OPARKA, K. J. & CHRISTIE, J. M. 2008. The

- photoreversible fluorescent protein iLOV outperforms GFP as a reporter of plant virus infection. *Proc Natl Acad Sci U S A*, 105, 20038-43.
- CHRISTIE, J. M., HITOMI, K., ARVAI, A. S., HARTFIELD, K. A., METTLER, M., PRATT, A. J., TAINER, J. A. & GETZOFF, E. D. 2012. Structural tuning of the fluorescent protein iLOV for improved photostability. *J Biol Chem*, 287, 22295-304.
- CLEMENTS, J. M., NEWHAM, P., SHEPHERD, M., GILBERT, R., DUDGEON, T. J., NEEDHAM, L. A., EDWARDS, R. M., BERRY, L., BRASS, A. & HUMPHRIES, M. J. 1994. Identification of a key integrin-binding sequence in VCAM-1 homologous to the LDV active site in fibronectin. *J Cell Sci*, 107, 2127-2135.
- COOPER, A. & KENNEDY, M. W. 2010. Biofoams and natural protein surfactants. *Biophys Chem*, 151, 96-104.
- COOPER, A., KENNEDY, M. W., FLEMING, R. I., WILSON, E. H., VIDELER, H., WOKOSIN, D. L., SU, T. J., GREEN, R. J. & LU, J. R. 2005. Adsorption of frog foam nest proteins at the air-water interface. *Biophys J*, 88, 2114-25.
- CRENSHAW, M. A. 1972. The Inorganic Composition of Molluscan Extrapallial Fluid. *Biological Bulletin*, 143, 506-512.
- CUI, X., BOLAND, T., D'LIMA, D. D. & LOTZ, M. K. 2012. Thermal Inkjet Printing in Tissue Engineering and Regenerative Medicine. *Recent patents on drug delivery & formulation*, 6, 149-155.
- CUI, X., GAO, G., YONEZAWA, T. & DAI, G. 2014. Human Cartilage Tissue Fabrication Using Three-dimensional Inkjet Printing Technology. *J Vis Exp*, 51294.
- CUSACK, M. & FREER, A. 2008. Biomineralization: elemental and organic influence in carbonate systems. *Chem Rev*, 108, 4433-54.
- DALBY, M. J., GADEGAARD, N. & OREFFO, R. O. C. 2014. Harnessing nanotopography and integrin-matrix interactions to influence stem cell fate. *Nat Mater*, 13, 558-569.
- DALBY, M. J., GADEGAARD, N., TARE, R., ANDAR, A., RIEHLE, M. O., HERZYK, P., WILKINSON, C. D. W. & OREFFO, R. O. C. 2007. The control of human mesenchymal cell differentiation using nanoscale symmetry and disorder. *Nat Mater*, 6, 997-1003.
- DALGETTY, L. & KENNEDY, M. W. 2010. Building a home from foam--tungara frog foam nest architecture and three-phase construction process. *Biol Lett*, 6, 293-6.
- DESAI, J. D. & BANAT, I. M. 1997. Microbial production of surfactants and their commercial potential. *Microbiology and Molecular Biology Reviews*, 61, 47-64.
- DI, Y. P. 2011. Functional roles of SPLUNC1 in the innate immune response against Gram-negative bacteria. *Biochem Soc Trans*, 39, 1051-5.
- ECKERSALL, P. D., KERR, M. G. & SNOW, D. H. 1982. An investigation into the proteins of horse sweat (*Equus caballus*). *Comparative Biochemistry and Physiology Part B: Comparative Biochemistry*, 73, 375-378.
- EDWARDS, J. R. & HAYASHI, J. A. 1965. Structure of a rhamnolipid from *Pseudomonas aeruginosa*. *Archives of Biochemistry and Biophysics*, 111, 415-421.
- EPSTEIN, A. K., POKROY, B., SEMINARA, A. & AIZENBERG, J. 2011. Bacterial biofilm shows persistent resistance to liquid wetting and gas penetration. *Proc Natl Acad Sci U S A*, 108, 995-1000.

- FENG, Q. L., FANG, Z., YAN, Z. G., XING, R., XIEL, P. & ZHANG, R. Q. 2009. The structure-function relationship of MS17, a matrix protein from pearl oyster *Pinctada fucata*. *Acta Biochimica Et Biophysica Sinica*, 41, 955-962.
- FLEMING, R. I., MACKENZIE, C. D., COOPER, A. & KENNEDY, M. W. 2009. Foam nest components of the tungara frog: a cocktail of proteins conferring physical and biological resilience. *Proc Biol Sci*, 276, 1787-95.
- FOX, H. W. & CHRISMAN, C. H. 1952. The Ring Method of Measuring Surface Tension for Liquids of High Density and Low Surface Tension. *The Journal of Physical Chemistry*, 56, 284-287.
- FRAIOLI, R., RECHENMACHER, F., NEUBAUER, S., MANERO, J. M., GIL, J., KESSLER, H. & MAS-MORUNO, C. 2015. Mimicking bone extracellular matrix: Integrin-binding peptidomimetics enhance osteoblast-like cells adhesion, proliferation, and differentiation on titanium. *Colloids and Surfaces B: Biointerfaces*, 128, 191-200.
- FRITH, J. E., MILLS, R. J., HUDSON, J. E. & COOPER-WHITE, J. J. 2012. Tailored Integrin-Extracellular Matrix Interactions to Direct Human Mesenchymal Stem Cell Differentiation. *Stem Cells and Development*, 21, 2442-2456.
- GAKHAR, L., BARTLETT, J. A., PENTERMAN, J., MIZRACHI, D., SINGH, P. K., MALLAMPALLI, R. K., RAMASWAMY, S. & MCCRAY, P. B., JR. 2010. PLUNC Is a Novel Airway Surfactant Protein with Anti-Biofilm Activity. *PLoS One*, 5, e9098.
- GARCIA-CABALLERO, A., RASMUSSEN, J. E., GAILLARD, E., WATSON, M. J., OLSEN, J. C., DONALDSON, S. H., STUTTS, M. J. & TARRAN, R. 2009. SPLUNC1 regulates airway surface liquid volume by protecting ENaC from proteolytic cleavage. *Proc Natl Acad Sci U S A*, 106, 11412-7.
- GARCÍA, A. J., SCHWARZBAUER, J. E. & BOETTIGER, D. 2002. Distinct Activation States of $\alpha 5\beta 1$ Integrin Show Differential Binding to RGD and Synergy Domains of Fibronectin. *Biochemistry*, 41, 9063-9069.
- GARLAND, A. L., WALTON, W. G., COAKLEY, R. D., TAN, C. D., GILMORE, R. C., HOBBS, C. A., TRIPATHY, A., CLUNES, L. A., BENCHARIT, S., STUTTS, M. J., BETTS, L., REDINBO, M. R. & TARRAN, R. 2013. Molecular basis for pH-dependent mucosal dehydration in cystic fibrosis airways. *Proc Natl Acad Sci U S A*, 110, 15973-8.
- GAUTAM, K. K. & TYAGI, V. K. 2006. Microbial Surfactants: A Review. *J Oleo Sci*, 55, 155-166.
- GESELLCHEN, F., BERNASSAU, A. L., DEJARDIN, T., CUMMING, D. R. S. & RIEHLE, M. O. 2014. Cell patterning with a heptagon acoustic tweezer - application in neurite guidance. *Lab Chip*, 14, 2266-2275.
- GLASSER, S. W., DETMER, E. A., IKEGAMI, M., NA, C. L., STAHLMAN, M. T. & WHITSETT, J. A. 2003. Pneumonitis and emphysema in sp-C gene targeted mice. *J Biol Chem*, 278, 14291-8.
- GOERKE, J. 1998. Pulmonary surfactant: functions and molecular composition. *Biochim Biophys Acta*, 1408, 79-89.
- GONZALEZ, J. J. M., HU, Y., GABELT, B. A. T., KAUFMAN, P. L. & PETERS, D. M. 2009. Identification of the Active Site in the Heparin II Domain of Fibronectin that Increases Outflow Facility in Cultured Monkey Anterior Segments. *Invest Ophthalmol Vis Sci*, 50, 235-241.
- GRAHAM, K. L., HALASZ, P., TAN, Y., HEWISH, M. J., TAKADA, Y., MACKOW, E. R., ROBINSON, M. K. & COULSON, B. S. 2003. Integrin-Using Rotaviruses Bind $\alpha 2\beta 1$ Integrin $\alpha 2$ I Domain via VP4 DGE Sequence and Recognize $\alpha X\beta 2$ and $\alpha V\beta 3$ by Using VP7 during Cell Entry. *J Virol*, 77, 9969-9978.

- GRIESE, M. 1999. Pulmonary surfactant in health and human lung diseases: state of the art. *Eur Respir J*, 13, 1455-76.
- GRONTHOS, S., STEWART, K., GRAVES, S. E., HAY, S. & SIMMONS, P. J. 1997. Integrin expression and function on human osteoblast-like cells. *J Bone Miner Res*, 12, 1189-97.
- GUSTAFSSON, M., CURSTEDT, T., JORNVALL, H. & JOHANSSON, J. 1997. Reverse-phase HPLC of the hydrophobic pulmonary surfactant proteins: detection of a surfactant protein C isoform containing Nepsilon-palmitoyl-lysine. *Biochem J*, 326 (Pt 3), 799-806.
- HAGISAWA, K., KINOSHITA, M., MIYAWAKI, H., SATO, S., MIYAZAKI, H., TAKEOKA, S., SUZUKI, H., IWAYA, K., SEKI, S., SHONO, S., SAITOH, D., NISHIDA, Y. & HANDA, M. 2016. Fibrinogen gamma-Chain Peptide-Coated Adenosine 5' Diphosphate-Encapsulated Liposomes Rescue Mice From Lethal Blast Lung Injury via Adenosine Signaling. *Crit Care Med*, 44, e827-37.
- HAKANPAA, J., LINDER, M., POPOV, A., SCHMIDT, A. & ROUVINEN, J. 2006. Hydrophobin HFBII in detail: ultrahigh-resolution structure at 0.75 Å. *Acta Crystallogr D Biol Crystallogr*, 62, 356-67.
- HAKANPÄÄ, J., PAANANEN, A., ASKOLIN, S., NAKARI-SETÄLÄ, T., PARKKINEN, T., PENTTILÄ, M., LINDER, M. B. & ROUVINEN, J. 2004. Atomic Resolution Structure of the HFBII Hydrophobin, a Self-assembling Amphiphile. *Journal of Biological Chemistry*, 279, 534-539.
- HATTAN, S. J., LAUE, T. M. & CHASTEEN, N. D. 2001a. Purification and characterization of a novel calcium-binding protein from the extrapallial fluid of the mollusc, *Mytilus edulis*. *J Biol Chem*, 276, 4461-8.
- HATTAN, S. J., LAUE, T. M. & CHASTEEN, N. D. 2001b. Purification and Characterization of a Novel Calcium-binding Protein from the Extrapallial Fluid of the Mollusc, *Mytilus edulis*. *Journal of Biological Chemistry*, 276, 4461-4468.
- HEALY, K. E., REZANIA, A. & STILE, R. A. 1999a. Designing Biomaterials to Direct Biological Responses. *Ann N Y Acad Sci*, 875, 24-35.
- HEALY, K. E., REZANIA, A. & STILE, R. A. 1999b. Designing biomaterials to direct biological responses. *Ann N Y Acad Sci*, 875, 24-35.
- HENNESSY, K. M., POLLOT, B. E., CLEM, W. C., PHIPPS, M. C., SAWYER, A. A., CULPEPPER, K. & BELLIS, S. L. 2009. The effect of collagen I mimetic peptides on mesenchymal stem cell adhesion and differentiation, and on bone formation at hydroxyapatite surfaces. *Biomaterials*, 30, 1898-1909.
- HERSEL, U., DAHMEN, C. & KESSLER, H. 2003. RGD modified polymers: biomaterials for stimulated cell adhesion and beyond. *Biomaterials*, 24, 4385-4415.
- HIGUCHI, A., LING, Q.-D., HSU, S.-T. & UMEZAWA, A. 2012. Biomimetic Cell Culture Proteins as Extracellular Matrices for Stem Cell Differentiation. *Chem Rev*, 112, 4507-4540.
- HOBLEY, L. 2013. BslA is a self-assembling bacterial hydrophobin that coats the *Bacillus subtilis* biofilm. *Proc. Natl Acad. Sci. USA*, 110, 13600-13605.
- HOBLEY, L., HARKINS, C., MACPHEE, C. E. & STANLEY-WALL, N. R. 2015. Giving structure to the biofilm matrix: an overview of individual strategies and emerging common themes. *FEMS Microbiol Rev*, 39, 649-69.
- HOBLEY, L., OSTROWSKI, A., RAO, F. V., BROMLEY, K. M., PORTER, M., PRESCOTT, A. R., MACPHEE, C. E., VAN AALTEN, D. M. & STANLEY-WALL, N. R. 2013a. BslA is a self-assembling bacterial hydrophobin that coats the *Bacillus subtilis* biofilm. *Proc Natl Acad Sci U S A*, 110, 13600-5.

- HOBLEY, L., OSTROWSKI, A., RAO, F. V., BROMLEY, K. M., PORTER, M., PRESCOTT, A. R., MACPHEE, C. E., VAN AALTEN, D. M. F. & STANLEY-WALL, N. R. 2013b. BslA is a self-assembling bacterial hydrophobin that coats the *Bacillus subtilis* biofilm. *Proceedings of the National Academy of Sciences*, 110, 13600-13605.
- HOFER, U. 2013. Bacterial physiology: A raincoat for *Bacillus subtilis*. *Nat Rev Micro*, 11, 660-661.
- HOU, S., LI, X., LI, X., FENG, X.-Z., WANG, R., WANG, C., YU, L. & QIAO, M.-Q. 2009. Surface modification using a novel type I hydrophobin HGFI. *Analytical and Bioanalytical Chemistry*, 394, 783-789.
- HU, Y., WINN, S. R., KRAJBICH, I. & HOLLINGER, J. O. 2003. Porous polymer scaffolds surface-modified with arginine-glycine-aspartic acid enhance bone cell attachment and differentiation in vitro. *Journal of Biomedical Materials Research Part A*, 64A, 583-590.
- HUA, S. Z. & PENNELL, T. 2009. A microfluidic chip for real-time studies of the volume of single cells. *Lab Chip*, 9, 251-6.
- HUANG, S., LIANG, N., HU, Y., ZHOU, X. & ABIDI, N. 2016. Polydopamine-Assisted Surface Modification for Bone Biosubstitutes. *BioMed Research International*, 2016, 2389895.
- HUGHES, M. A., BRENNAN, P. M., BUNTING, A. S., SHIPSTON, M. J. & MURRAY, A. F. 2014. Cell patterning on photolithographically defined parylene-C: SiO₂ substrates. *J Vis Exp*.
- HUI, C. Y., JAGOTA, A., LIN, Y. Y. & KRAMER, E. J. 2002. Constraints on Microcontact Printing Imposed by Stamp Deformation. *Langmuir*, 18, 1394-1407.
- HUMPHRIES, M. J., AKIYAMA, S. K., KOMORIYA, A., OLDEN, K. & YAMADA, K. M. 1986. Identification of an alternatively spliced site in human plasma fibronectin that mediates cell type-specific adhesion. *J Cell Biol*, 103, 2637-2647.
- HYNES, R. O. 1999. Cell adhesion: old and new questions. *Trends in Cell Biology*, 9, M33-M37.
- HYNES, R. O. 2002. Integrins. *Cell*, 110, 673-687.
- JAMES, L. W., AMIT, K., HANS, A. B., ENOCH, K. & GEORGE, M. W. 1996. Microcontact printing of self-assembled monolayers: applications in microfabrication. *Nanotechnology*, 7, 452.
- JANSSEN, M. I., VAN LEEUWEN, M. B., SCHOLTMEIJER, K., VAN KOOTEN, T. G., DIJKHUIZEN, L. & WOSTEN, H. A. 2002a. Coating with genetic engineered hydrophobin promotes growth of fibroblasts on a hydrophobic solid. *Biomaterials*, 23, 4847-54.
- JANSSEN, M. I., VAN LEEUWEN, M. B. M., SCHOLTMEIJER, K., VAN KOOTEN, T. G., DIJKHUIZEN, L. & WÖSTEN, H. A. B. 2002b. Coating with genetic engineered hydrophobin promotes growth of fibroblasts on a hydrophobic solid. *Biomaterials*, 23, 4847-4854.
- JI, B., CUSACK, M., FREER, A., DOBSON, P. S., GADEGAARD, N. & YIN, H. 2010. Control of crystal polymorph in microfluidics using molluscan 28 kDa Ca²⁺-binding protein. *Integrative Biology*, 2, 528-535.
- JOHANSSON, J. & CURSTEDT, T. 1997. Molecular Structures and Interactions of Pulmonary Surfactant Components. *European Journal of Biochemistry*, 244, 675-693.
- JOSHI, S. J., GEETHA, S. J. & DESAI, A. J. 2015. Characterization and Application of Biosurfactant Produced by *Bacillus licheniformis* R2. *Appl Biochem Biotechnol*, 177, 346-61.

- KAM, L. C., SHEN, K. & DUSTIN, M. L. 2013. Micro- and nanoscale engineering of cell signaling. *Annu Rev Biomed Eng*, 15, 305-26.
- KENNEDY, M. W. 2011. Latherin and other biocompatible surfactant proteins. *Biochem Soc Trans*, 39, 1017-22.
- KHAN, F., HE, M. & TAUSSIG, M. J. 2006. Double-Hexahistidine Tag with High-Affinity Binding for Protein Immobilization, Purification, and Detection on Ni-Nitrilotriacetic Acid Surfaces. *Analytical Chemistry*, 78, 3072-3079.
- KHOW, O. & SUNTRARACHUN, S. 2012. Strategies for production of active eukaryotic proteins in bacterial expression system. *Asian Pacific Journal of Tropical Biomedicine*, 2, 159-162.
- KISHORE, U., GREENHOUGH, T. J., WATERS, P., SHRIVE, A. K., GHAI, R., KAMRAN, M. F., BERNAL, A. L., REID, K. B. M., MADAN, T. & CHAKRABORTY, T. 2006. Surfactant proteins SP-A and SP-D: Structure, function and receptors. *Mol Immunol*, 43, 1293-1315.
- KOBAYASHI, I. & SAMATA, T. 2006. Bivalve shell structure and organic matrix. *Materials Science and Engineering: C*, 26, 692-698.
- KOBAYASHI, K. & IWANO, M. 2012. BslA(YuaB) forms a hydrophobic layer on the surface of *Bacillus subtilis* biofilms. *Mol Microbiol*, 85, 51-66.
- KOMORIYA, A., GREEN, L. J., MERVIC, M., YAMADA, S. S., YAMADA, K. M. & HUMPHRIES, M. J. 1991. The minimal essential sequence for a major cell type-specific adhesion site (CS1) within the alternatively spliced type III connecting segment domain of fibronectin is leucine-aspartic acid-valine. *Journal of Biological Chemistry*, 266, 15075-15079.
- KREDI, D. 2015. *Improving interfaces for nerve repair*. PhD, University of Glasgow.
- KRUSS Young- Laplace equation. KRUSS.
- KU, S. H., LEE, J. S. & PARK, C. B. 2010. Spatial Control of Cell Adhesion and Patterning through Mussel-Inspired Surface Modification by Polydopamine. *Langmuir*, 26, 15104-15108.
- KUMAR, A. & WHITESIDES, G. M. 1993. Features of gold having micrometer to centimeter dimensions can be formed through a combination of stamping with an elastomeric stamp and an alkanethiol "ink" followed by chemical etching. *Applied Physics Letters*, 63, 2002-2004.
- KWAN, A. H. Y., WINEFIELD, R. D., SUNDE, M., MATTHEWS, J. M., HAVERKAMP, R. G., TEMPLETON, M. D. & MACKAY, J. P. 2006. Structural basis for rodlet assembly in fungal hydrophobins. *Proc Natl Acad Sci U S A*, 103, 3621-3626.
- LEE, J. N., JIANG, X., RYAN, D. & WHITESIDES, G. M. 2004. Compatibility of mammalian cells on surfaces of poly(dimethylsiloxane). *Langmuir*, 20, 11684-91.
- LEE, J. N., PARK, C. & WHITESIDES, G. M. 2003. Solvent compatibility of poly(dimethylsiloxane)-based microfluidic devices. *Analytical Chemistry*, 75, 6544-54.
- LI, B., QIU, Y., GLIDLE, A., COOPER, J., SHI, H. & YIN, H. 2014. Single cell growth rate and morphological dynamics revealing an "opportunistic" persistence. *Analyst*, 139, 3305-13.
- LINDER, M., SZILVAY, G. R., NAKARI-SETALA, T., SODERLUND, H. & PENTTILA, M. 2002. Surface adhesion of fusion proteins containing the hydrophobins HFBI and HFBII from *Trichoderma reesei*. *Protein Sci*, 11, 2257-66.
- LINDER, M. B., SZILVAY, G. R., NAKARI-SETÄLÄ, T. & PENTTILÄ, M. E. 2005. Hydrophobins: the protein-amphiphiles of filamentous fungi. *FEMS Microbiology Reviews*, 29, 877-896.

- LIU, Z., YU, X. & WAN, L. 2016. Capillary rise method for the measurement of the contact angle of soils. *Acta Geotechnica*, 11, 21-35.
- LUSSI, J. W., FALCONNET, D., HUBBELL, J. A., TEXTOR, M. & CSUCS, G. 2006. Pattern stability under cell culture conditions—A comparative study of patterning methods based on PLL-g-PEG background passivation. *Biomaterials*, 27, 2534-2541.
- MA, P. X. 2008. Biomimetic materials for tissue engineering. *Adv Drug Deliv Rev*, 60, 184-98.
- MACKENZIE, C. D., SMITH, B. O., MEISTER, A., BLUME, A., ZHAO, X., LU, J. R., KENNEDY, M. W. & COOPER, A. 2009. Ranaspumin-2: structure and function of a surfactant protein from the foam nests of a tropical frog. *Biophys J*, 96, 4984-92.
- MARIN, F., LUQUET, G., MARIE, B. & MEDAKOVIC, D. 2008. Molluscan shell proteins: primary structure, origin, and evolution. *Curr Top Dev Biol*, 80, 209-76.
- MARKET, W. S. 2016. *World Surfactant Market - Report.pdf* [Online]. <http://www.acmite.com/brochure/Brochure-Global-Surfactant-Market-Report.pdf>. [Accessed January 2017].
- MCCANN, T. J., MASON, W. T., MEIKLE, M. C. & MCDONALD, F. 1997. A collagen peptide motif activates tyrosine kinase-dependent calcium signalling pathways in human osteoblast-like cells. *Matrix Biol*, 16, 273-83.
- MCDONALD, R. E., FLEMING, R. I., BEELEY, J. G., BOVELL, D. L., LU, J. R., ZHAO, X., COOPER, A. & KENNEDY, M. W. 2009. Latherin: A Surfactant Protein of Horse Sweat and Saliva. *PLoS One*, 4, e5726.
- MCINERNEY, M. J., JAVAHERI, M. & NAGLE, D. P. 1990. Properties of the biosurfactant produced by *Bacillus licheniformis* strain JF-2. *Journal of Industrial Microbiology*, 5, 95-101.
- MEISTER, K., BÄUMER, A., SZILVAY, G. R., PAANANEN, A. & BAKKER, H. J. 2016. Self-Assembly and Conformational Changes of Hydrophobin Classes at the Air-Water Interface. *The Journal of Physical Chemistry Letters*, 7, 4067-4071.
- MELTON, K. R., NESSLEIN, L. L., IKEGAMI, M., TICHELAAR, J. W., CLARK, J. C., WHITSETT, J. A. & WEAVER, T. E. 2003. SP-B deficiency causes respiratory failure in adult mice. *Am J Physiol Lung Cell Mol Physiol*, 285, L543-9.
- MISOGIANES, M. J. & CHASTEEN, N. D. 1979. A chemical and spectral characterization of the extrapallial fluid of *Mytilus edulis*. *Analytical Biochemistry*, 100, 324-334.
- MORRIS, R. J., BRANDANI, G. B., DESAI, V., SMITH, B. O., SCHOR, M. & MACPHEE, C. E. 2016. The Conformation of Interfacially Adsorbed Ranaspumin-2 Is an Arrested State on the Unfolding Pathway. *Biophys J*, 111, 732-42.
- MORSE, M. M. M. A. D. E. 2005. Fractal intermediates in the self-assembly of silicatein filaments. *PNAS*, 102, 11657-11662.
- MRKSICH, M. 2009. Using self-assembled monolayers to model the extracellular matrix. *Acta Biomater*, 5, 832-41.
- MYERS, D. 2005a. The Organic Chemistry of Surfactants. *Surfactant Science and Technology*. John Wiley & Sons, Inc.
- MYERS, D. 2005b. An Overview of Surfactant Science and Technology. *Surfactant Science and Technology*. John Wiley & Sons, Inc.
- NAKAOKA, R., HIRANO, Y., MOONEY, D. J., TSUCHIYA, T. & MATSUOKA, A. 2013. Study on the potential of RGD- and PHSRN-modified alginates as artificial

- extracellular matrices for engineering bone. *Journal of Artificial Organs*, 16, 284-293.
- NIE, Z. & KUMACHEVA, E. 2008. Patterning surfaces with functional polymers. *Nat Mater*, 7, 277-90.
- NITSCHKE, M., SCHMACK, G., JANKE, A., SIMON, F., PLEUL, D. & WERNER, C. 2002. Low pressure plasma treatment of poly(3-hydroxybutyrate): toward tailored polymer surfaces for tissue engineering scaffolds. *J Biomed Mater Res*, 59, 632-8.
- NOMIZU, M., WEEKS, B. S., WESTON, C. A., KIM, W. H., KLEINMAN, H. K. & YAMADA, Y. 1995. Structure-activity study of a laminin $\alpha 1$ chain active peptide segment Ile-Lys-Val-Ala-Val (IKVAV). *FEBS Letters*, 365, 227-231.
- ORLA PROTEIN TECHNOLOGIES. <http://www.orlaproteins.com/cell-culture-surfaces.aspx> [Online].
- OSTROWSKI, A., MEHERT, A., PRESCOTT, A., KILEY, T. B. & STANLEY-WALL, N. R. 2011. YuaB functions synergistically with the exopolysaccharide and TasA amyloid fibers to allow biofilm formation by *Bacillus subtilis*. *J Bacteriol*, 193, 4821-31.
- PAANANEN, A., VUORIMAA, E., TORKKELI, M., PENTTILA, M., KAURANEN, M., IKKALA, O., LEMMETYINEN, H., SERIMAA, R. & LINDER, M. B. 2003. Structural hierarchy in molecular films of two class II hydrophobins. *Biochemistry*, 42, 5253-8.
- PETRIE, T. A., CAPADONA, J. R., REYES, C. D. & GARCIA, A. J. 2006. Integrin specificity and enhanced cellular activities associated with surfaces presenting a recombinant fibronectin fragment compared to RGD supports. *Biomaterials*, 27, 5459-70.
- PIERSCHBACHER, M. D. & RUOSLAHTI, E. 1987. Influence of stereochemistry of the sequence Arg-Gly-Asp-Xaa on binding specificity in cell adhesion. *J Biol Chem*, 262, 17294-8.
- PINTO, R. A., HAWGOOD, S., CLEMENTS, J. A., BENSON, B. J., NAIDU, A., HAMILTON, R. L. & WRIGHT, J. R. 1995. Association of surfactant protein C with isolated alveolar type II cells. *Biochim Biophys Acta*, 1255, 16-22.
- PLOW, E. F., HAAS, T. A., ZHANG, L., LOFTUS, J. & SMITH, J. W. 2000. Ligand Binding to Integrins. *Journal of Biological Chemistry*, 275, 21785-21788.
- PYTELA, R., PIERSCHBACHER, M. D., ARGRAVES, S., SUZUKI, S. & RUOSLAHTI, E. 1987. [27] Arginine-glycine-aspartic acid adhesion receptors. *Methods in Enzymology*. Academic Press.
- QIN, D., XIA, Y. & WHITESIDES, G. M. 2010a. Soft lithography for micro- and nanoscale patterning. *Nat Protoc*, 5, 491-502.
- QIN, D., XIA, Y. & WHITESIDES, G. M. 2010b. Soft lithography for micro- and nanoscale patterning. *Nat. Protocols*, 5, 491-502.
- QIU, Z.-Y., CHEN, C., WANG, X.-M. & LEE, I.-S. 2014. Advances in the surface modification techniques of bone-related implants for last 10 years. *Regenerative Biomaterials*, 1, 67-79.
- RALF, S., MARTIN, B., THOMAS, P. & STEPHAN, H. 2012. Droplet based microfluidics. *Reports on Progress in Physics*, 75, 016601.
- RATNER, B. D. & BRYANT, S. J. 2004. Biomaterials: where we have been and where we are going. *Annu Rev Biomed Eng*, 6, 41-75.
- REDICK, S. D., SETTLES, D. L., BRISCOE, G. & ERICKSON, H. P. 2000. Defining Fibronectin's Cell Adhesion Synergy Site by Site-Directed Mutagenesis. *J Cell Biol*, 149, 521-527.
- REIS, R. S., PACHECO, G. J., PEREIRA, A. G. & FREIRE, D. M. G. 2013. Biosurfactants: Production and Applications.

- REZANIA, A. & HEALY, K. E. 1999a. Biomimetic Peptide Surfaces That Regulate Adhesion, Spreading, Cytoskeletal Organization, and Mineralization of the Matrix Deposited by Osteoblast-like Cells. *Biotechnology Progress*, 15, 19-32.
- REZANIA, A. & HEALY, K. E. 1999b. Integrin subunits responsible for adhesion of human osteoblast-like cells to biomimetic peptide surfaces. *Journal of Orthopaedic Research*, 17, 615-623.
- ROBERTS, J. N. 2013. *Enzyme-Responsive RGD-Functionalised Substrates to Influence Mesenchymal Stem Cells*. PhD, University of Glasgow.
- RON, S. R., SANTOS, J. C. & CANNATELLA, D. C. 2006. Phylogeny of the tungara frog genus *Engystomops* (= *Physalaemus pustulosus* species group; Anura: Leptodactylidae). *Mol Phylogenet Evol*, 39, 392-403.
- ROSANO, G. L. & CECCARELLI, E. A. 2014. Recombinant protein expression in *Escherichia coli*: advances and challenges. *Front Microbiol*, 5, 172.
- RUOSLAHTI, E. 1996a. RGD and other recognition sequences for integrins. *Annu Rev Cell Dev Biol*, 12, 697-715.
- RUOSLAHTI, E. 1996b. RGD AND OTHER RECOGNITION SEQUENCES FOR INTEGRINS. *Annu Rev Cell Dev Biol*, 12, 697-715.
- RYAN, M. J. 1980. Female mate choice in a neotropical frog. *Science*, 209, 523-5.
- RYAN, M. J. 1985. .The Túngara frog *Chicago, IL: The University of Chicago Press*.
- SAHA, K., IRWIN, E. F., KOZHUKH, J., SCHAFFER, D. V. & HEALY, K. E. 2007. Biomimetic interfacial interpenetrating polymer networks control neural stem cell behavior. *Journal of Biomedical Materials Research Part A*, 81A, 240-249.
- SAHIN, S., BLIZNYUK, O., ROVALINO CORDOVA, A. & SCHROËN, K. 2016. Microfluidic EDGE emulsification: the importance of interface interactions on droplet formation and pressure stability. 6, 26407.
- SAITO, M., YIN, L.-J., KOBAYASHI, I. & NAKAJIMA, M. 2005. Preparation characteristics of monodispersed oil-in-water emulsions with large particles stabilized by proteins in straight-through microchannel emulsification. *Food Hydrocolloids*, 19, 745-751.
- SANO, H. & KUROKI, Y. 2005. The lung collectins, SP-A and SP-D, modulate pulmonary innate immunity. *Mol Immunol*, 42, 279-287.
- SARASHINA, I. & ENDO, K. 2006. Skeletal matrix proteins of invertebrate animals: Comparative analysis of their amino acid sequences. *Paleontological Research*, 10, 311-336.
- SCHINDELIN, J., ARGANDA-CARRERAS, I., FRISE, E., KAYNIG, V., LONGAIR, M., PIETZSCH, T., PREIBISCH, S., RUEDEN, C., SAALFELD, S., SCHMID, B., TINEVEZ, J.-Y., WHITE, D. J., HARTENSTEIN, V., ELICEIRI, K., TOMANCAK, P. & CARDONA, A. 2012. Fiji: an open-source platform for biological-image analysis. *Nat Meth*, 9, 676-682.
- SCHOENWAEELDER, S. M. & BURRIDGE, K. 1999. Bidirectional signaling between the cytoskeleton and integrins. *Current Opinion in Cell Biology*, 11, 274-286.
- SCHOLTMEIJER, K., JANSSEN, M. I., GERSSEN, B., DE VOCHT, M. L., VAN LEEUWEN, B. M., VAN KOOTEN, T. G., WÖSTEN, H. A. B. & WESSELS, J. G. H. 2002. Surface Modifications Created by Using Engineered Hydrophobins. *Applied and Environmental Microbiology*, 68, 1367-1373.
- SCHULER, M., HAMILTON, D. W., KUNZLER, T. P., SPRECHER, C. M., DE WILD, M., BRUNETTE, D. M., TEXTOR, M. & TOSATTI, S. G. 2009. Comparison of the

- response of cultured osteoblasts and osteoblasts outgrown from rat calvarial bone chips to nonfouling KRSR and FHRRKA-peptide modified rough titanium surfaces. *J Biomed Mater Res B Appl Biomater*, 91, 517-27.
- SCHULZ, A., LIEBECK, B. M., JOHN, D., HEISS, A., SUBKOWSKI, T. & BOKER, A. 2011. Protein-mineral hybrid capsules from emulsions stabilized with an amphiphilic protein. *Journal of Materials Chemistry*, 21, 9731-9736.
- SHEKARAN, A. & GARCIA, A. J. 2011. Extracellular matrix-mimetic adhesive biomaterials for bone repair. *J Biomed Mater Res A*, 96, 261-72.
- SIEBERS, M. C., TER BRUGGE, P. J., WALBOOMERS, X. F. & JANSEN, J. A. 2005. Integrins as linker proteins between osteoblasts and bone replacing materials. A critical review. *Biomaterials*, 26, 137-146.
- STRALEY, K. S. & HEILSHORN, S. C. 2009. Independent tuning of multiple biomaterial properties using protein engineering. *Soft Matter*, 5, 114-124.
- SZILVAY, G. R., PAANANEN, A., LAURIKAINEN, K., VUORIMAA, E., LEMMETYINEN, H., PELTONEN, J. & LINDER, M. B. 2007. Self-assembled hydrophobin protein films at the air-water interface: structural analysis and molecular engineering. *Biochemistry*, 46, 2345-54.
- TAKADA, Y., YE, X. & SIMON, S. 2007. The integrins. *Genome Biol*, 8, 215.
- TALLAWI, M., ROSELLINI, E., BARBANI, N., CASCONI, M. G., RAI, R., SAINT-PIERRE, G. & BOCCACCINI, A. R. 2015. Strategies for the chemical and biological functionalization of scaffolds for cardiac tissue engineering: a review. *J R Soc Interface*, 12, 20150254.
- TARRAN, R. & REDINBO, M. R. 2014. Mammalian short palate lung and nasal epithelial clone 1 (SPLUNC1) in pH-dependent airway hydration. *Int J Biochem Cell Biol*, 52, 130-5.
- TASHIRO, K., SEPHEL, G. C., WEEKS, B., SASAKI, M., MARTIN, G. R., KLEINMAN, H. K. & YAMADA, Y. 1989. A synthetic peptide containing the IKVAV sequence from the A chain of laminin mediates cell attachment, migration, and neurite outgrowth. *Journal of Biological Chemistry*, 264, 16174-16182.
- VAN DIJKE, K. C., SCHROËN, K., VAN DER PADT, A. & BOOM, R. 2010. EDGE emulsification for food-grade dispersions. *Journal of Food Engineering*, 97, 348-354.
- VANCE, S. J. 2012. *The relationship between structure and function in natural surfactant proteins*. PhD, University of Glasgow.
- VANCE, S. J., MCDONALD, R. E., COOPER, A., KENNEDY, M. W. & SMITH, B. O. 2014. Resonance assignments for latherin, a natural surfactant protein from horse sweat. *Biomol NMR Assign*, 8, 213-6.
- VANCE, S. J., MCDONALD, R. E., COOPER, A., SMITH, B. O. & KENNEDY, M. W. 2013a. The structure of latherin, a surfactant allergen protein from horse sweat and saliva. *Journal of the Royal Society Interface*, 10, 20130453.
- VANCE, S. J., MCDONALD, R. E., COOPER, A., SMITH, B. O. & KENNEDY, M. W. 2013b. The structure of latherin, a surfactant allergen protein from horse sweat and saliva. *Journal of the Royal Society Interface*, 10.
- VEIS, A. 1990. Biomineralization. Cell Biology and Mineral Deposition. Kenneth Simkiss and Karl M. Wilbur. Academic Press, San Diego, CA, 1989. xiv, 337 pp., illus. \$69.95; On Blomineralization. Heinz A. Lowenstam and Stephen Weiner. Oxford University Press, New York, *Science*, 247, 1129-1130.

- VEIS, A. 2010. Crystals and Life: An Introduction. *Biomineralization*. John Wiley & Sons, Ltd.
- WALTON, W. G., AHMAD, S., LITTLE, M. S., KIM, C. S., TYRRELL, J., LIN, Q., DI, Y. P., TARRAN, R. & REDINBO, M. R. 2016. Structural Features Essential to the Antimicrobial Functions of Human SPLUNC1. *Biochemistry*, 55, 2979-91.
- WANG, Z., COLLIGHAN, R. J., GROSS, S. R., DANEN, E. H., OREND, G., TELCI, D. & GRIFFIN, M. 2010. RGD-independent cell adhesion via a tissue transglutaminase-fibronectin matrix promotes fibronectin fibril deposition and requires syndecan-4/2 alpha5beta1 integrin co-signaling. *J Biol Chem*, 285, 40212-29.
- WEICHEL, M., SCHMID-GRENDELMEIER, P., RHYNER, C., ACHATZ, G., BLASER, K. & CRAMERI, R. 2003. Immunoglobulin E-binding and skin test reactivity to hydrophobin HCh-1 from *Cladosporium herbarum*, the first allergenic cell wall component of fungi. *Clinical & Experimental Allergy*, 33, 72-77.
- WEIGT, L. A., CRAWFORD, A. J., RAND, A. S. & RYAN, M. J. 2005. Biogeography of the tungara frog, *Physalaemus pustulosus*: a molecular perspective. *Mol Ecol*, 14, 3857-76.
- WEINER, S. & HOOD, L. 1975. Soluble protein of the organic matrix of mollusk shells: a potential template for shell formation. *Science*, 190, 987-9.
- WELLE, A., WEIGEL, S. & BULUT, O. D. 2014. Patterning of polymeric cell culture substrates. *Methods Cell Biol*, 119, 35-53.
- WOSTEN, H. A. & DE VOCHT, M. L. 2000. Hydrophobins, the fungal coat unravelled. *Biochim Biophys Acta*, 1469, 79-86.
- WÖSTEN, H. A., SCHUREN, F. H. & WESSELS, J. G. 1994. Interfacial self-assembly of a hydrophobin into an amphipathic protein membrane mediates fungal attachment to hydrophobic surfaces. *The EMBO Journal*, 13, 5848-5854.
- WÖSTEN, H. A. B., RUARDY, T. G., VAN DER MEI, H. C., BUSSCHER, H. J. & WESSELS, J. G. H. 1995. Interfacial self-assembly of a Schizophyllum commune hydrophobin into an insoluble amphipathic protein membrane depends on surface hydrophobicity. *Colloids and Surfaces B: Biointerfaces*, 5, 189-195.
- WÖSTEN, H. A. B. & SCHOLTMEIJER, K. 2015. Applications of hydrophobins: current state and perspectives. *Appl Microbiol Biotechnol*, 99, 1587-1597.
- WU, C., SCOTT, J. & SHEA, J.-E. 2012. Binding of Congo Red to Amyloid Protofibrils of the Alzheimer Aβ(9-40) Peptide Probed by Molecular Dynamics Simulations. *Biophys J*, 103, 550-557.
- WU, N., DAI, J. & MICALE, F. J. 1999. Dynamic Surface Tension Measurement with a Dynamic Wilhelmy Plate Technique. *J Colloid Interface Sci*, 215, 258-269.
- YASHINA, A., MELDRUM, F. & DEMELLO, A. 2012. Calcium carbonate polymorph control using droplet-based microfluidics. *Biomicrofluidics*, 6, 22001-2200110.
- YIN, H., JI, B., DOBSON, P. S., MOSBAHI, K., GLIDLE, A., GADEGAARD, N., FREER, A., COOPER, J. M. & CUSACK, M. 2009. Screening of biomineralization using microfluidics. *Analytical Chemistry*, 81, 473-8.
- YIN, Y., HUANG, J., PAINE, M. L., REINHOLD, V. N. & CHASTEEN, N. D. 2005. Structural Characterization of the Major Extrapallial Fluid Protein of the Mollusc *Mytilus edulis*: Implications for Function. *Biochemistry*, 44, 10720-10731.

- YOKOSAKI, Y., MATSUURA, N., HIGASHIYAMA, S., MURAKAMI, I., OBARA, M., YAMAKIDO, M., SHIGETO, N., CHEN, J. & SHEPPARD, D. 1998. Identification of the Ligand Binding Site for the Integrin $\alpha 9\beta 1$ in the Third Fibronectin Type III Repeat of Tenascin-C. *Journal of Biological Chemistry*, 273, 11423-11428.
- ZALTASH, S., PALMBLAD, M., CURSTEDT, T., JOHANSSON, J. & PERSSON, B. 2000. Pulmonary surfactant protein B: a structural model and a functional analogue. *Biochim Biophys Acta*, 1466, 179-86.
- ZHANG, L., IKEGAMI, M., CROUCH, E. C., KORFHAGEN, T. R. & WHITSETT, J. A. 2001. Activity of pulmonary surfactant protein-D (SP-D) in vivo is dependent on oligomeric structure. *J Biol Chem*, 276, 19214-9.
- ZHMUD, B. V., TIBERG, F. & HALLSTENSSON, K. 2000. Dynamics of Capillary Rise. *J Colloid Interface Sci*, 228, 263-269.
- ZHU, X. & ASSOIAN, R. K. 1995. Integrin-dependent activation of MAP kinase: a link to shape-dependent cell proliferation. *Molecular Biology of the Cell*, 6, 273-282.